The role of interleukin-10 in normal and aberrant late lung development

Inaugural Dissertation

submitted to the

Faculty of Medicine

in partial fulfilment of the requirements

for the degree of Doctor in Human Biology

(*Doctor biologiae hominis - Dr. biol. hom.*)

of the Justus Liebig University Giessen

by

Lignelli, Ettore

of

Rome, Lazio, Italy

Giessen (2021)

Aus dem Fachbereich der Medizin Justus-Liebig-Universität Gießen

Betreuer:

Prof. Dr. Werner Seeger

Gutachter:

Prof. Dr. Saverio Bellusci

Datum der Verteidigung:

17. Februar 2022

1 Table of contents

2 List of Figures

3 List of Tables

4 List of Abbreviations

7-AAD	7-amino-actinomycin D
AECI	Alveolar epithelial type I cell
AECII	Alveolar epithelial type II cell
alv	alveoli
alv epi	alveolar epithelium
APC	allophycocyanin
BPD	bronchopulmonary dysplasia
BSA	bovine serum albumin
CD	cluster of differentiation
CE	coefficient of error
CV	coefficient of variation
Cy7	cyanine 7
DAPI	4′,6-diamidino-2-phenylindole
dNTP	deoxynucleotide triphosphate
DUSP	dual-specificity phosphatase
E	embryonic days
EpCAM	epithelial cell adhesion molecule
FC	fold change
FITC	fluorescein isothiocyanate
FSC-A	forward scatter area
FSC-H	forward scatter height
Gsk3β	glycogen synthase kinase 3β
IFN	interferon
IL	interleukin
IL-10 KO	global interleukin-10 knockout
IP	intraperitoneal
Ly-6C	lymphocyte antigen 6 complex, locus C
MLI	arithmetic mean linear intercept
M-MLV	Moloney Murine Leukaemia Virus
N	number
N.D.	not detected
N_V	numerical density
P	postnatal day
P (corr)	corrected P-value
PAMPs	pathogen-associated molecular patterns
par	parenchyma
PBS	phosphate buffered saline
PE	phycoerythrin
PFA	paraformaldehyde
pro-SPC	prosurfactant protein C
PRR	pattern recognition receptor
RT-PCR	reverse transcription polymerase chain reaction
S	surface area
Sbno2	protein strawberry notch 2
SDS	sodium dodecyl sulfate
SSC-A	side scatter area
STAT3	signal transducer and activator of transcription 3
S_V	surface density

TEMED	N,N,N',N'-tetramethyl ethylenediamine
TNFR1B	tumor necrosis factor receptor superfamily member 1B
TNF	tumor necrosis factor
TR-AM	tissue resident alveolar macrophages
TTP	tristetraprolin
V	volume
V_V	volume density
τ (sep)	arithmetic mean septal thickness

5 Abstract

Bronchopulmonary dysplasia (BPD) is a chronic lung disease characterized by stunted lung development, simplification of alveoli and chronic inflammation. The anti-inflammatory cytokine interleukin (IL)-10, considered the keystone of anti-inflammatory immunomodulation, has been documented to be significantly downregulated in the hyperoxia (85% O_2)-based murine model of BPD, suggesting administration of this cytokine as a potential therapeutic modality. Daily exogenous administration of IL-10 did not impact the lung architecture of mice exposed to 21% O_2 (normoxia) or hyperoxia; furthermore, no alterations were observed in global IL-10 knockout mice exposed to either normoxia or hyperoxia. Refining the dosage by administering IL-10 solely on the first postnatal day (P) 1 induced an aggravation of the septal thickening which is one of the hallmarks of BPD, while having no observable effect in mice exposed to normoxia. No changes were also observed in mice treated with IL-10 at P3, regardless of the oxygen concentrations. Immunohistochemistry imaging revealed an increase in the abundance of fibroblasts in the septa of IL-10 treated mice exposed to hyperoxia. Flow cytometric analysis of whole lung homogenates isolated from IL-10-treated mice revealed that treatment with IL-10 rescues the eosinophilic environment associated with the chronic inflammatory component of BPD while significantly altering the composition of the T cell compartment of the immune response by raising the absolute T cell counts when administered at P1, but not at P3. A deeper analysis of T cell subsets revealed that IL-10 administration raises $CD4^+$ cell count in mice treated at P1, while no impact was observed in mice treated at P3. The $CD8^+$ cell count was reduced in mice exposed to normoxia and treated with IL-10 both at P1 and at P3, while $CD4^+$ $CD25^+$ cell count dropped in mice exposed to both normoxia and hyperoxia. An analysis conducted on whole lungs transcriptomes of mice exposed to hyperoxia and treated with IL-10 at P1 reported a switch from a strong anti-inflammatory profile observed at P2 to a profile more oriented towards the epithelial-mesenchymal transition at P3. To date, this is the first study providing detailed insights into the potential of IL-10 as a therapeutic to be employed in the treatment of BPD. These data delineate a clear picture of IL-10 as a complex, multi-layered molecule whose harnessing for translational purposes, although promising, constitutes a delicate challenge.

6 Zusammenfassung

Bronchopulmonale Dysplasie (BPD) ist eine chronische Lungenkrankheit, die durch verkümmerte Lungenentwicklung, Simplifikation der Alveolen und chronische Entzündung gekennzeichnet ist. Das entzündungshemmende Zytokin Interleukin (IL)-10, das als Grundpfeiler der antiinflammatorischen Immunmodulation gilt, wird im Hyperoxie-Maus-Modell (85 % Sauerstoffkonzentration) wesentlich herabreguliert, was nahelegt, dass die Verabreichung dieses Zytokins einen potenziellen Therapieansatz darstellt. Die tägliche exogene Verabreichung vonIL-10 zeigte keinen Einfluss auf die Lungenarchitektur von Mäusen in Normoxie und Hyperoxie, ebenso waren – unabhängig von der Sauerstoffkonzentration – keine Veränderungen bei IL-10 Knockout-Mäusen zu beobachten. Die Präzisierung der Dosis durch die Verabreichung von IL-10 ausschließlich am ersten postnatalen Tag (first postnatal day, P1) führte zu einer Verschlimmerung der Septumverdickung, eines der Kennzeichen der BPD, zeigte jedoch keinen beobachtbaren Effekt bei Mäusen in Normoxie. Ebenso konnte kein Effekt bei jenen Mäusen festgestellt werden, die an P3 mit IL-10 behandelt wurden, unabhängig von der Sauerstoffkonzentration. Die Immunhistochemie -Bildgebung zeigte einen Anstieg in der Anzahl von alveolaren Epithelzellen Typ II und Fibroblasten in den Septa der mit IL-10 behandelten Mäusen in Hyperoxie. Die durchflusszytometrische Analyse von ganzen Lungenhomogenaten, die von Mäusen isoliert wurden, die mit exogenem IL-10 behandelt wurden, zeigten ein Erhalten der eosinophilen Milieus, die mit der chronischen Entzündungskomponente der BPD in Verbindung gebracht wird. Die tiefergehende Analyse der T-Zellen Subsets zeigte, dass die Verabreichung von IL-10 eine Erhöhung der Anzahl der $CD4^+$ Zellen bei den an P1 behandelten Mäusen zur Folge hatte, wohingegen kein Effekt bei an P3 behandelten Mäusen zu beobachten war. Die Anzahl von $CD8^+$ Zellen verringerte sich bei Mäusen in Normoxie, sowohl bei Behandlung an P1 als auch an P3. Die Anzahl von $CD4^+CD25^+$ Zellen verringerte sich bei Mäusen sowohl in Normoxie als auch Hyperoxie. Die durchgeführte Analyse ganzer Lungentranskriptome von Mäusen in Hyperoxie, die an P1 mit IL-10 behandelt wurden, zeigte einen Wechsel von einem an P2 beobachteten stark antiinflammatorischen Profil hin zu einem eher remodellierenden Profil an P3. Bis dato ist dies die erste Studie, die detaillierte Einblicke in das Potenzial von IL-10 als Therapeutikum für BPD liefert. Diese Daten skizzieren ein klares Bild von IL-10 als komplexes, vielschichtiges Molekül, dessen Nutzen für translationale Zwecke – obgleich vielversprechend – eine heikle Herausforderung darstellt.

7 Introduction

7.1 Lung development in human and mouse

Mitochondria must rely on a steady supply of oxygen and on an equally steady removal of the carbon dioxide produced to provide the host organism with energy. Lungs are uniquely positioned to effectively facilitate this exchange, performed by the main functional unit, the alveolus. Oxygen-rich air transits through the upper airways (comprised of nose, trachea, bronchi, and bronchioles) to reach the lung parenchyma, and, through the alveolar ducts, the alveolar sacs, which are comprised of alveoli. In the alveolus, blood loaded with carbon dioxide is exposed to oxygenated air through the extremely thin barrier an alveolus provides between the outside world and the bloodstream (56). Oxygenated blood is then distributed through the organism, to provide fuel for the respiratory process. During gestation, the respiratory system undergoes a complex developmental process (174, 175). As illustrated in Figure 1 and described in (71), there are five main stages of mammalian lung development: embryonic, pseudoglandular, canalicular, saccular and alveolar. These phases are mostly shared between humans and mice, with the main difference being the stage at which the organism is born, saccular for the mouse, and alveolar for the human. Lungs originate from the anterior foregut endodermal bud, during the embryonic phase (gestational days [G]26 to G49 in humans and embryonic days [E] 9 to E12 in mice) (20). After one first act of branching into two individual buds, the precursors of the main airways, of the pulmonary vein and of the pulmonary artery are the first structures to form. In the pseudoglandular phase (G35-G119 in humans, E12-E16 in mice) further branching of the structure generates the conducting airways and terminal bronchioles, including nerve and blood vessel support networks. It is in the following phase, the canalicular phase (G112-G182 in humans, E16-E17 in mice), that the first rudimentary alveoli are formed. Alveolar epithelial type I cells (AECI) and alveolar epithelial type II cells (AECII), in conjunction with the first capillaries, start differentiating in this phase, thus setting up the first scaffolding for the air-blood barrier (22, 150). The following stage, the saccular stage (G168-G266 in humans, E17-postnatal day [P]4 in mice), takes its name from the elongated formations branching from the terminal bronchioles, the saccules. Each saccule is characterised by indentations of mesenchymal cells that will evolve into the alveoli proper, exponentially expanding the gas exchange area (60).The architecture of the future alveolus is already visible in the presence of septa, which comprise the main surface of the gas exchange

area and give structure to the parenchyma. Each septum hosts capillaries embedded in mesenchymal connective tissue and is paved with AECI. Conversely, AECII are progenitor cells which differentiate to AECI during development or repair and are crucial in keeping the alveolus patent by secreting surfactant, a phospholipoprotein that reduces surface tension and therefore the pressure difference needed for lung inflation (176). The late development of the lung is characterized by secondary septation, which further expands the surface available for gas exchange; this last phase, the alveolar phase, is where the human and mouse developmental processes start to majorly diverge. While in humans the alveolar phase takes place in an extended period that goes from G252 to young adulthood, in mice alveolarization is entirely postnatal, spanning a timeframe between P4 and P14. Importantly, mouse pup lungs are competent for gas exchange at birth, while human babies born in the saccular stage are considered premature and require medical intervention and support (21, 64, 129, 170). Perinatal practices for the management of preterm respiration involve mechanical ventilation to forcefully supply an adequate amount of oxygen to the lungs. The subsequent barotrauma and oxygen toxicity injury often result in chronic lung disease, particularly bronchopulmonary dysplasia (BPD) (140).

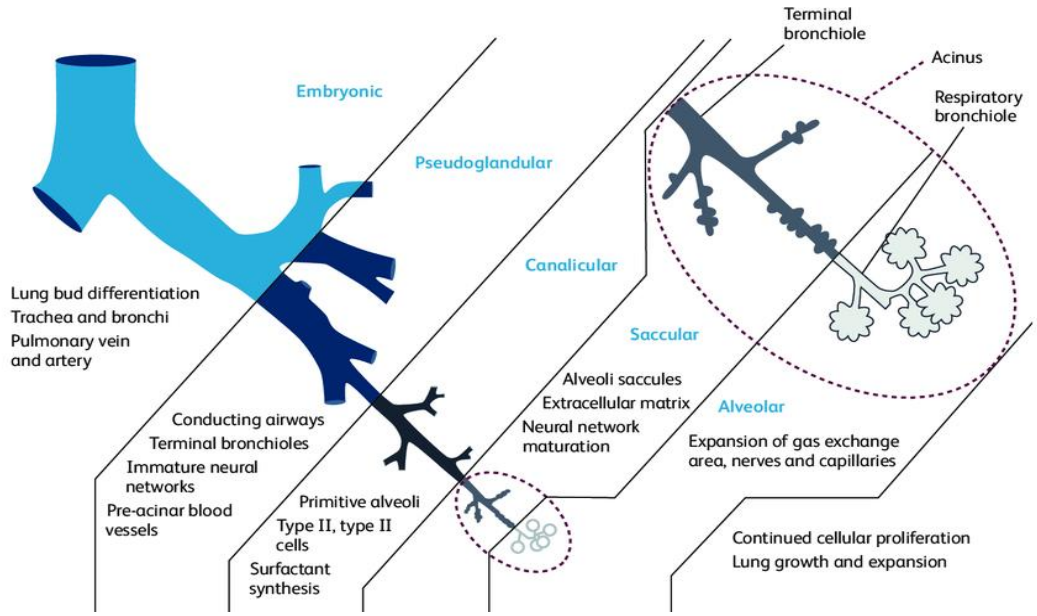

Figure 1. Main phases of mammalian lung development.
The five main phases of mammalian lung development are embryonic, pseudoglandular, canalicular, saccular and alveolar. Mice pups are born in the saccular developmental phase with fully functional lungs, while human infants born at the same stage are considered preterm. Figure adapted from (103).

7.2 Bronchopulmonary dysplasia

Described and named for the first time in 1967 by Northway and colleagues (118), BPD is a chronic disease of the lung with high prevalence in premature (born before 36 weeks of gestation) infants who received oxygen supplementation via mechanical ventilation (4, 46). Between 40% and 45% of extremely preterm infants develop BPD (173), a disease characterized by a strong, unchecked inflammatory response and underlined by high levels of pro-inflammatory cytokines like tumor necrosis factor- (TNF-) α and interferon (IFN) γ, in addition to angiogenic factors (11, 140). As the disease develops, dysregulated tissue repair and outright arrest of alveolarization lead to the formation of fewer, enlarged alveoli with thickened septa and consequently a vastly reduced gas exchange surface emerges, persisting for life (107, 137). The definition and characteristics of BPD have evolved in the five decades since a first description of this disease was presented (67, 157). As understanding of this illness deepened, severe fibrosis, the hallmark of "old" BPD, has been replaced as a critical diagnostic factor with a constellation of various levels of severity, established in relation to the oxygen needs of the infant. Today, BPD can be referred to as mild, moderate, or severe, based on oxygen requirements at <32 weeks of gestational age (57). Investigation of the complex network of pathophysiological processes involved in the onset and progress of BPD requires a robust scientific model to develop managing strategies and potential therapeutic approaches. Due to the scarcity of human material for direct study, animal models have been crucial for progressing research on BPD (114, 160); the undeniable convenience and versatility of the mouse model, combined with the constant refining of disease modelling techniques (115), has nevertheless brought this model to prominence.

7.3 The murine model of bronchopulmonary dysplasia

For the purpose of this study, wild-type and transgenic mice have been employed in every instance of animal experimentation (see Materials and Methods). The primary experimental model used was a BPD mouse model based on high concentration of oxygen in the inspired air (85% O_2, hyperoxia) (105, 115, 116), which results in changes in lung architecture that closely resemble changes observed in humans (Figure 2), as opposed to mice exposed to the standard oxygen concentrations detected in breathable air (21% O_2, normoxia). These mice, exposed from the day of birth to hyperoxia, present larger, fewer alveoli, thickening of the septa and irregular vascularization. Furthermore, there is abundant evidence supporting the assumption

that the hyperoxia-based murine model of BPD successfully replicates a chronic inflammation milieu, one of the key determinants of BPD in humans (35, 113, 177), characterised by a stark increase in the levels of pro-inflammatory cytokines and inflammatory cells in the lung tissue and lavage fluids. Non-resolved inflammation contributes greatly to BPD; the persistent generation of reactive oxygen species negatively impacts lung repair and alveolarization, chiefly by inhibiting secondary septation and vascular development (177).

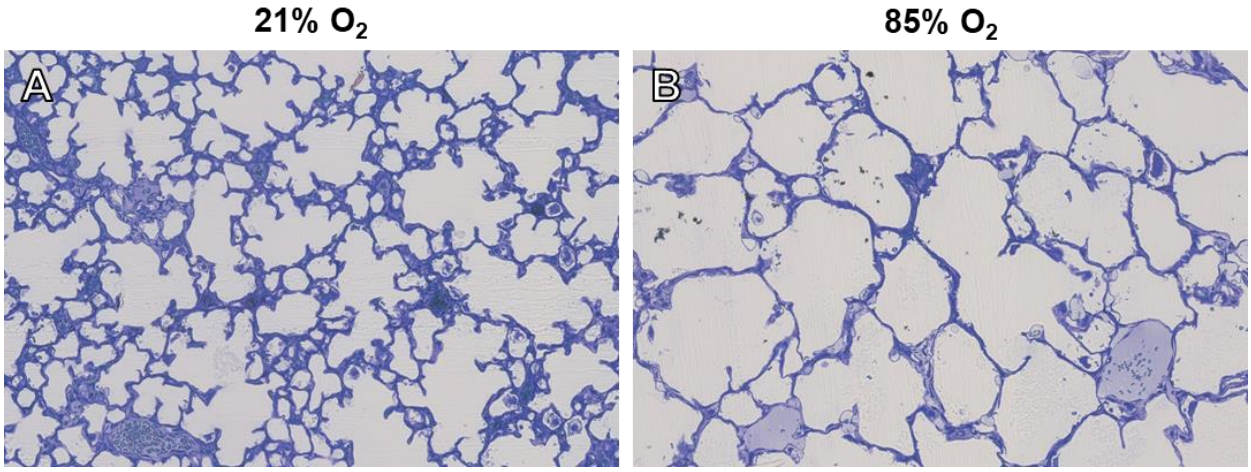

Figure 2. Comparison between lung architecture in P14 mouse pups exposed to normoxia and hyperoxia. Mouse pups exposed to normoxia achieve normal lung development and full alveolarization (A), while mouse pups exposed to hyperoxia achieve aberrant lung development (B). Image adapted from (94).

7.4 Inflammation as a pathogenic mediator of bronchopulmonary dysplasia

Inflammation plays a key role in the hyperoxia model as one of the main mediators of aberrant lung development. Simple exposure of the developing lungs to standard levels of oxygen is injurious and can severely impact the development of the preterm lung. Mechanical ventilation exacerbates this effect since ventilator-induced lung injury in human preterm infants generates an inflammatory event after a week of ventilation. Specifically, hyperoxia elicits a two-pronged response: influx of inflammatory cells (leukocytes) and an increased synthesis of pro- and anti-inflammatory mediators (cytokines). The influx of leukocytes is believed to be the main cause of stunted alveolarization (139), while altered homeostasis of cytokines is common in infants who develop BPD, leading to a chronic inflammatory environment (9, 78).

7.4.1 Leukocytes

Leukocytes are the cellular component of the blood tasked with defence against infection and disease. From a common, multipotent hematopoietic progenitor, two main cell lineages, myeloid and lymphoid, branch out. The myeloid branch gives rise to structural blood components (which include erythrocytes and thrombocytes), to mast cells, and to myeloblasts, which further differentiate into granulocytes and monocytes (122). Granulocytes are divided into three subsets based on the staining features of the granules stored in the cytoplasm: neutrophils, eosinophils, and basophils. These cells enact a broad response to pathogens not linked to specific antigens (16). Of importance, eosinophilia has been amply documented in patients who develop BPD, and the intensification of eosinophil infiltration is believed to correlate with the severity of the pathology (18, 161, 180). Monocytes are the largest type of leukocyte. The macrophage, the mature form of monocytes, is tasked with the phagocytosis of pathogens and the cellular debris resulting from infection. Additionally, these cells are responsible for the secretion of a large number of pro- and anti-inflammatory cytokines (124). A second form of macrophages, the tissue resident macrophages, derive from precursor cells in the egg yolk; in the lung, these macrophages colonize the alveolar space in the first three days of life (51). The lymphoid branch originating from the multipotent hematopoietic progenitors gives rise to lymphocytes. Lymphocytes are divided into natural killer cells, responsible for cytotoxic innate immunity, and B and T cells, which mount an adaptive immune response against previously identified pathogens. While B cells are tasked with the secretion of antibodies, $CD8^+$ T cells perform cytotoxic functions against infected or cancerous cells; $CD4^+$ T cells support other parts of the cellular immune response in identifying and neutralizing pathogens, while $CD4^+$ $CD25^+$ T cells maintain immunological tolerance (55). A schematic representation of leukocyte lineages can be found in Figure 3.

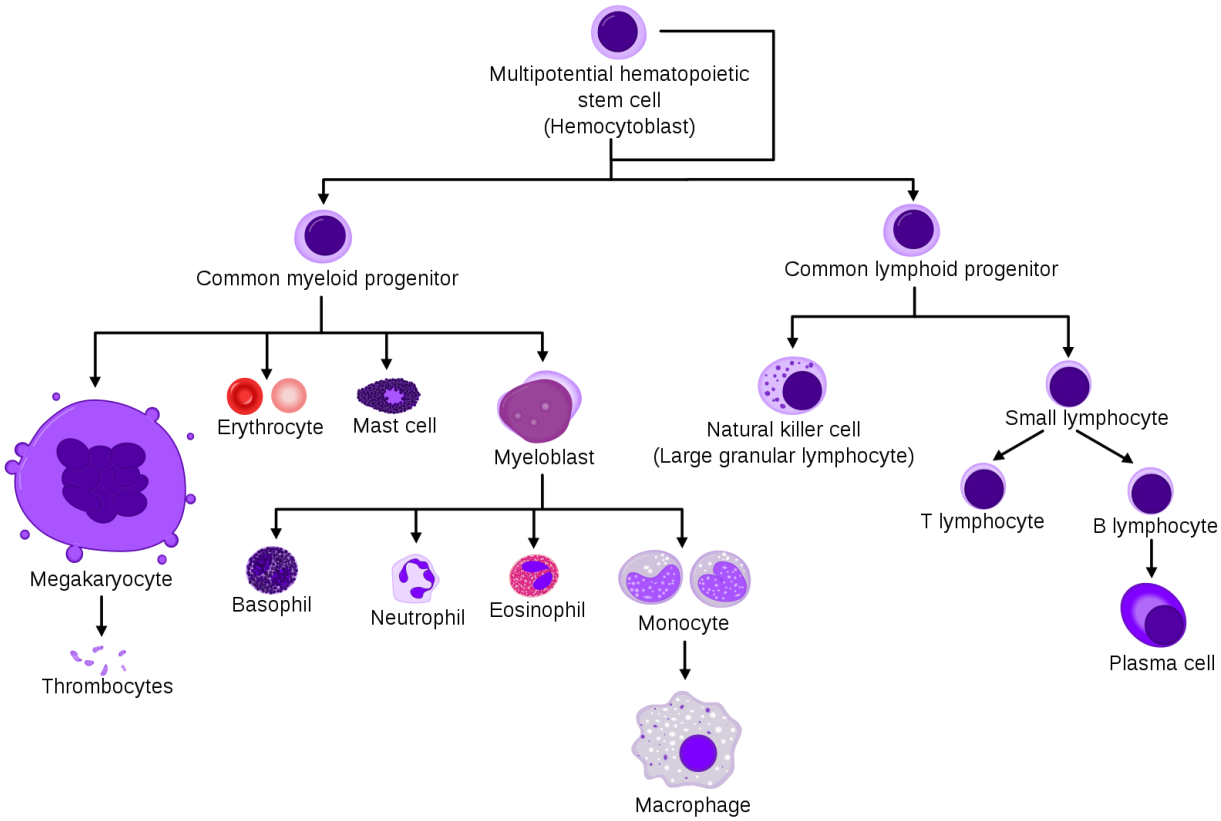

Figure 3. Leukocyte lineage branching.
Leukocytes originate from two main branches of white blood cells, the myeloid lineage, and the lymphoid lineage, which in turn originate from a common hematopoietic progenitor. While granulocytes and macrophages derive from a common myeloid progenitor, natural killer cells and lymphocytes share a common lymphoid progenitor. Image by A. Rad and M. Häggström, under CC-BY-SA 3.0 license.

After the initiation of mechanical ventilation, epithelial and endothelial cell injury leads to increased permeability of the vascular compartment (172, 177), which in turn facilitates an influx of platelets, granulocytes, and macrophages (47). Studies involving lavage fluid analysis detected a distinct prevalence of granulocytes in tracheal secretions (73), while neutrophils, the most represented subset of granulocytes, are led to the alveolar space by an intense cytokine response (25, 38). Studies on infants reported that these remarkably high levels of granulocytes persist for weeks before subsiding (121); the majority of these infants eventually developed BPD and would end up having persistent leukocyte infiltration for the first few months of life (48). Acting in synergy with granulocytes, macrophages have also been reported to further the lung injury process. In infants, macrophages have been reported to play a trophic role in the development of a plurality of organs (128), including the lung (72). Activated macrophages secrete toxic oxygen metabolites, which can quickly overtake the innate cell defence established by antioxidant enzymes, in addition to intensifying the influx of neutrophils through chemoattractants (13, 76). As the permanence of leukocytes in the lungs stretches through the chronic phase, macrophages switch to a pro-fibrotic state and activate the secretion of growth

factors, including the transforming growth factor (TGF) -β (17). Cytopathology examinations of lavage fluids isolated from infants that received forced ventilation have demonstrated that macrophages are indeed the most represented cell type (99). In addition to altered lung architecture, premature infants who developed BPD face an elevated, lifelong respiratory infections risk; further investigations on the link between inflammation and BPD pointed to a systemic inflammatory response and a transient leukemoid reaction in the foetus as elements crucial to the development of BPD (183),(184). Lymphocytes are tasked with mounting an adaptive, targeted cellular response against pathogens (59) and significant, persistent alterations of this adaptive immune response in BPD have indeed been confirmed by additional studies. Infants who progress to BPD present a reduced total T cell count since the first day of life (12), while other subsets of T cells present considerable alterations. In experiments on preterm baboons, subjects that developed BPD registered a higher $CD4^+$ cell count (136), while in very low birth weight infants (below 1,500 g) $CD4^+$ T cells are significantly more represented than $CD8^+$ (130, 154). This corroborates the findings of a study on dexamethasone treatment (125) reporting that in patients undergoing standard drug regimen the $CD4^+/CD8^+$ ratio was significantly lower, thus validating the hypothesis that the beneficial effects of dexamethasone could be attributable to a reduction in $CD4^+$ cells abundance. A model of $CD4^+$-mediated lung injury in chronic pulmonary inflammation as a result of autoaggression has been proposed by Bruder and colleagues (19).

7.4.2 Cytokines

Ventilation-induced lung injury elicits a complex cascade of inflammatory mediators; among these, cytokines, adhesion molecules, hormones, and growth factors are responsible of directing the vast majority of this response (15). Cytokines, small peptides secreted by a multitude of cell types, including immune, epithelial, and endothelial cells (169), comprise both pro-inflammatory and anti-inflammatory molecules. Although it was previously believed that this duality represented a rigid subdivision without any point of contact between pro- and anti-inflammatory cytokines, subsequent studies refined and deepened our understanding of the roles cytokines play in innate and adaptive immunity regulation. It is now widely accepted that many cytokines routinely cross these boundaries and can exert both inhibitory and stimulatory effects on the immune response (8, 98, 142). One especially notable example is the anti-inflammatory activity resulting from the interaction of TNF-α with one specific receptor, the tumor necrosis factor receptor superfamily member 1B (TNFR1B) (151). Originally

considered a co-stimulator of T cells and B cells (74), TNFR1B has been subsequently validated as a key element through which regulatory T cells exert immunosuppressive activity. Additionally, a subgroup of cytokines has been demonstrated to direct the migration of immune cells; these chemotactic cytokines, aptly named chemokines, regulate cell trafficking in both pro- and anti-inflammatory contexts through concentration gradients, immunological sites of action and co-factors (155). Chemokines are considered the main mediators of the influx of granulocytes and macrophages associated with the development of BPD in mechanically ventilated infants (99). As a whole, cytokine pro-inflammatory patterns revolve around the activation of intracellular signalling, like the activation and upregulation of the nuclear factor κ-light-chain-enhancer of activated B (NF-κB) cells pathway, which is critical for the development of lung injury following ventilation (Figure 4) (158). The sheer number of and the complex relations between cytokines represent the biggest obstacle preventing a full and complete understanding of all the regulatory mechanisms and interactions that underlie such a sprawling network of functions. While many pro-inflammatory cytokines are routinely involved in the pathways related to inflammation, among the anti-inflammatory cytokines, interleukin (IL) -10 is widely considered to have a prominent, if not the most important, role in the modulation of the inflammatory response (106, 155, 186).

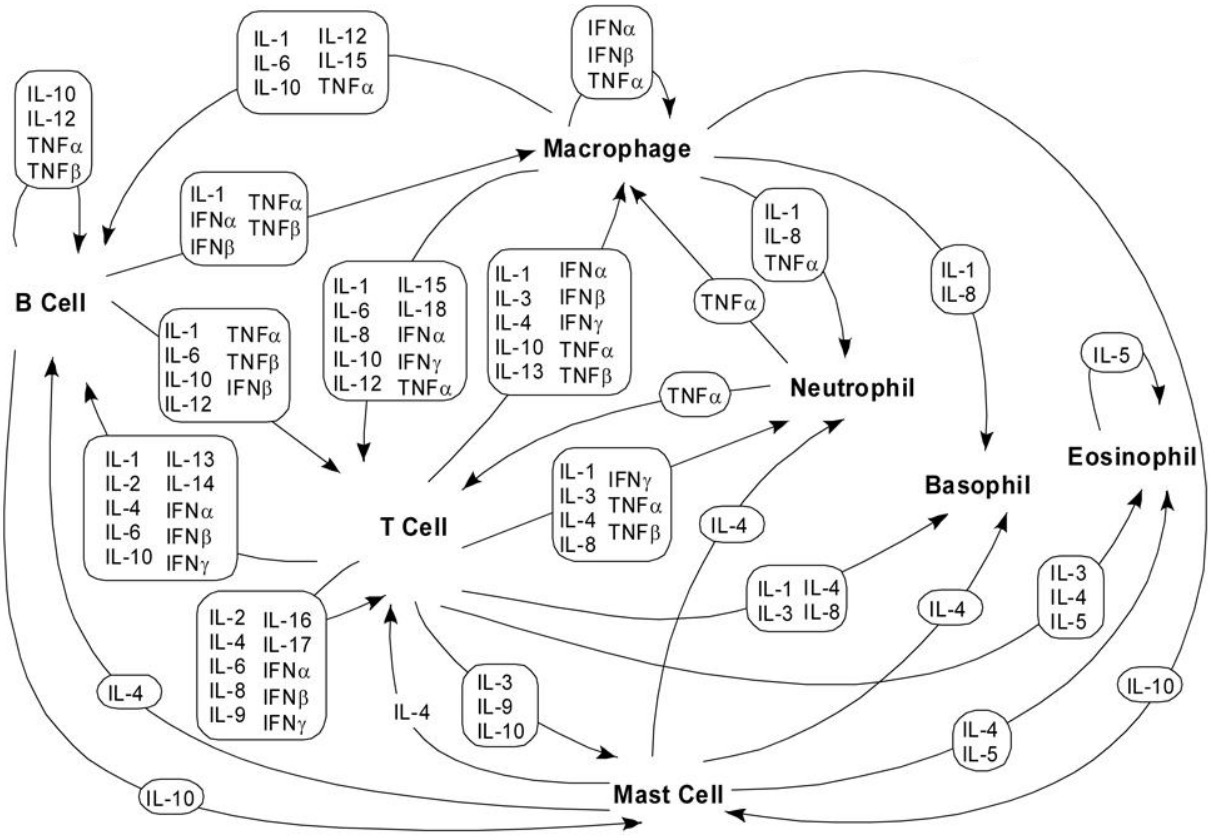

Figure 4. Overview of the main cytokine network nodes.
The main effector cells of the immune system (B cells, T cells, macrophages, mast cells, neutrophils, basophils, and eosinophils) all require strict and carefully choreographed coordination to effectively respond to pathogens. This level of organization is achieved through a complex, multifaceted cytokine network (186). IFN, interferon; IL, interleukin; TNF, tumor necrosis factor.

7.5 Interleukin-10

Originally named cytokine synthesis inhibitory factor, or CSIF, IL-10 was discovered 31 years ago by Fiorentino and coworkers (37) in a study reporting the crucial role of this molecule in the interplay between two subsets of $CD4^+$ cells, defined as T helper (Th) 1 and 2. Furthermore, this study reported on the synthesis of IL-10 by Th2 and the inhibitory effects of this cytokine on the activity of Th1 cells. In addition to Th2 cells, a wide variety of other cell types secrete IL-10. Monocytes, circulating and resident macrophages and all granulocytes except basophils have been documented to produce IL-10 (106), and so do lymphocytes (Th1 $CD4^+$, $CD8^+$, $CD4^+$ $CD25^+$ T regulatory cells and B cells) (40). Other cellular sources of IL-10 include epithelial cells (66) and neoplastic cells (65). The expression patterns of IL-10 are tightly regulated. In leukocytes, the activation of pattern recognition receptors, which sense molecules from pathogens and are expressed mainly by innate immune cells, elicit the parallel expression of inflammatory cytokines and IL-10, in a strict choreography balancing the immune response

(80), which relies on the activation of the mitogen-activated protein kinase (MAPK) (144). Production of IL-10 by macrophages and dendritic cells is an especially varied, multi-stage process which sees many different and intersecting crossroads and pathways, involving many other co-receptors and cytokines, like CD40, dectin-1 and DC-SIGN (123). In T cells, conditions and stimuli required for the regulation of IL-10 secretion are interwoven with T cells activation and differentiation pathways, thus ensuring a feedback loop to prevent autoaggression (143). Conversely, the regulation of IL-10 production by non-immune cell types is still poorly understood. The mechanisms regulating IL-10 production in epithelial cells, in particular, have been studied mostly in intestinal epithelial cells; *Il10* knockout mice are routinely employed in studies involving intestinal bowel disease, chronic enterocolitis and Crohn's disease (43, 61). It is striking then, to date, the impact of IL-10 deregulation in the lung, an organ with a strong epithelial cell component, has not yet been investigated.

7.5.1 IL-10 receptor and signalling

All members of the interleukin family initiate signalling cascades by binding to a heterodimeric receptor (127). Interleukin-10 specifically binds to a receptor complex formed by units IL-10Rα and IL-10Rβ; while IL-10Rα is specific for leukocytes, IL-10Rβ is common to all interleukin receptors (185). Dimerization of the IL-10R complex initiates a signalling cascade that, through the phosphorylation of the Janus kinase 1 (JAK1) and the tyrosine kinase 2 (Tyk2), allows the recruitment of the signal transducer and activator of transcription 3 (STAT3) (178). Although the exact mechanisms with which STAT3 mediates the anti-inflammatory effects of IL-10 have not yet been clearly established, activation of STAT3 has been reported to be a key requirement for this function (82, 179), and deletion of STAT3 results in chronic enterocolitis similar in magnitude to the effects of deletion of IL-10 itself (Figure 5) (166). Among the proposed models of IL-10/STAT3 action, the one achieving the widest consensus is the induction of a plethora of additional anti-inflammatory actors, including genes coding for the transcription factors E26 and ETS variant transcription factor 3 (34), RNA destabilizing factors like tristetraprolin, or the direct inhibition of relevant microRNAs, as seen in the case of miR-155 (95, 148).

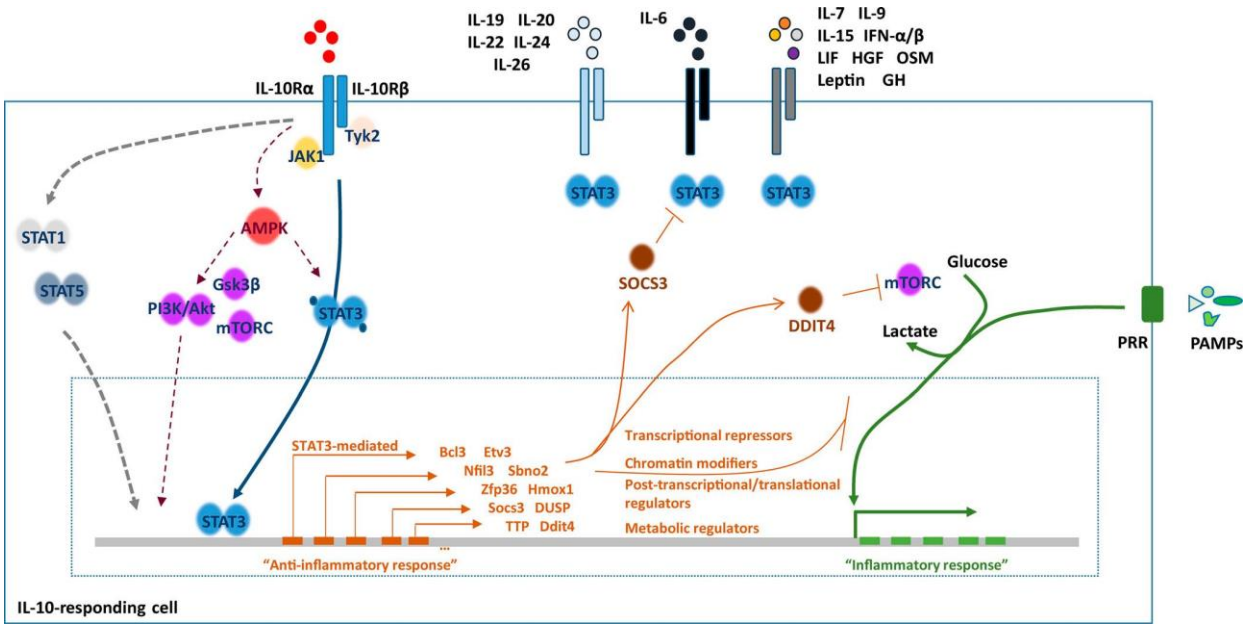

Figure 5. Overview of IL-10 signalling.
Binding of IL-10 to its receptor initiates a signalling cascade resulting in the induction of a STAT3-mediated anti-inflammatory response. Through mechanisms still not fully understood, STAT3 activation by IL-10 can also alternatively elicit a switch to a pro-inflammatory response. AMP, adenosine monophosphate; AMPK, AMP-activated protein kinase; Bcl3, B cell lymphoma 3-encoded protein; DDIT4, DNA-damage-inducible transcript 4; DUSP, dual-specificity phosphatase; ETS, Etv3, ETS variant transcription factor 3; GH, growth hormone; Gsk3β, glycogen synthase kinase 3β; HGF, hepatocyte growth factor; Hmox1, heme oxygenase (decycling) 1; IL, interleukin; IFN, interferon; JAK1, Janus kinase 1; LIF, leukaemia inhibitory factor; mTORC, mammalian target of rapamycin complex; Nfil3, nuclear factor, interleukin 3 regulated; OSM, oncostatin M; PAMPs, pathogen-associated molecular patterns; PI3K, phosphoinositide 3-kinase; PRR, pattern recognition receptor; Sbno2, protein strawberry notch 2; SOCS3, suppressor of cytokine signalling 3; STAT, signal transducer and activator of transcription; TTP, tristetraprolin; Tyk2, tyrosine kinase 2; Zfp36, zinc finger protein 36 homolog. Adapted from (145).

7.5.2 IL-10 as a key anti-inflammatory mediator

In the context of inflammation, IL-10 has been described as the main actor responsible for the de-escalation of cellular immune response. Macrophages, in particular, have been extensively described as the main target of IL-10 (190). By specifically suppressing NF-κB target genes (63), IL-10 inhibits antigen presentation, production of immunostimulatory cytokines like TNF-α and IL-6 and the direct pathogen elimination enacted by reactive oxygen species in macrophages (26, 28, 31), thus strongly limiting the subsequent inflammatory response. In neutrophils, IL-10 acts as a disruptor of both the NF-κB and the interferon regulatory factor inflammatory pathways (63). Deletion of *Il10* restricted to T cells has been reported to elicit an effect comparable to a global deletion of IL-10 in viral infection models, including a

remarkable inhibitory effect on T cells themselves (165). Historically thought of exerting this activity mainly via antigen-presenting cells (91), IL-10 has also been reported to directly target T cells and induce anergy (49). Conversely, inactive $CD8^+$ T cells respond to IL-10 by proliferating and increasing production of IFNγ (111). Outside of immune cells, an extended range of IL-10 interactions with different cell types during inflammation has been amply documented. In neurons, IL-10 has been demonstrated to exert a protective effect against potential damage due to infection or excessive inflammatory response, and support survival (188). A similar role has been ascribed to IL-10 in the adipose tissue (87). Of note, through its interactions with STAT3, IL-10 has recently been identified as a promoter of wound repair, directly impacting extracellular matrix deposition and fibroblasts and epithelial cells metabolism and proliferation (10, 131).

7.5.3 IL-10 manipulation as a therapeutic modality

Due to its key role in inflammation and disease, IL-10 manipulation has been widely regarded as a promising therapeutic modality. The wide-ranging network of interactions it is embedded into has nevertheless proven the effects of an actual treatment difficult to predict and modulate. Following the generation of the first IL-10 deficient mice by Kühn and coworkers (79) and the subsequent adoption of this mouse line as a model of chronic enterocolitis, exogenous IL-10 administration has been at the forefront of inflammatory bowel disease medical research. A large cohort of studies has demonstrated that systemic treatment with IL-10, either by administration or by localized overexpression, widely improves colitis outcomes in different animal models of the disease (52, 163), although human application is still in its infancy (24). The anti-inflammatory role of IL-10 has also been immediately regarded as a potential immune escape mechanism for tumours, and this theory has been amply validated by studies in various animal models (52, 89). Nonetheless, IL-10 has also been linked to an improved antitumoral response in solid tumor patients via a reported $CD8^+$-enhancing activity (112), thus adding to the scope of its effects. This complexity of IL-10 interactions is especially evident in autoimmune diseases. Administering IL-10 to patients affected by psoriasis and rheumatoid arthritis is indeed promising (168), while in systemic lupus erythematosus, inhibiting IL-10 levels and activity appears a more convincing strategy (88). The conflicting outcomes of these studies indicate that the use of IL-10 as a therapeutic modality is currently of unclear clinical viability, and desperately call for studies on a wider range of biological systems.

7.5.4 IL-10 in pulmonary physiology and disease

In preterm infants that develop BPD, IL-10 levels have been repeatedly reported to be lower than in term infants, or in infants who would not develop BPD (42, 68, 135), thus suggesting a link between the anti-inflammatory role of this cytokine and the chronic inflammation which is one of the core constituents of BPD. However, the body of knowledge accrued around the role of IL-10 in lung disease has been developed chiefly in the areas of infection, allergy, and cancer. Mice in which *Il10* was knocked out exhibit heightened production of inflammatory cytokines like IL-4, IL-6 and IFNγ, thus leading to a much more severe inflammatory response in an infection model based on intranasal instillation of ovalbumin (138). Furthermore, in a model of allergic bronchopulmonary aspergillosis, IL-10 knockout mice exhibited as severe a reaction (50). In the context of cancer immunology, the pleiotropic activity of IL-10 has emerged as the catalyst for several antithetic observations. Non-small cell lung cancer patients presenting higher levels of IL-10 had better survival rates (45), while the opposite was observed in melanoma (117). These diametrically opposed effects have been pinned on the cell type targeted by IL-10 and on different responses of T cells to IL-10, based on the effector stage of the cells at the moment of therapy (145). Of note, high levels of IL-10 have been linked to acute pro-inflammatory effects, including heightened production of IFNγ and reduced counts of haemoglobin and platelets (167). While reversible, these effects have been proven to be independent from the various conditions studied in these projects (84). The mechanisms underlying this pro-inflammatory activity of IL-10 are currently unknown. Strikingly, the immense body of knowledge about the role of IL-10 in inflammation belies the comparatively small amount that is known about the implications of mutation of *Il10* and the dysregulation of IL-10 in the aberrant lung development, and especially in BPD. Several studies have confirmed a link between the high IL-10 producer-1082 G allele and moderate protection from BPD (33), (181), but in the vast majority of studies, variance in IL-10 levels is reported as an indirect risk predictor for BPD and other diseases, as well as a readout element for experiments involving treatments with other potential therapeutics (42, 96, 58, 187). Most recently, a paper by Kalymbetova and colleagues (72) has expanded on the known roles of resident macrophages in the hyperoxia-based mouse model of BPD, to include that of key mediators of arrested alveolarization; however, although the vast majority of lung inflammation and disease studies consider expression levels and the dynamics of IL-10 activity, to date no studies have been undertaken to elucidate the direct impact of IL-10 in normal and aberrant lung development.

8 Hypothesis and aims of the study

The cytokine IL-10 is the keystone of the anti-inflammatory immune response, ensuring effective protection of the host against excess responses to external insults and pathogens. Although the mechanisms of action of this molecule are well understood and reporting expression levels and efficacy of IL-10 are often key in the readout of inflammation studies, viability as a therapeutic modality is unclear. Furthermore, truly little is known about the impact of IL-10 on postnatal lung development. It is therefore critical to elucidate its impact *in vivo*, in normal and aberrant lung development.

The aims of this study are the following:

1. To investigate the impact of IL-10 on lung morphology in normal and aberrant lung development.
2. To evaluate the impact of IL-10 on the cellular immune response, in regard to the relative abundance of specific leukocyte subsets, in normal and aberrant lung development.
3. To delineate the effects of IL-10 administration on the normal and aberrant lung development transcriptomes, with a focus on the critical early postnatal days.

9 Materials and Methods

9.1 Materials

9.1.1 Technical Equipment

The technical equipment employed in all experimental procedures is reported in table 1.

Table 1. Technical equipment.
The catalogue number is reported as stated on manufacturers' websites, or, if not provided, a double number sign (##) is reported.

Device	Company and Location	Catalogue ID
Design-Based Stereology		
Agar cutting mould	Made in house	##
Agar cubic mould	Made in house	##
Askina® Brauncel® cellulose swabs	B.Braun, Germany	9051015
Feather's Trimming Blade	Medical AG, Germany	No. 130, type S-35
Histobloc	Kulzer GmbH, Germany	64708995
Histoform Q Embedding Mould	Kulzer GmbH, Germany	12025
Macro Lens	Nikon Corporation, Japan	JAA637DA
Microtome	Leica, Germany	RM2255
Microtome Knife	Leica, Germany	14021604813
NanoZoomer-XR	Miltenyi biotec, Germany	C12000
Needles, G24	CML supply, USA	901-24-050
Enzyme-Linked Immunosorbent Assay		
CELLSTAR® 96 Well Plates	Greiner Bio-One GmbH, Germany	655180
Nanoquant Tecan Infinite® 200 Pro	Tecan Group Ltd., Switzerland	M200PRO
Digital SLR camera	Nikon Corporation, Japan	D5300
Experimental Animal Model of BPD		
Oxygen Chamber for Animal Cages	BioSpherix, Ltd., USA	##

Table 1, continued.

Oxygen Controller ProOx 110	BioSpherix, Ltd., USA	##
Flow cytometric analysis		
100 µm Cell Strainer	Greiner Bio-One GmbH, Germany	542000
40 µm Cell Strainer	Greiner Bio-One GmbH, Germany	542040
BD FACSARIA III	BD Biosciences, USA	##
GentleMACS™ Dissociator	Miltenyi biotec, Germany	130-093-235
LSRFortessa	BD Biosciences, USA	##
Mouse genotyping		
Mastercycler ep Gradient	Eppendorf, Germany	##
Immunoblotting		
Biorad PowerPac 200	Bio-Rad, USA	BP-200
Precellys® 24	VWR, USA	P000669-PR240-A
ImageQuant™ LAS 4000	GE Healthcare, USA	##
Mini-PROTEAN® Tetra Cell Casting Module	Bio-Rad, USA	1658024
Nanoquant Tecan Infinite® 200 Pro	Tecan Group Ltd., Switzerland	##
Refrigerated Microcentrifuge	VWR, USA	CT15RE
Transfer-blot® Turbo™ Transfer System	Bio-Rad, USA	1704150
Immunohistochemistry and confocal microscopy		
Laser Scanning Microscope	Zeiss, Germany	LSM 710
Microtome	Leica, Germany	CM3050S
Microtome Blades	Thermo Fisher Scientific, USA	MX35 ULTRA
Polymerase Chain Reaction (PCR)		
Royal Bio-Imaging System-Intas Gel iX Imager	Intas Biopharmaceuticals, India	##
Thermocycler	PeqLab, VWR, UK	4484073
White Light Transilluminator	UVP, LLC, Germany	TW-26

Table 1, continued.

Reverse transcription PCR		
MicroAmp™ Fast Optical 96-Well Reaction Plate, 0.1 mL	Thermo Fisher Scientific, USA	4346907
MicroAmp™ Optical Adhesive Film	Thermo Fisher Scientific, USA	4311971
NanoDrop One Microvolume UV Vis Spectrophotometer	Thermo Fisher Scientific, USA	ND-ONE-W
Precellys 24-Dual homogenizer	VWR, USA	P000669-PR240-A
QuantStudio™ 3 Real-Time PCR System	Thermo Fisher Scientific, USA	A28567
RNA sequencing		
LabChip Gx Touch 24	PerkinElmer, USA	CLS138162
NextSeq500 sequencing system	Illumina, USA	SY-415-1001

9.1.2 Reagents

The reagents and chemicals employed in all experimental procedures are reported in table 2.

Table 2. Reagents and chemicals.
The catalogue number is reported as stated on manufacturers' websites, or, if not provided, a double number sign (##) is reported.

Name	Company, Location	Catalogue ID
Design-based stereology		
Agar	Sigma-Aldrich, Germany	05039
Azure II	Sigma-Aldrich, Germany	861065
Glutaraldehyde 50%	Serva Electrophoresis GmbH, Germany	23116.02
Hepes Solution	Sigma-Aldrich, Germany	H0887
Methylene Bleu	Carl Roth Gmbh & Co. Kg, Germany	A514.1
m-Xylol	Carl Roth Gmbh & Co. Kg, Germany	3791.1
N,N-Dimethylformamide	Sigma-Aldrich, Germany	494488
Osmium Tetroxide	Carl Roth Gmbh & Co. Kg, Germany	8371.3
Paraformaldehyde	Sigma-Aldrich, Germany	P6148
Phosphate buffered saline, 1×	Sigma-Aldrich, Germany	D1408
Silica Gel	Carl Roth Gmbh & Co. Kg, Germany	P077.1
Sodium Cacodylate Trihydrate	Serva Electrophoresis GmbH, Germany	15540.03
Technovit® 3040 Powder, Yellow	Kulzer GmbH, Germany	64708806
Technovit® 7100	Kulzer GmbH, Germany	64709003
Technovit® Universal Liquid	Kulzer GmbH, Germany	66022678
Uranyl Acetate	Serva Electrophoresis GmbH, Germany	77870.02
Enzyme-linked immunosorbent assay		
Mouse IL-10 Quantikine ELISA kit	R&D Systems, USA	M1000B
Experimental animal model of BPD		
AccuStart™ II Mouse Genotyping Kit	Quantabio, USA	733-2236

Table 2, continued.

NARCOREN®	Merial GmbH, Hallbergmoos, Germany	##
RNaseZAP™	Sigma-Aldrich, Germany	R2020
Flow cytometric analysis		
Deoxyribonuclease I	Merck KGaA, Germany	260913
Dispase	Corning Incorporated, USA	354235
Dulbecco's Modified Eagle Medium	Thermo Fisher Scientific, USA	61965
Flow Cytometry Staining Buffer	Invitrogen, USA	00422226
Gamunex-C	Grifols, Spain	##
Penicillin-Streptomycin	Thermo Fisher Scientific, USA	15140122
Mouse genotyping		
Agarose NEEO Ultra-Quality	Carl Roth, Germany	2267
Ethidium bromide	Promega, USA	H5041
Immomix™	Bioline, UK	BIO-25020
Immunoblotting		
4× Laemmli Sample Buffer	Bio-Rad, USA	1610747
2-Mercaptoethanol	Sigma-Aldrich, Germany	M6250
Ammonium Sulphate	Sigma-Aldrich, Germany	A2939
Bovine Serum Albumin	Sigma-Aldrich, Germany	A3059
cOmplete™	Merck KGaA, Germany	11836170001
Glycine	Carl Roth Gmbh & Co. Kg, Germany	3187.3
Powdered Milk	Carl Roth Gmbh & Co. Kg, Germany	T145.5
Precision Plus Protein™ Dual Colour Standards	Bio-Rad, USA	1610374
Quick Start™ Bradford 1× Dye Reagent	Bio-Rad, USA	5000205
Restore™ PLUS Western Blot Stripping Buffer	Thermo Fisher Scientific, USA	46428
Radioimmunoprecipitation assay buffer	Sigma-Aldrich, Germany	R0278
Rotiphorese® 50x TAE Puffer	Carl Roth Gmbh & Co. Kg, Germany	CL86

Table 2, continued.

Rotiphorese® Gel 30 (37,5:1)	Carl Roth Gmbh & Co. Kg, Germany	3029.1
SDS Solution (10% w/v)	Promega, USA	V6553
Sodium Orthovanadate	Sigma-Aldrich, Germany	S6508
SuperSignal™ West Femto Maximum Sensitivity Substrate	Thermo Fisher Scientific, USA	34096
TEMED	Bio-Rad, USA	1610800
Trans-Blot® Turbo™ Mini Nitrocellulose Transfer Packs	Bio-Rad, USA	1704158
Immunohistochemistry and confocal microscopy		
4′,6-diamidino-2-phenylindole (DAPI)	Thermo Fisher Scientific, USA	D3571
Acetone, > 99.7% (v/v)	Carl Roth Gmbh & Co. Kg, Germany	CP40.2
Bovine serum albumin	Thermo Fisher Scientific, USA	11733046
Citric acid monohydrate	Sigma-Aldrich, Germany	C1909
Dako Pen	Agilent, USA	S2002
DePeX	Serva, Germany	18243.01
Ethanol ≥ 99.8 %	Carl Roth Gmbh & Co. Kg, Germany	K928.3
Fluoromount W	Serva Electrophoresis, Germany	21634
Paraformaldehyde	Sigma-Aldrich, Germany	P6148
ROTI®Histol	Carl Roth Gmbh & Co. Kg, Germany	6640.1
Tween® 20	Promega, Germany	H5152
Polymerase chain reaction (PCR)		
5× Green GoTaq® Flexi Buffer	Promega, USA	M891A
Agarose NEEO Ultra-Quality	Carl Roth Gmbh & Co. Kg, Germany	2267
dNTP Mix (10 mM)	Promega, USA	U1511
Ethidium Bromide Solution	Promega, USA	H5041
Extracta DNA Prep kit	Quantabio, USA	97065-350
GeneAmp™ 10× PCR Buffer	Thermo Fisher Scientific, USA	4379878

Table 2, continued.

GoTaq® Hot Start Polymerase (500 u)	Promega, USA	M5005
Magnesium Chloride (25 mM)	Promega, USA	A351
M-MLV Reverse Transcriptase	Thermo Fisher Scientific, USA	28025-021
Nuclease-Free Water	Thermo Fisher Scientific, USA	AM9930
Random Hexamers (50 µM)	Thermo Fisher Scientific, USA	N8080127
RNase Inhibitor	Applied Biosystems, USA	N8080119
Reverse transcription polymerase chain reaction (RT-PCR)		
miRNeasy® Mini kit	Qiagen, Germany	217004
Nuclease-Free Water	Thermo Fisher Scientific, USA	AM9930
Platinum™ SYBR™ Green qPCR SuperMix-UDG	Thermo Fisher Scientific, USA	11733046
RNA sequencing		
RNase-Free DNase Set	Qiagen, Germany	79254
VAHTS Stranded mRNA-seq Library Prep Kit	Vazyme, China	NR612

9.1.3 Software

All software used is reported in table 3.

Table 3. Software.
The catalogue number is reported as stated on manufacturers' websites, or, if not provided, a double number sign (##) is reported.

Name	Company
Camera Control Pro 2	Nikon Corporation, Japan
DIVA software	BD Biosciences, USA
Flexiware 8	SCIREQ, Canada
GraphPad Prism 7.0	GraphPad Software, USA
ImageJ	NIH, USA
ImageQuant LAS 4000	GE Healthcare, United Kingdom
IntasGelCaptureEntry	Intas Biopharmaceuticals, India
Magellan	Tecan, Switzerland
Microsoft Office	Microsoft, USA
NDP.scan	Hamamatsu Photonics, Japan
NDP.view2	Hamamatsu Photonics, Japan
StepOne™ and StepOnePlus™ Software v2.3	Thermo Fisher Scientific, USA
Visiopharm's newCAST™	Visiopharm A/S, Denmark
ZEN 3.1 Blue Edition	Zeiss, Germany

9.2 Methods

9.2.1 Mouse treatments and experimental animal procedures

9.2.1.1 C57BL/6J wild type mice

C57BL/6J wild type mice (*Mus musculus*) were purchased from vendors Charles River Laboratories, USA and Janvier Labs, France.

9.2.1.2 Hyperoxia-based mouse model of bronchopulmonary dysplasia

Newborn mouse pups were randomized to equal litter size per nursing dam, placed into oxygen chambers and exposed to normoxia or hyperoxia conditions within the first 4 hours of birth from P1 to P14 (115). Oxygen was maintained at constant concentrations using an automated oxygen control system and it was monitored daily. Mice were maintained on a 12:12 hours dark:light cycle and provided with food and water *ad libitum*. To limit oxygen toxicity, nursing dams were rotated every 24 h (39). Newborn mouse lungs were collected at P1, P2 and P3, representative of early developmental stages preceding peak bulk secondary septation; at P5, representative of peak bulk secondary septation; or at P14, representative of the ending stage of secondary septation (129, 150). Newborn mouse pups were killed by pentobarbital overdose via intraperitoneal (IP) injection.

9.2.1.3 C57BL/6J.129P2-*Il10*^{tm1Cgn} mice

C57BL/6J.129P2-*Il10*^{tm1Cgn} global IL-10 knockout (henceforth referred to as IL-10 KO) mice were kindly donated by doctor André Bleich, from the Medizinische Hochschule Hannover. The generation of this mouse strain was described elsewhere by Kühn and coworkers (79). Mice were bred under specific pathogen free conditions to minimize the incidence of colitis. Tail biopsies were collected from newborn mice and genomic DNA was isolated using the AccuStart™ II Mouse Genotyping Kit. Wild type and mutant alleles were determined by PCR, screening for the IL-10, targeted mutation 1, University of Cologne (79) mutation. Amplicons were resolved in a 1.5% agarose gel prepared in Tris-acetate-EDTA (TAE) buffer and visualized by ethidium bromide. The amplification reagents, primers and the PCR cycling conditions, as provided by the donor lab, are listed respectively in Table 4, Table 5, and Table 6. Representative figures of the PCR amplification of genomic DNA and of the steady-state levels of *Il10* mRNA in wild type and C57BL/6J.129P2-*Il10*^{tm1Cgn} mice are reported respectively in Figure 6 and Figure 7.

Table 4. Reagents employed for C57BL/6J.129P2-Il10^{tm1Cgn} mouse strain genomic DNA amplification.

Component	Volume (µl)
Nuclease-free H_2O	16.5
Immomix™	5
Wild type forward primer	0.5
Common reverse primer	0.5
Mutant forward primer	0.5
Genomic DNA	2
Total	25

Table 5. List of primers employed for C57BL/6J.129P2-Il10^{tm1Cgn} mouse strain genomic DNA amplification.

Primer	Sequence (5′ - 3′)
Wild type forward	GCCTTCAGTATAAAAGGGGGACC
Reverse common	GTGGGTGCAGTTATTGTCTTCCCG
Mutant forward	CCTGCGTGCAATCCATCTTG

Table 6. PCR cycling conditions for C57BL/6J.129P2-Il10tm1Cgn mouse strain genomic DNA amplification.

Step	Reaction		Temperature	Time
1	Denaturation		94 °C	30 s
2	Denaturation	35×	94 °C	30 s
3	Annealing		55 °C	1 min
4	Extension		68 °C	1 min
5	Final Elongation		68 °C	5 min
6	Storage		4 °C	∞

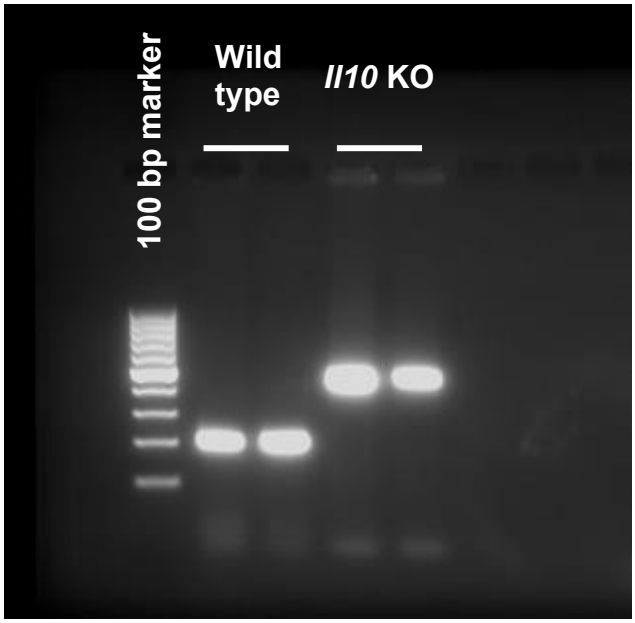

Figure 6. Polymerase chain reaction amplification of genomic DNA isolated from tail biopsies of wild type and C57BL/6J.129P2-*Il10*^{tm1Cgn} mice.
Tail biopsies were collected from wild type and C57BL/6J.129P2-Il10^{tm1Cgn} (*Il10* KO) mice at P14. Amplicons were resolved on 2% agarose gel and visualized by ethidium bromide. Bp, base pairs; KO, knockout.

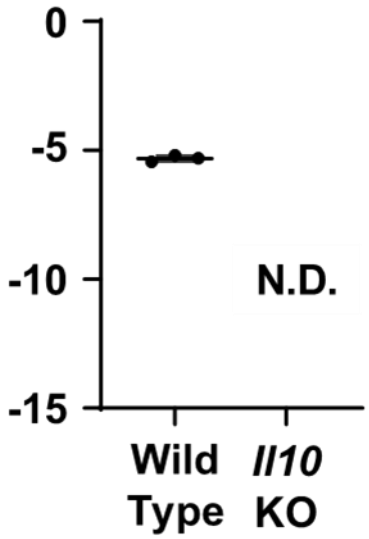

Figure 7. Steady-state levels of *Il10* in wild type and C57BI/6J.129P2-*Il10*^{tm1Cgn} mice.
Steady-state messenger RNA levels for *Il10* were assessed by real-time reverse transcriptase-polymerase chain reaction in total RNA pools isolated from the lungs of wild type and C57BI/6J.129P2-Il10^{tm1Cgn} (*Il10* KO) mouse pups at P14. Data represent mean ± SD. IL, interleukin; KO, knockout; N.D., not detected.

9.2.1.4 Interleukin-10 administration

On P1, mouse pups were randomized to generate litters of equal size per nursing dam and administered via intraperitoneal (IP) injections, daily, between P1 and P14, or on P1, or on P3, 50, 100 or 150 µg/kg recombinant mouse IL-10 protein, diluted in sterile phosphate-buffered saline (PBS). Vehicle PBS was injected as control. Experimental animals were exposed from P1 to normoxia or hyperoxia and sacrificed at P14.

9.2.2 Total RNA isolation

Total RNA was isolated from mouse lungs using the miRNeasy® Mini kit. A fraction of the lung was placed into 2 ml tubes containing ceramic beads and homogenized using a Precellys 24-Dual homogenizer. Total RNA from lung tissue was resuspended in 50 µl nuclease-free water.

9.2.3 Gene expression analysis

The concentration of total RNA was determined using a NanoDrop One Microvolume UV-Vis Spectrophotometer. For messenger RNA (mRNA) analysis, 1000 ng of total RNA were diluted in 20 µl of nuclease-free water and denatured via heating for 10 minutes at 70 °C in a thermocycler. The mRNA was then retrotranscribed into complementary DNA by using the components listed in Table 7.

Table 7. Components used to retrotranscribe messenger RNA into complementary DNA for gene expression analysis.
Steps, reactions, temperature, and the reaction time for one sample are as previously established (2).

Component	Volume (µl)
Nuclease-free H_2O	1
GeneAmp™ 10× PCR Buffer	4
Magnesium chloride Solution (25 mM)	8
dNTP Mix (10 mM)	2
Random Hexamers (50 µM)	2
RNase Inhibitor (20 U/µl)	1
M-MLV Reverse Transcriptase (50 U)	2
RNA (1,000 ng/µl)	20
Total	40

Abbreviations: dNTP, deoxynucleotide triphosphates; M-MLV, Moloney Murine Leukaemia Virus.

Table 8. Protocol employed to retrotranscribe messenger RNA into complementary DNA for gene expression analysis.
The steps, the reactions, the temperature, and the reaction time for one sample were previously established in our laboratory (2).

Step	Reaction	Temperature	Time
1	Incubation	21 °C	10 min
2	Extension	43 °C	75 min
3	Enzyme inactivation	95 °C	5 min
4	Storage	4 °C	∞

The reaction was performed according to the protocol listed in Table 8. At the end of the procedure, the complementary DNA was diluted in 60 µl nuclease-free water. The amplification was carried out using Platinum™ SYBR™ Green qPCR SuperMix-UDG reagents in a QuantStudio™ 3 Real-Time PCR System**.** The cycling protocol used in all experiments is reported in Table 9.

Table 9. RT-PCR cycling protocol.
The steps, the reactions, the temperature, and the reaction time for one sample were previously established in our laboratory (2).

Step	Reaction		Temperature	Time
1	Denaturation		95 °C	5 min
2	Denaturation	40x	95 °C	5 s
3	Annealing		59 °C	5 s
4	Extension		72 °C	30 s
5	Final Extension		72 °C	15 min
6	Melting Curve Analysis			30 min
7	Storage		4 °C	∞

Changes in the difference between cycle thresholds were defined as a technical replicate mean of $Ct_{(reference\ gene)} - Ct_{(gene\ of\ interest)}$, with the *Polr2a* gene used as the reference gene. Primers were purchased from Eurofins Scientific. The primer pairs were designed intron-spanning and were experimentally validated. The primers and the primer sequences employed in in the mRNA analysis are listed in Table 10.

Table 10. List of primers used for mRNA analysis.

Gene	Forward (5′ - 3′)	Reverse (5′ - 3′)
Il10	TCAAGGATGCACATCAAAAGGC	AGGCAGCAACTTCCTCCCT
Il10ra	CCCATTCCTCGTCACGATCTC	TCAGACTGGTTTGGGATAGGTTT
Il10rb	ACCTGCTTTCCCCAAAACGAA	TGAGAGAAGTCGCACTGAGTC
Ifng	ATGAACGCTACACACTGCATC	CCATCCTTTTGCCAGTTCCTC
Tnf	CCCTCACACTCAGATCATCTTCT	GCTACGACGTGGGCTACAG
Tnfrsf1b	ACACCCTACAAACCGGAACC	AGCCTTCCTGTCATAGTATTCCT
Polr2a	CTAAGGGGCAGCCAAAGAAAC	CCATTCAGCATACAACTCTAGGC

9.2.4 Total protein isolation

Whole-lung protein content was isolated from mouse lungs using a protein lysis buffer (1 mM sodium orthovanadate and 1mM cOmplete™, Mini, EDTA-free Protease Inhibitor Cocktail dissolved in 1 ml radioimmunoprecipitation assay buffer). A fraction of the lung was placed into 2 ml tubes containing ceramic beads and homogenized using a Precellys 24-Dual homogenizer. Lung lysates were placed on ice for 10 min, transferred into a 1.5 ml tube and centrifuged at 13,000 rpm for 15 min using a refrigerated microcentrifuge at 4°C. The supernatant was then transferred in a new tube. In order to measure protein concentration, a Bradford assay was performed on the lysates. The samples and an aliquot of the lysis buffer were diluted 1:50 in water, and 10 µl per well were pipetted in a 96 well plate. Serial dilutions of bovine serum albumin (BSA), containing 0.05 µg, 0.1 µg, 0.2 µg, 0.3 µg, 0.4 µg and 0.5 µg of protein, were used for the generation of a standard curve. An equal volume of 10 µl of these dilutions were added to the 96 well plate. For the assay, 200 µl of Quick Start™ Bradford 1× Dye Reagent were added to each well in use, incubated for 5 min at room temperature and read by an Infinite® 200 PRO spectrophotometer at a 570 nm wavelength. The protein concentration from each sample was calculated by optical density extrapolation from the BSA standard curve created as reference, using the Magellan software.

9.2.5 Enzyme-linked immunosorbent assay

The assay was performed exactly as specified by manufacturer instructions. All reagents included in the Mouse IL-10 Quantikine ELISA kit were brought to room temperature and standards and controls were prepared fresh from kit stocks. An aliquot of whole lung protein extract was diluted to reach a working concentration of 500 pg/ml**.** Kit plates were populated as for instructions with duplicates of the standards necessary to generate a standard curve, the provided control protein, and the experimental samples, then left in incubation for 2 h at room temperature in light agitation. Each well was then aspirated and washed 4× with 400 µl of proprietary Wash Buffer; the plate was then inverted and blotted against a paper towel. 100 µl of proprietary Mouse IL-10 Conjugate was added to each well and incubated for 2 h at room temperature in light agitation. Each well was aspirated and washed 4× with 400 µl of proprietary Wash Buffer, then the plate was inverted and blotted against a paper towel. Then, 100 µl of proprietary Substrate Solution was then added to each well and incubated for 30 min in the dark at room temperature, followed by the addition of 100 µl of proprietary Stop Solution. The optical density of each well was then determined using an Infinite® 200 PRO spectrophotometer set at a wavelength of 450 nm, with a correction wavelength set at 540 nm,

and concentration values were calculated by extrapolation from the reference standard curve using the Magellan software.

9.2.6 Immunoblotting

35 µg of total lung lysate from each sample were mixed with 4× Laemmli sample buffer containing 5% β-mercaptoethanol. Proteins were denatured for 10 minutes on 95°C, loaded on a 10% sodium dodecyl sulfate (SDS) polyacrylamide gel and resolved by running at 100 mV in running buffer. When the visible part of the sample reached the bottom of the resolving gel, the gel was removed from the running cassette and the resolved proteins were transferred to a nitrocellulose membrane using the Trans-Blot Turbo Transfer System kit. The membrane was washed for 2 min in double-distilled water and incubated for 1 h in a solution of 5% (m/v) milk powder and 0.1% (v/v) Tween ™ 20 diluted in PBS, as blocking buffer. The membrane was then incubated overnight with the appropriate primary antibody, diluted in the same blocking buffer, at 4 °C. The membrane was subsequently washed in fresh washing buffer for 6× 5 min and incubated for 1 h at room temperature in the appropriate horseradish peroxidase-conjugated secondary antibody, diluted in blocking buffer. The membrane was then washed in washing buffer for 6× 5 min, and finally incubated in SuperSignal® West Femto chemiluminescent substrate for 5 min at room temperature. The protein bands were visualized using an ImageQuant LAS 4000 instrument. Gel and buffer preparation for western blot are listed in Table 11. The primary and secondary antibodies used in western blot analysis are respectively listed in Table 12 and Table 13.

Table 11. Gel and buffer preparation for western blot.

Stacking Gel	Resolving Gel
5% Rotiphorese® Gel 30 (37,5:1) 125 mM Tris-Cl, pH=6.8 0.05% SDS 0.05% Ammonium Sulphate 0.065% TEMED	10% Rotiphorese® Gel 30 (37,5:1) 375 mM Tris-Cl, pH=8.8 0.05% SDS 0.05% Ammonium Sulphate 0.065% TEMED
Running Buffer	Blocking Buffer
250 mM Tris-Cl 2.5 M Glycine 1% SDS	1× PBS 0.2% Tween® 20 5% Powdered Milk
Washing Buffer	
1× PBS 0.2% Tween® 20	

Abbreviations: PBS, phosphate buffered saline; SDS, sodium dodecyl sulphate; TEMED, N,N,N',N'-tetramethyl ethylenediamine.

Table 12. Primary antibodies used in immunoblotting procedures.

Target	Host	Dilution	Catalogue Number	Company
IL-10	Mouse	1:1,000	sc-8438	Santa Cruz Biotechnology, USA
β-Actin	Rabbit	1:3,000	4967	Cell Signaling Technology, USA

Abbreviations: IL, interleukin.

Table 13. Secondary antibodies used in immunoblotting procedures.

Target	Host	Dilution	Catalogue Number	Company
Rabbit IgG	Goat	1:3,000	32460	Thermo Fisher Scientific, USA
Mouse IgG	Goat	1:3,000	32430	Thermo Fisher Scientific, USA

9.2.7 Design-based stereology

The architecture of the lung was analysed through design-based stereology, performed following the recommendations laid out by the American Thoracic Society and the European Respiratory Society (62). Newborn mouse pups were sacrificed at P14 and lungs were fixed by instillation of fixative through intratracheal cannulation with a blunt needle, gauge 24. A hydrostatic pressure of 20 cmH_2O was maintained on the fixative at all times. The fixative was composed of 1.5% (w/v) paraformaldehyde (PFA), 1.5% (w/v) glutaraldehyde 50% and 150 mM Hepes solution, in PBS, pH 7.4. The lungs were isolated intact, together with thymus, oesophagus, trachea, and heart and fixed for 24 h at 4 °C. Thymus, oesophagus, trachea, and heart were then carefully removed. At the end of the fixation period, excess moisture on the lungs was delicately absorbed by dabbing dry with cellulose swabs. Once dried, lungs were carefully embedded in 2% agar as per random uniform sampling methodology protocols (64, 152) and cut in 3 mm sections. Sections were laid on graph paper and pictures of each section was taken in the same orientation using a professional photographing camera. An estimate of lung volume was then obtained by analysing these pictures through the Cavalieri principle, using the ImageJ software (102). The lung pieces were removed from the agar embedding and placed into a glass vial, under a fume hood, for the plastic embedding procedure. Briefly, the lung pieces were washed 4× 5 min, with a solution of 0.1 M sodium cacodylate trihydrate, and then incubated in 1% (w/v) osmium tetroxide for 2 h. Lungs were washed again 4× 5 min, repeated 4 times, with a solution of 0.1 M sodium cacodylate trihydrate, then washed with double-distilled water, repeated 8 times, and incubated with 2.5% (w/v) uranyl acetate overnight. Lungs were then washed with double-distilled water 4× 5 min, and dehydrated by immersion 2× 1 h, in 70% acetone, 2× 1 h, in 90% acetone and for 1 h in 100% acetone. Lungs were subsequently kept overnight in an infiltration solution made of equal parts 1:1 100% acetone:glycol methacrylate and Hardener 1 (Technovit® 7100). The lungs were then incubated in pure Technovit® 7100 overnight. Afterwards, the solution was drained and replaced with an infiltration solution composed of a mix of 3 ml of fresh Technovit® 7100 and 200 µl of Hardener 2. Samples in this solution were kept in agitation for 3 minutes, removed from the solution and placed into the embedding mould. After 2 min, an appropriate amount of infiltration solution composed of Technovit and Hardener 2, fresh from agitation, was poured over the samples into the embedding moulds, until fully immersed. Embedded lungs were kept in the fume hood for 48 h to allow the glycol methacrylate to fully solidify. Cutting supports were then placed over each lung and an appropriate amount of a mixture composed of 10 g of

Technovit® 3040 Powder and 5 ml of Technovit® Universal Liquid was poured slowly between each support and embedded lung and left to solidify for a minimum of 4 h. Every block was subsequently sectioned using a microtome. To determine the total number of alveoli and the alveolar density, a series of sections 2 μm thick were cut from the lung block. Every first and third section of a consecutive series was placed on a glass slide and used for analysis through the physical disector approach (64, 164). All additional parameters included in the analysis, namely mean linear intercept (MLI), arithmetic mean septal thickness and total surface area of gas exchange, were derived by the analysis of 4 sections per block, from which every tenth cut section was picked (92, 94, 105, 108-110, 120, 152). Sections on glass slides were stained with Richardson stain (132) and scanned using a digital slide scanner. The analysis was assessed using the Visiopharm newCAST™ computer-assisted stereology system (Figure 8). Septal thickness, MLI, total surface area of gas exchange, as well as alveolar number and alveolar density, were estimated as described by our group (92, 105). For each parameter, 3-10% of each section was analysed. The coefficient of error (CE) and the coefficient of variation (CV) were measured for each stereological parameter. A quotient threshold of 0.5 was set to validate the precision of the measurements.

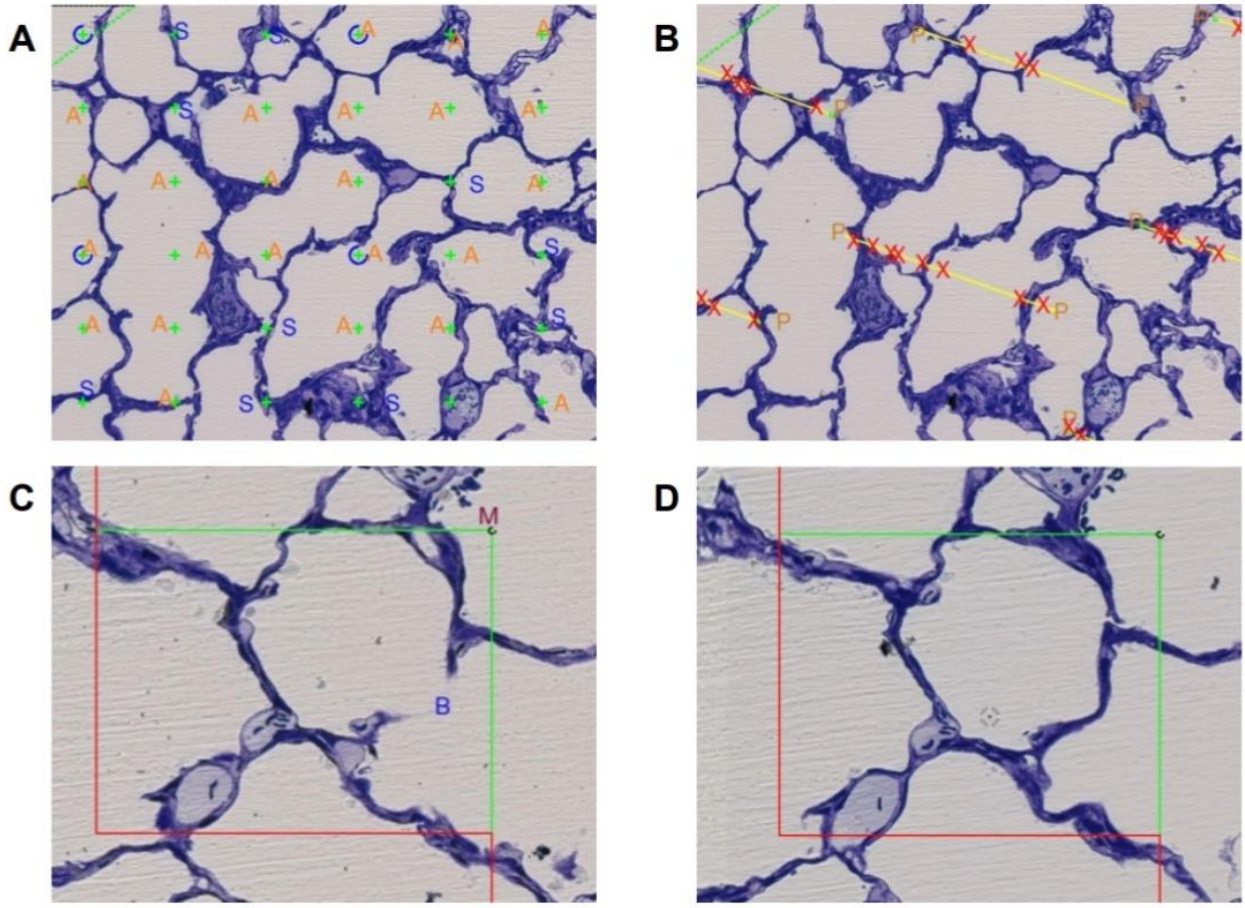

Figure 8. Design-based stereology employed for lung morphology measurements.
Representative pictures of the computer-based analysis performed through the Visiopharm ® software. (A) Air spaces and septa are differentiated by marking points falling in the alveolar space with an A, and on a septum with a B. (B) A grid composed of evenly spaced lines superimposed to the image allows for the assessment of surface area density, by marking each crossing point through a septum (X) and whenever one of the line extremities falls into parenchyma (P). In order to quantify the number of alveoli in the lung, physical disector images were compared to identify instances in which an alveolus appears to be in an "open" (C) state, *versus* a "closed" (D) state. B marks the "bridge" formed between two septa "closing" the alveolus and is counted as a single event. Every random counting field visualized by the software is shared by the disected images and counted only once (M).

9.2.8 Flow cytometric analysis of select immune cell populations in the lungs

Multicolour flow cytometric analysis was performed with an LSR Fortessa flow cytometer, using DIVA software. Lungs from P14 wild type mice injected with PBS or IL-10 at P1 or P3 and exposed to normoxia or hyperoxia from P1 to P14 were prepared by instilling approximately 300 µl of dispase, followed by incubation for 30 min at 37 °C. Lungs were then immersed in Dulbecco's Modified Eagle Medium containing 10 mM Hepes, 1% (v/v) penicillin-streptomycin and 0.01% deoxyribonuclease I from bovine pancreas, and homogenized using a gentleMACS™ dissociator. The homogenates were filtered using a 100 µm and a 40 µm cell strainer. The filtered lung cell suspension was then washed with PBS and

centrifuged at 1,300 g for 15 min at 4 °C. The pellet was then resuspended in flow cytometry staining buffer containing 10% Gamunex-C and incubated with the appropriate fluorochrome-labelled antibodies (see protocols in sections 8.2.8.1 and 8.2.8.2) for 20 min at 4 °C. Cells were then washed between staining steps with Flow Cytometry Staining Buffer and stained 10 min before analysis with 7-amino-actinomycin D (7-AAD) for dead cells exclusion. 100,000 events per lung cell suspension were set as the counting-stop setting, and absolute cell numbers are presented. Data analysis was performed with Prism 8 software.

9.2.8.1 T cell staining protocol and gating strategy

The staining protocol and the gating strategy employed for all flow cytometry experiments on T cells are reported respectively in Table 14 and Figure 9.

Table 14. Antibodies used for T cell staining.

Cell type	Target	Fluorochrome	Clone	Company
-	Dead cells	7-AAD	-	Thermo Fisher Scientific
Leukocytes	CD45	APC-Cy7	30F11	BD Biosciences, USA
T cells	CD3	APC	145-2C11	BioLegend, USA
Cytotoxic T cells	CD8a	PE-Cy7	53-6.7	BioLegend, USA
Helper T cells	CD4	FITC	GK 1.5	BioLegend, USA
Regulatory T cells	CD25	Pacific Blue	PC61	BioLegend, USA

Abbreviations: 7-AAD, 7-amino-actinomycin D; APC, allophycocyanin; CD, cluster of differentiation; Cy7, cyanine 7; FITC, fluorescein isothiocyanate; PE, phycoerythrin.

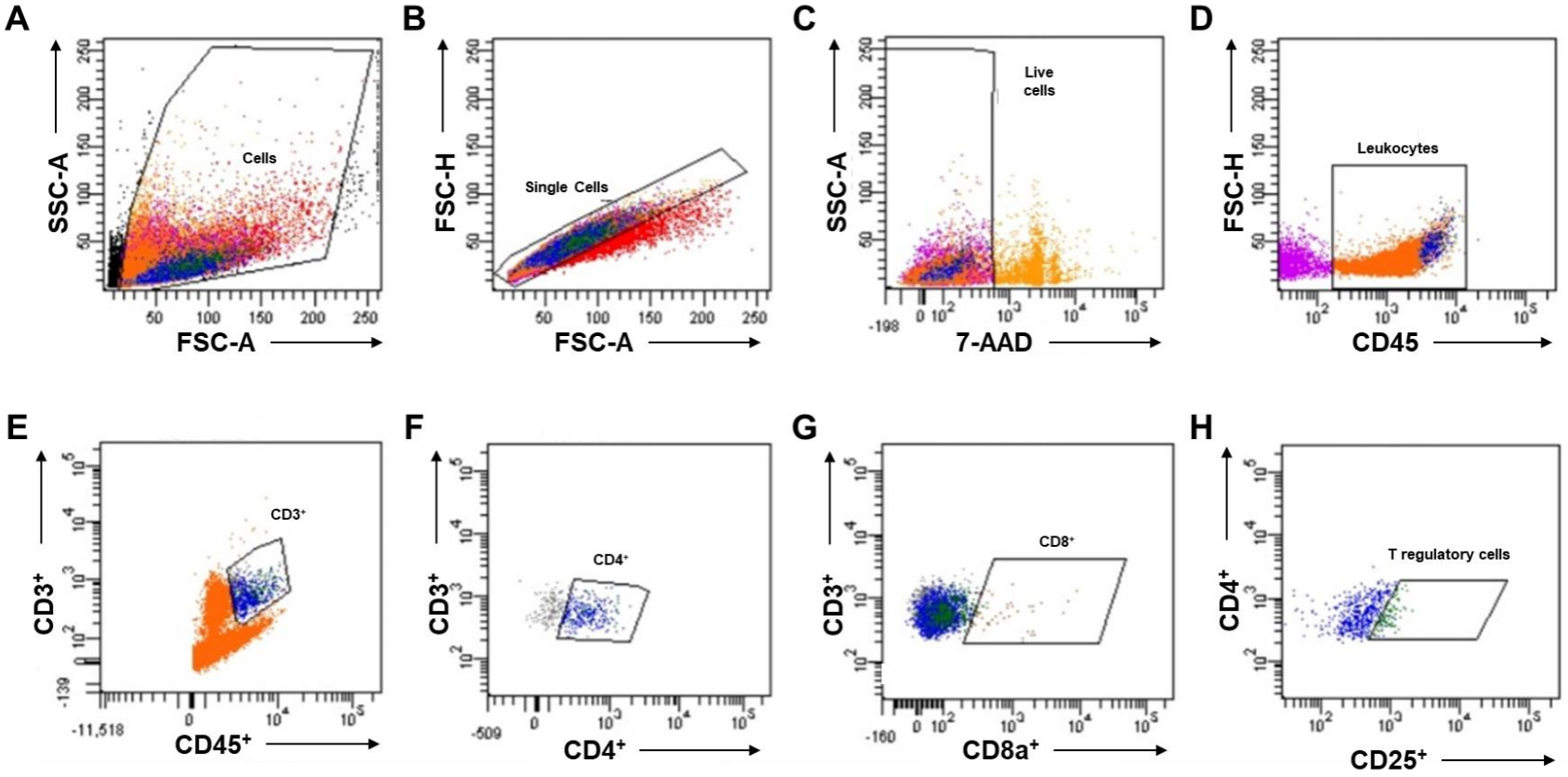

Figure 9. Gating strategy for fluorescence-activated cell sorting of adaptive immunity cells in whole lung tissue lysates.
Representative dot plots of multicolour-stained cells isolated from lung homogenates obtained from P14 mice. Panels A to E illustrate the gating progression from total input gating to $CD3^+$ cells gating; panels F and G were gated on panel E, while panel H was gated on panel F. Alive leukocytes ($7\text{-}AAD^-$ $CD45^+$ cells) were differentiated according to CD3, CD8, CD4 and CD25 expression. $CD3^+$ $CD45^+$ cells represent T cells, $CD3^+$ $CD4^+$ represent $CD4^+$ cells, $CD3^+$ $CD8a^+$ cells represent $CD8^+$ cells, CD4+ $CD25^+$ cells represent T regulatory cells. 7-AAD, 7-Aminoactinomycin D; CD3, cluster of differentiation 3; CD4, cluster of differentiation 4; CD8a, cluster of differentiation 8a; CD25, Interleukin-2 receptor alpha chain; CD45, Protein tyrosine phosphatase, receptor type, C; FSC-A, forward scatter area; FSC-H, forward scatter height; SSC-A, side scatter area.

9.2.8.2 Innate immunity staining protocol and gating strategy

The staining protocol and the gating strategy employed for all flow cytometry experiments on T cells are reported in Table 15 and Figure 10.

Table 15. Innate immune cells staining protocol.

Cell type	Target	Fluorochrome	Clone	Company
Leukocytes	CD45	APC-Cy7	30F11	BD Biosciences, USA
Macrophages	CD206	APC	C068C2	BioLegend, USA
Monocytes	Ly-6C	FITC	HK1.4	BioLegend, USA
Neutrophils	CD24	PE-Cy7	M1/69	BioLegend, USA
Tissue-resident macrophages	CD11b	Pacific Blue	M1/70	BioLegend, USA

Abbreviations: APC, allophycocyanin; CD, cluster of differentiation; Cy7, cyanine 7; FITC, fluorescein isothiocyanate; Ly-6C, lymphocyte antigen 6 complex, locus C; PE, phycoerythrin.

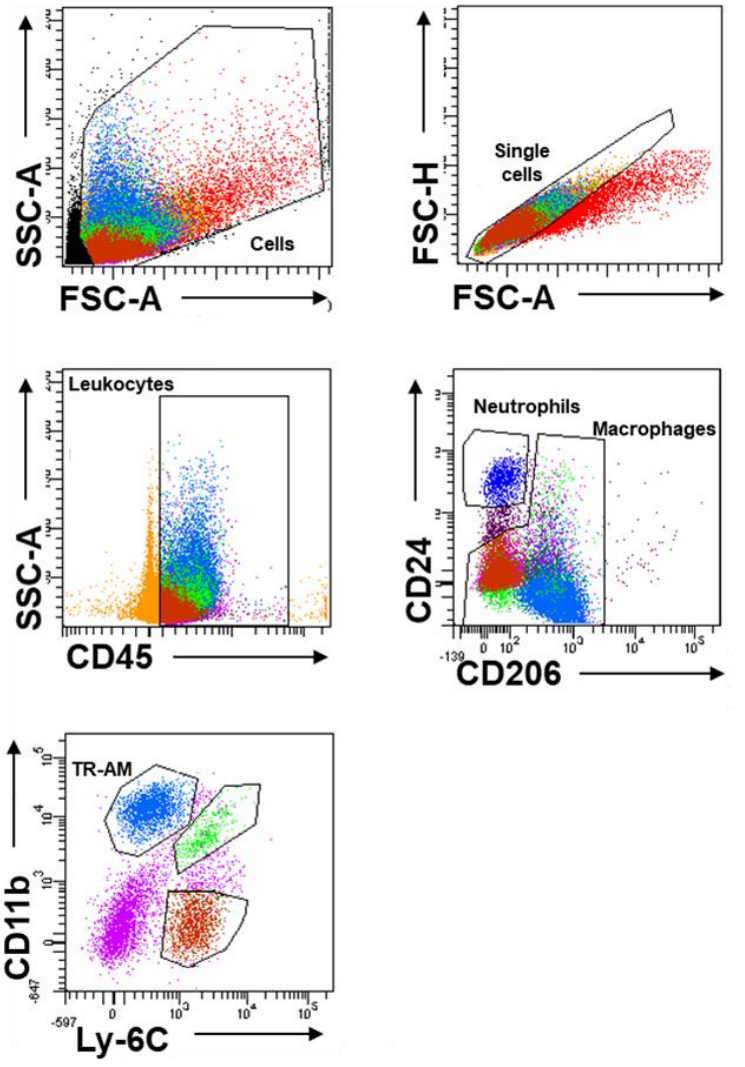

Figure 10. Gating strategy for fluorescence-activated cell sorting of innate immunity cells in whole lung tissue lysates.
Representative dot plots of multicolour-stained cells isolated from lung homogenates obtained from P14 mice. Leukocytes ($CD45^+$ cells) were differentiated according to CD11b, CD24, CD206 and Ly-6C expression. $CD24^+CD206^-$ cells represent neutrophils, $CD24^-CD206^+$ represent macrophages, $CD11b^+$ $Ly\text{-}6C^-$ cells represent tissue-resident macrophages. CD, cluster of differentiation; FSC-A, forward scatter area; FSC-H, forward scatter height; Ly-6C, lymphocyte antigen 6 complex, locus C; SSC-A, side scatter area; TR-AM, tissue-resident alveolar macrophages.

9.2.9 Immunohistochemistry and confocal microscopy

9.2.9.1 Lung isolation, fixation and embedding in paraffin

Mouse pups were sacrificed at P14. The lungs were perfused transcardially with PBS and instilled with 4% PFA at a constant pressure of 20 mmH_2O. Lungs were dissected out of the thoracic cavity, fixed overnight at 4 °C in 4% PFA and then dehydrated through sequential immersions in 100%, 96% and 70% ethanol. Lungs were then embedded in paraffin and 5 µm sections were cut and mounted on glass slides.

9.2.9.2 Immunohistochemistry

Slides were heated at 60 °C for 1 h to melt paraffin, then dewaxed by immersion in ROTI®Histol 3× 10 min. Slides then underwent rehydration via immersion in ethanol at progressively higher dilutions: 2× 5 min, in 100% ethanol; 5 min in 96% ethanol; 5 min in 70% ethanol. Sections were then washed for 5 min in PBS in light agitation and boiled for 20 min in citrate buffer [0.21% (m/v) citric acid monohydrate, 0.05% Tween™ 20 (v/v) at pH 6]. After cooling, slides were washed for 5 min in PBS in light agitation and sections were encircled in a hydrophobic layer using a Dako Pen, before blocking with 5% (m/v) BSA for 1 h. After washing for 5 min in PBS in light agitation, sections were incubated overnight with the appropriate primary antibodies (see Table 16 below). After washing in light agitation 6× 5 min in PBS, slides were incubated for 1 h at room temperature with the appropriate secondary antibodies (see Table 17 below). After washing in light agitation 6× 5 min, in PBS, sections were counterstained for 5 min in 4',6-diamidino-2-phenylindole (DAPI) diluted 1:1,000 in PBS. Slides were mounted with DePeX and covered with a cover glass. Images were taken using a laser scanning microscope and analysed using the ZEN 3.1 Blue Edition software.

Table 16. Primary antibodies used in the immunohistochemistry stainings.

Target	Host	Dilution	Catalogue Number	Company
CD45	Rabbit	1:200	SAB4502541	Merck, Germany
EpCAM	Rabbit	1:800	42515S	Cell Signaling Technology, USA
IgG isotype control	Goat	1:100	403004	Biolegend, USA
IgG isotype control	Rabbit	1:100	401502	Biolegend, USA
Podoplanin	Goat	1:100	AF3244	R&D Systems, USA
Prosurfactant protein C	Rabbit	1:500	AB3786	Merck, Germany
Vimentin	Rabbit	1:500	GTX100619	GeneTex, USA

Abbreviations: CD, cluster of differentiation; EpCAM, Epithelial cell adhesion molecule.

Table 17. Secondary antibodies employed in the immunohistochemistry stainings.

Fluorophore	Host/Target	Dilution	Catalogue Number	Company
Alexa Fluor 647	Rabbit/Goat	1:500	A21446	Invitrogen, USA
Alexa Fluor 555	Goat/Rabbit	1:500	A21428	Invitrogen, USA
Alexa Fluor 488	Goat/Rabbit	1:500	A11008	Invitrogen, USA

9.2.10 RNA sequencing

For RNA sequence analysis, total RNA was isolated from P1, P2 and P3 mouse lungs using the miRNeasy® Mini kit combined with on-column DNase digestion to avoid contamination by genomic DNA. RNA and library preparation integrity were verified with LabChip Gx Touch 24. A total of 300 ng of RNA were used as input for VAHTS Stranded mRNA-seq Library preparation following the manufacturer's protocol. Sequencing was performed on a NextSeq500 sequencing system using v2 chemistry, resulting in an average of 39M reads per library with a 1x75 base pairs single end setup. The resulting raw reads were assessed for quality, adapter content and duplication rates with FastQC (7). Trimmomatic version 0.39 was employed to trim reads after a quality drop below a mean of Q20 in a window of five nucleotides (14). Only reads between 30 and 150 nucleotides were cleared for further analyses. Trimmed and filtered reads were aligned versus the Ensembl mouse genome version mm10 (GRCm38.p5) using STAR 2.6.1d with the parameter "--outFilterMismatchNoverLmax 0.1" to increase the maximum ratio of mismatches to mapped length to 10% (32). The number of reads aligning to genes was counted with featureCounts tool from the Subread package 1.6.5 (86). Only reads mapping at least partially inside exons were admitted and aggregated per gene. Reads overlapping multiple genes or aligning to multiple regions were excluded. Differentially expressed genes were identified using DESeq2 version 1.26.0 (90). Only genes with a minimum fold change of ± 2 (log2 = ±1), a maximum Benjamini-Hochberg corrected *P* value of 0.05, and a minimum combined mean of 5 reads were deemed to be significantly differentially expressed. The Ensemble annotation was enriched with UniProt data (release 06.06.2014) based on Ensembl gene identifiers (Activities at the Universal Protein Resource).

9.2.11 Statistical analysis

Statistics and graphs were performed using GraphPad Prism 8.0. Values are presented as mean ± SD. Differences between groups were evaluated by one-way ANOVA with Tukey's post hoc test, or by two-way ANOVA with Bonferroni's multiple comparisons test. Differences between two group comparisons were performed with an unpaired Student's t-test. The presence of outliers was verified by Grubbs' test. *P* values below 0.05 were considered as significant.

10 Results

10.1 Expression levels of IL-10 and IL-10 receptor in normal and aberrant lung development

Although low levels of IL-10 in ventilated infants have been reported to correlate with BPD (68), there is no information, to date, on the expression levels of *Il10* mRNA and the synthesis of IL-10 throughout late lung development. Expression levels of *Il10* mRNA, which codes for IL-10, and of *Ilra* and *Ilrb*, which respectively code for the subunit α and β of the IL-10 receptor (henceforth abbreviated as IL10R), have, therefore, been profiled in whole lung homogenates isolated from mice exposed to normoxia or hyperoxia to model BPD (115). Lung homogenates have been isolated from P3, P5 and P14 mouse pups, to chart levels respectively at the pre-, peak, and post-alveolarization phases of lung development. While no change was observed at P3, the steady-state levels of *Il10* deviate significantly between mice exposed to normoxia and hyperoxia at P5 and P14 (Figure 11), revealing a marked drop during the peak alveolarization phase, which is still present at the end of the whole alveolarization process. While the steady-state levels of *Il10ra* mRNA are significantly lower at high oxygen concentration at P3, the steady-state levels of the mRNAs coding for both dimers of IL10R are unchanged at P5 and are both significantly downregulated in mice exposed to normoxia at P14. To assess the steady-state levels of IL-10 protein abundance in the developing mouse lungs, whole lung protein lysates have been isolated from mouse pups exposed to normoxia and hyperoxia at P3, P5 and P14 and analysed by western blot (Figure 12A) and enzyme-linked immunosorbent assay (Figure 12B). IL-10 levels are starkly reduced in the lungs of mice exposed to hyperoxia, compared to mice exposed to normoxia, throughout the whole late lung development process. These data indicate that IL-10 levels are significantly reduced during the course of aberrant late lung development, and that such low levels are achieved from early on in the late lung development process. The expression levels of both IL-10 receptor subunits at P14 in mice exposed to hyperoxia, compared to those exposed to normoxia, are higher, suggesting that in the mouse model of BPD the activation of the IL-10 signalling cascade is not prevented by the inability of target cells to bind IL-10.

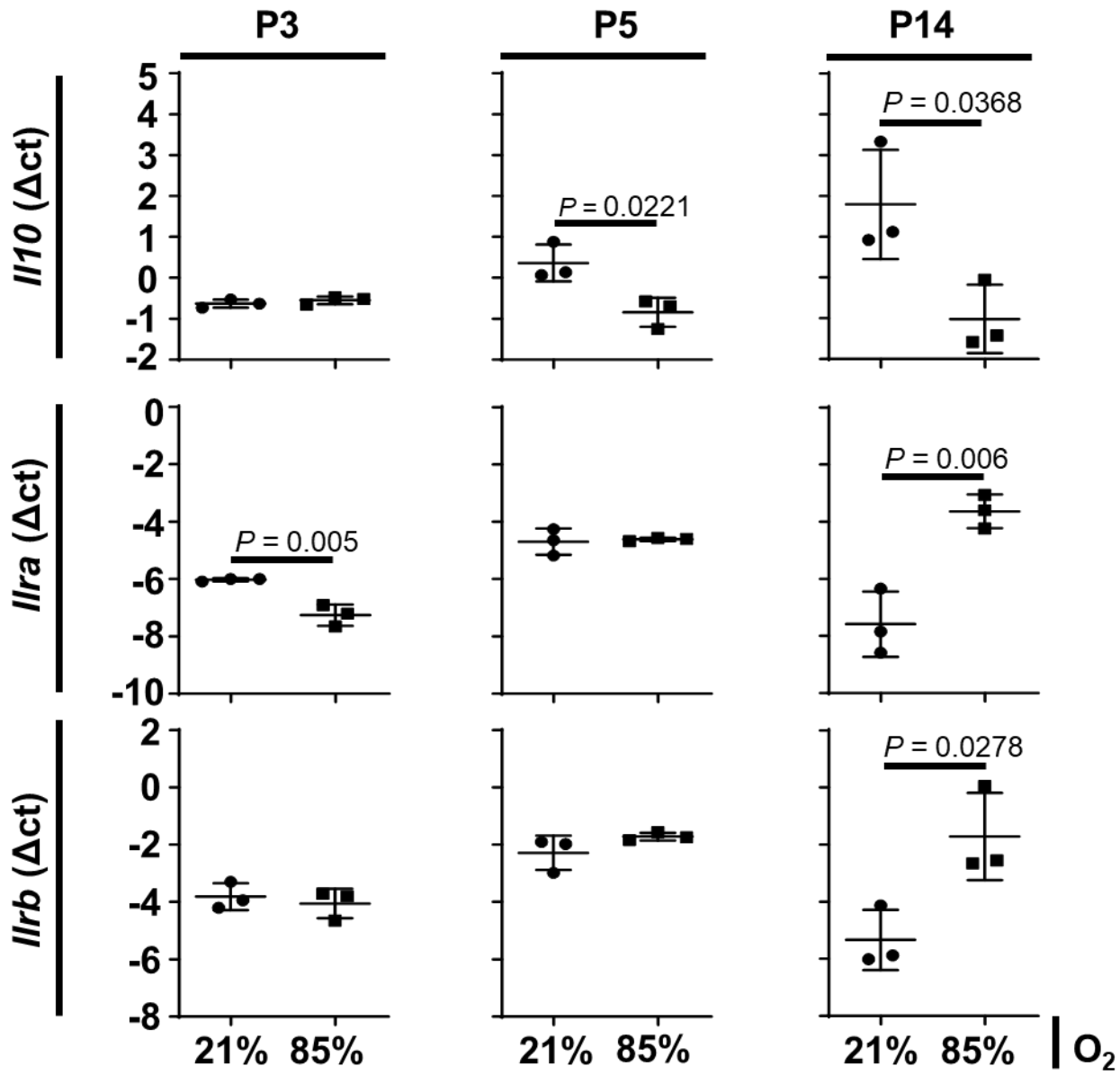

Figure 11. Assessment of steady-state mRNA levels of *Il10*, *Ilra* and *Ilrb* during lung development.
The steady-state mRNA levels for *Il10*, *Ilra* and *Ilrb* were assessed by real-time polymerase chain reaction in total RNA pools isolated from the lungs of mouse pups at P3, P5 and P14 that had been exposed to 21% O_2 or 85% O_2. Data represent mean ± SD. *P* values were determined by unpaired Student´s t-test (N=3). Only the statistical comparisons where $P < 0.05$ are presented.

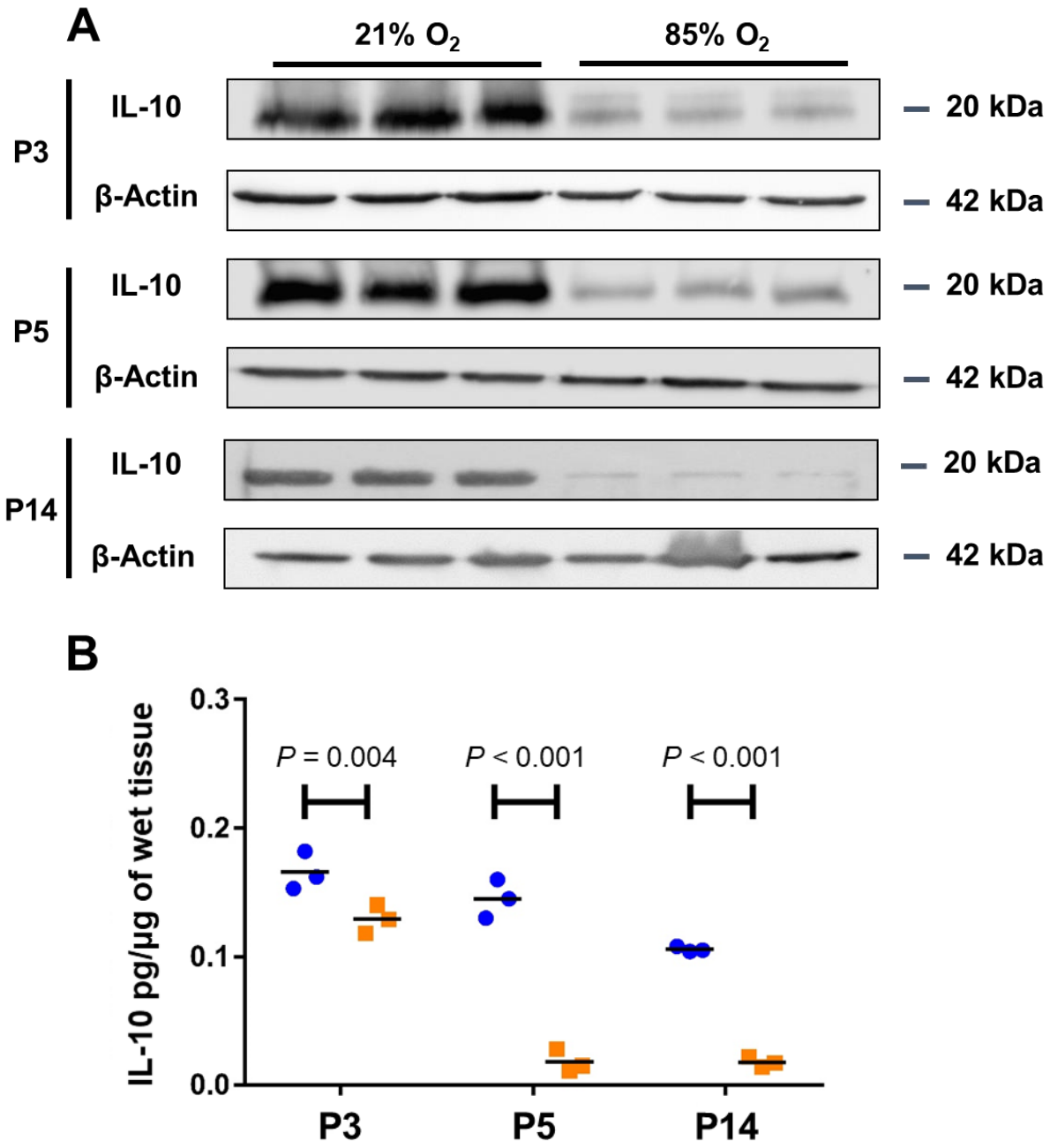

Figure 12. IL-10 protein expression in lung homogenates of mouse pups exposed to normoxia and hyperoxia.
(A) IL-10 protein levels were assessed by western blot in lung homogenates of P3, P5 and P14 mouse pups exposed to either normoxia or hyperoxia (N=3 animals per group). (B) IL-10 protein abundance was quantified by enzyme-linked immunosorbent assay in lung homogenates of P3, P5 and P14 mouse pups exposed to either normoxia or hyperoxia (N=3 animals per group). Data represents means ± SD. *P* values were determined by unpaired Student's *t*-test. Only the statistical comparisons where $P < 0.05$ are presented.

10.2 Experimental IL-10 dose

To maximize recombinant IL-10 availability to the lungs throughout the experimental period, a daily injection regime was selected, and IP injections were chosen as the delivery modality

to minimize handling of mouse newborn pups in the crucial first days of life. To assess the most effective experimental IL-10 dose, a range of three progressively higher doses of recombinant IL-10 were administered via IP injections daily to different mouse litters. Newborn C57BL/6J wild type mice exposed from P1 until P14 to either normoxia or hyperoxia were therefore injected daily with 50, 100 or 150 μg/kg of recombinant IL-10 or PBS as a control. Detection of changes in the gene expression of selected anti-inflammatory and pro-inflammatory factors was performed as an assessment of effective IL-10 delivery. To assess the impact of systemic IL-10 administration locally in the lung, the expression of the genes coding for pro-inflammatory molecules IFNγ, TNF-α, and anti-inflammatory molecule TNFR1B were assessed in whole lung homogenates. Lungs were collected at P14 for detection of *Ifng* (Figure 13A), *Tnf* (Figure 13B) and *Tnfrsf1b* (Figure 13C) steady-state mRNA levels by RT-PCR. Compared to mice exposed to normoxia, steady-state levels of *Ifng*, *Tnf* and *Tnfrsf1b* mRNA were elevated in mice exposed to hyperoxia. Daily injections of 50 μg/kg IL-10 reduced the expression of *Ifng* and *Tnf* mRNA in mice subjected to hyperoxia and further raised those of *Tnfrsf1b*, suggesting a strong anti-inflammatory effect can be achieved with this dosage. Conversely, the mRNA levels for these genes in mice injected with IL-10 and subjected to normoxia are consistently higher than in mice injected with vehicle, suggesting that, in absence of inflammation, exogenous IL-10 administration elicits a pro-inflammatory response. A similar effect is achieved at both 100 and 150 μg/kg. Daily IP injections of 50 μg/kg IL-10 were then selected as the dosage most likely to stimulate the desired anti-inflammatory activity of IL-10 in the hyperoxia model of BPD.

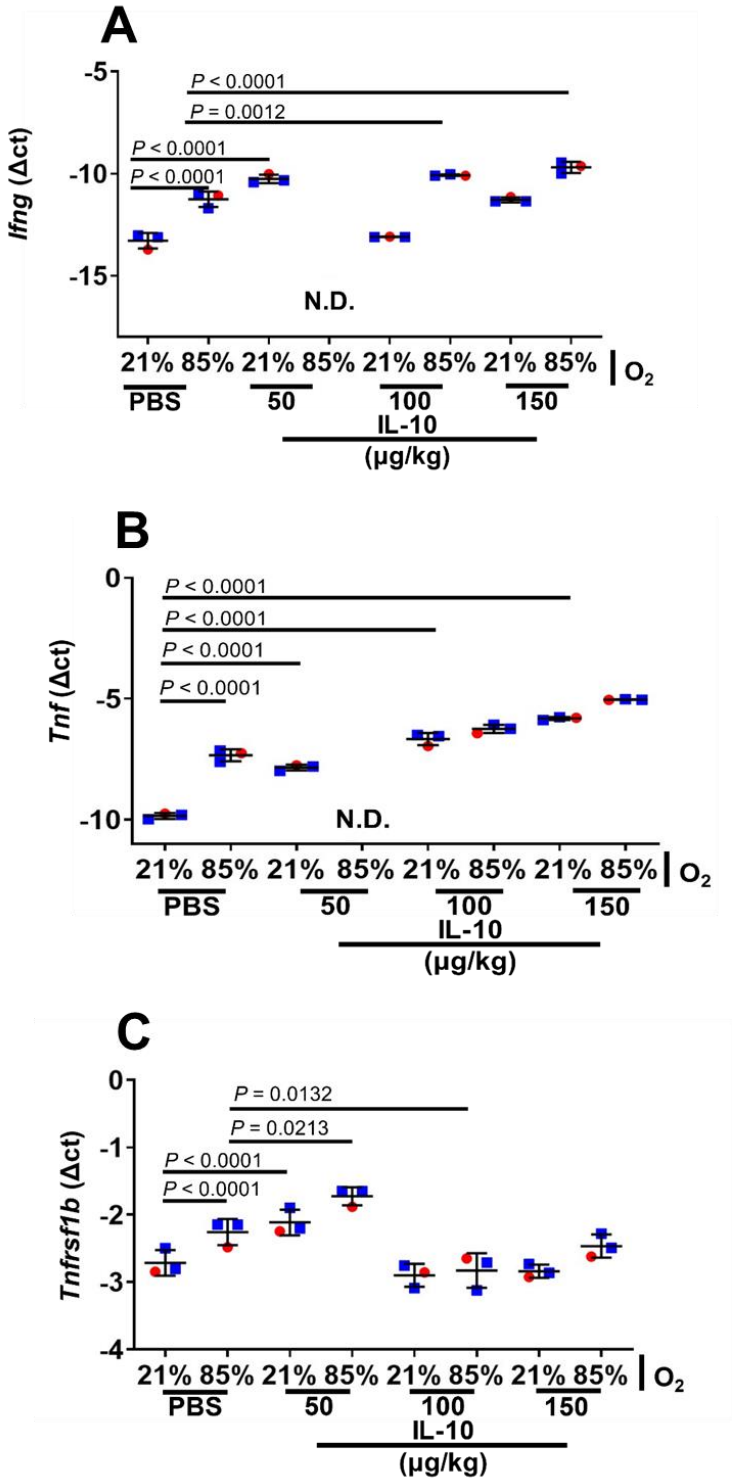

Figure 13. Steady-state mRNA levels of *Ifng*, *Tnf* and *Tnfrsf1b* in the lungs of P14 mice injected daily with IL-10.

Steady-state mRNA levels for (A) *Ifng*, (B) *Tnf* and (C) *Tnfrsf1b* were assessed by RT-PCR in total RNA pools isolated from the lungs of mouse pups at P14 that had been exposed to 21% O_2 or 85% O_2 since P1. Pups received daily IP injections of the reported doses of recombinant IL-10. Data represent mean ± SD. *P* values were determined by one-way ANOVA with Tukey's *post hoc* test (N=3). Only the statistical comparisons where $P < 0.05$ are presented. Blue square: males; red circles: females. For clarity, only one PBS control is reported; the trends of all controls are comparable.

10.3 Impact of daily administration of IL-10 on normal and aberrant lung development

C57BL/6J wild type mouse pups were exposed to normoxia and hyperoxia from P1 to P14. Daily IP administration of recombinant IL-10 did not impact lung architecture over the period from P1 to P14 in newborn mice pups exposed to normoxia, compared to newborn mouse pups injected daily with PBS (Figure 14E, F *versus* A, B, complete data set in Table 18). No impact was detected in newborn mice pups injected daily with IL-10 and exposed to hyperoxia compared to newborn mouse pups injected daily with PBS and exposed to hyperoxia (Figure 14G, H *versus* C, D). No significant change was observed in the volume/body mass ratio (Figure 14I), septal thickness (Figure 14J), surface area of gas exchange (Figure 14K), MLI (Figure 14L), alveolar density (Figure 14M) or total number of alveoli (Figure 14N). These data indicate that daily administration of IL-10 does not impact normal or aberrant late lung development.

10.4 Impact of global deletion of *Il10* on normal and aberrant lung development

Mice were generated as reported by Kühn and coworkers (79) and were a kind gift of Dr André Bleich, from the Medizinische Hochschule Hannover. For this experiment, C57BL/6J wild type and IL-10 KO mouse pups were exposed to normoxia and hyperoxia from P1 to P14. Global deletion of IL-10 does not impact lung architecture over the period from P1 to P14 in newborn mice pups exposed to normoxia, compared to wild type newborn mouse pups exposed to normoxia (Figure 15E, F *versus* A, B, complete data set in Table 19). No impact was detected in global IL-10 knockout newborn mice pups exposed to hyperoxia compared to wild type newborn mouse exposed to hyperoxia (Figure 15G, H *versus* C, D). No significant change was observed in the volume/body mass ratio (Figure 15I), septal thickness (Figure 15J), surface area of gas exchange (Figure 15K), MLI (Figure 15L), alveolar density (Figure 15M) or total number of alveoli (Figure 15N). Thus, global deletion of IL-10 does not impact normal or aberrant late lung development.

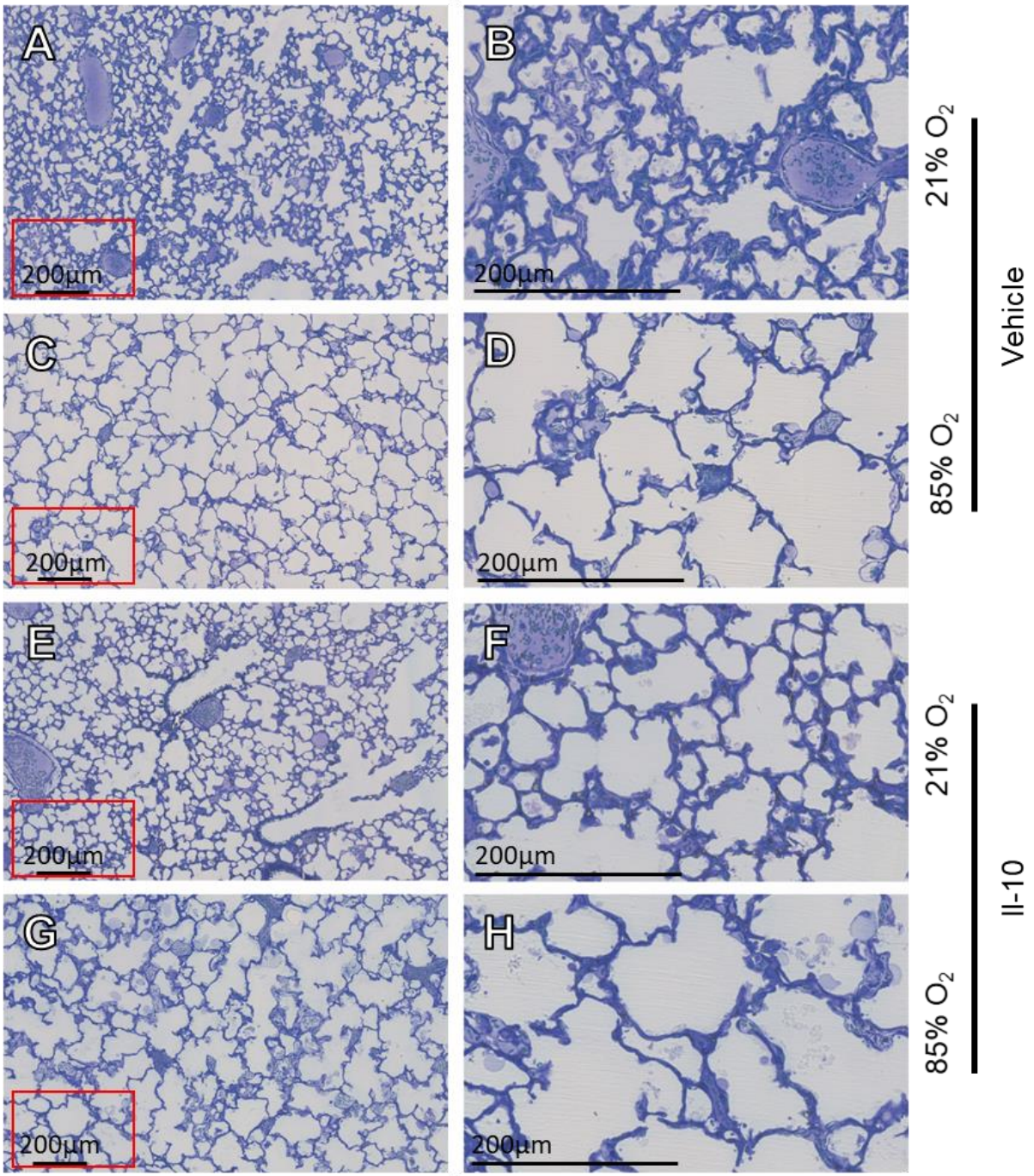

Figure 14. Stereological analysis of lung structure in P14 mice injected daily with PBS or IL-10.
C57BL/6J wild type mice were injected daily with PBS or recombinant IL-10 and exposed to normoxia or hyperoxia from P1 to P14. Lungs were harvested and processed for analysis of the lung structure by design-based stereology on P14. (A, C, E, G) Lower magnification images from lungs. (B, D, F, H) Higher magnification images derived from the red rectangle on the corresponding image on the bottom left, to highlight changes in septal thickness. Each image is representative of images of lung sections obtained from four other mice within each experimental group. Design-based stereology was employed to assess (I) volume/mass ratios, (J) septal thickness, (K) surface area of gas exchange, (L) mean linear intercept (MLI), (M) alveolar density and (N) number of alveoli. Data represent mean ± S.D. Data comparisons were made by one-way ANOVA with Tukey's *post hoc* test (N=5). Only the statistical comparisons where $P < 0.05$ are presented. Blue square: males; red circles: females.

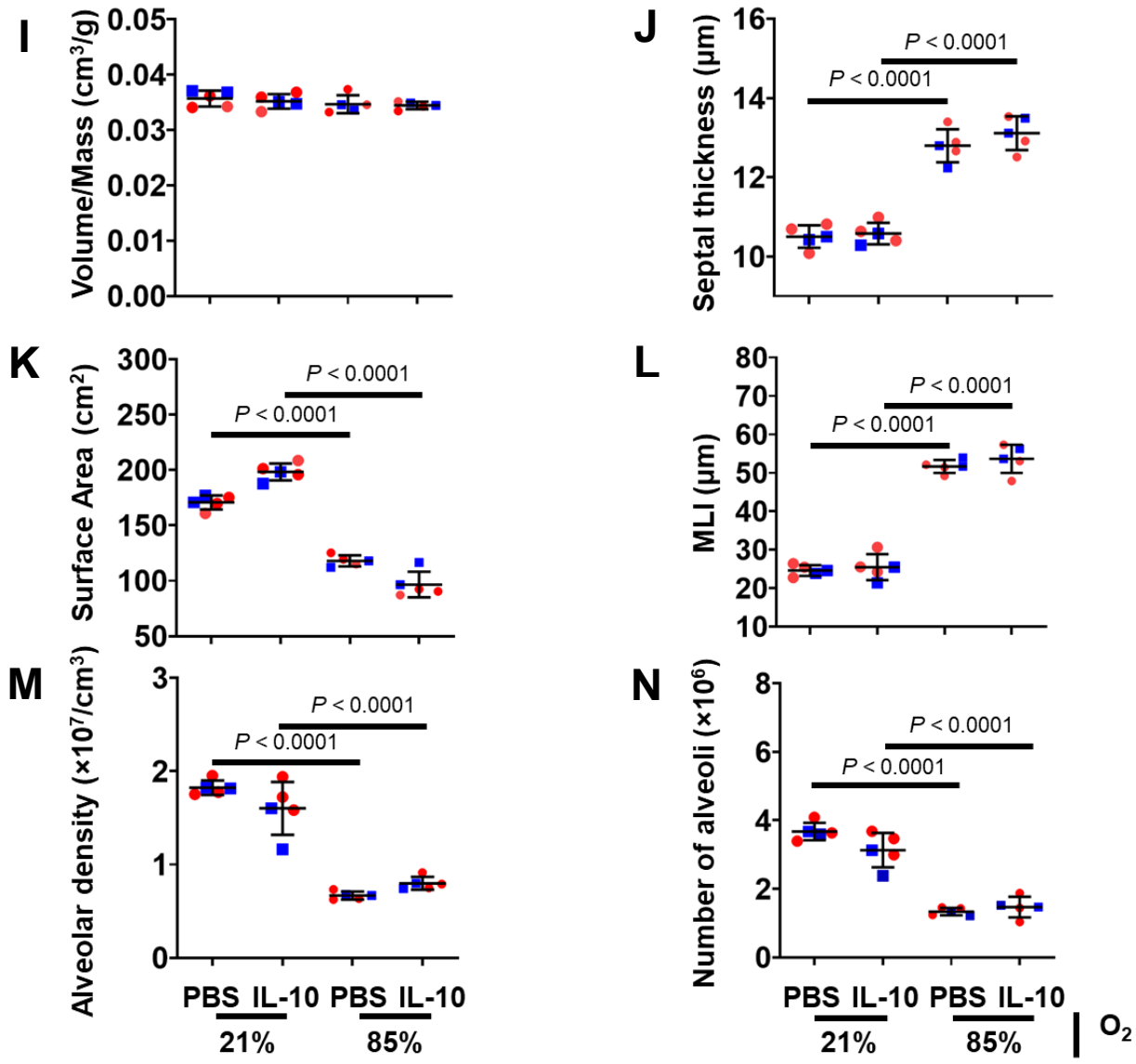

Figure 14, continued.

Parameter			21% O_2						85% O_2								
			PBS			IL-10			PBS						IL-10		
			mean ± SD			mean ± SD			mean ± SD			*P* value *vs.* PBS /21% O_2			mean ± SD		*P* value *vs.* PBS /85% O_2
V (lung) [cm^3]			0.22 ± 0.03			0.21 ± 0.01			0.22 ± 0.01			0.9976			0.22 ± 0.06		0.9536
CE	*CV*	CE^2/CV^2	0.006	0.138	0.25	0.043	0.087	0.25	0.019	0.079	0.25				0.015	0.031	0.25
V_V (par/lung) [%]			90.61 ±1.99			91.01 ± 2.96			89.34 ± 3.59			0.9836			89.46 ± 4.46		0.9999
N (alv, lung) 10^6			3.67 ± 0.25			3.13 ± 0.50			1.33 ± 0.10			<0.0001			1.47 ± 0.29		0.9113
CE	*CV*	CE^2/CV^2	0.030	0.06	0.2	0.071	0.15	0.2	0.036	0.08	0.2				0.091	0.20	0.2
N_V (alv/par) 10^7 [cm^{-3}]			1.82 ± 0.01			1.60 ± 0.08			0.66 ± 0.04			<0.0001			0.79 ± 0.06		0.5395
S_V [cm^{-1}]			786.40 ± 29.32			731.78 ± 31.60			505.02 ± 24.41			<0.0001			460.98 ± 32.26		0.7721
S (alv epi, lung) [cm^2]			164.67 ± 12.57			181.17 ± 17.81						106.13 ± 14.31		<0.0001	96.66 ± 11.64		0.6292
CE	*CV*	CE^2/CV^2	0.034	0.176	0.2	0.043	0.198	0.2	0.005	0.112	0.2				0.053	0.120	0.2
τ (sep) [µm]			10.50 ± 0.28			10.58 ± 0.26						12.79 ± 0.41		<0.0001	13.11 ± 0.42		0.5148
CE	*CV*	CE^2/CV^2	0.011	0.026	0.2	0.011	0.038	0.2	0.014	0.032	0.2				0.014	0.036	0.2
MLI [µm]			24.59 ± 1.41			25.45 ± 3.35						51.67 ± 1.69		<0.0001	53.62 ± 3.66		0.6740
CE	*CV*	CE^2/CV^2	0.025	0.057	0.2	0.058	0.131	0.2	0.014	0.032	0.2				0.030	0.068	0.2

Table 18. Full stereological analysis at P14 of lung structure in mice injected daily with PBS or IL-10.

Abbreviations: alv, alveoli; alv epi, alveolar epithelium; *CV*, coefficient of variation; IL-10, interleukin-10; MLI, mean linear intercept; *N*, number; N_V, numerical density; par, parenchyma; *S*, surface area; S_V, surface density; τ (sep), arithmetic mean septal thickness; *V*, volume; V_V, volume density. Values are presented as mean ± SD, $n = 5$ lungs for each group. One-way ANOVA with Tukey's *post hoc* analysis was used to determine *P* values.

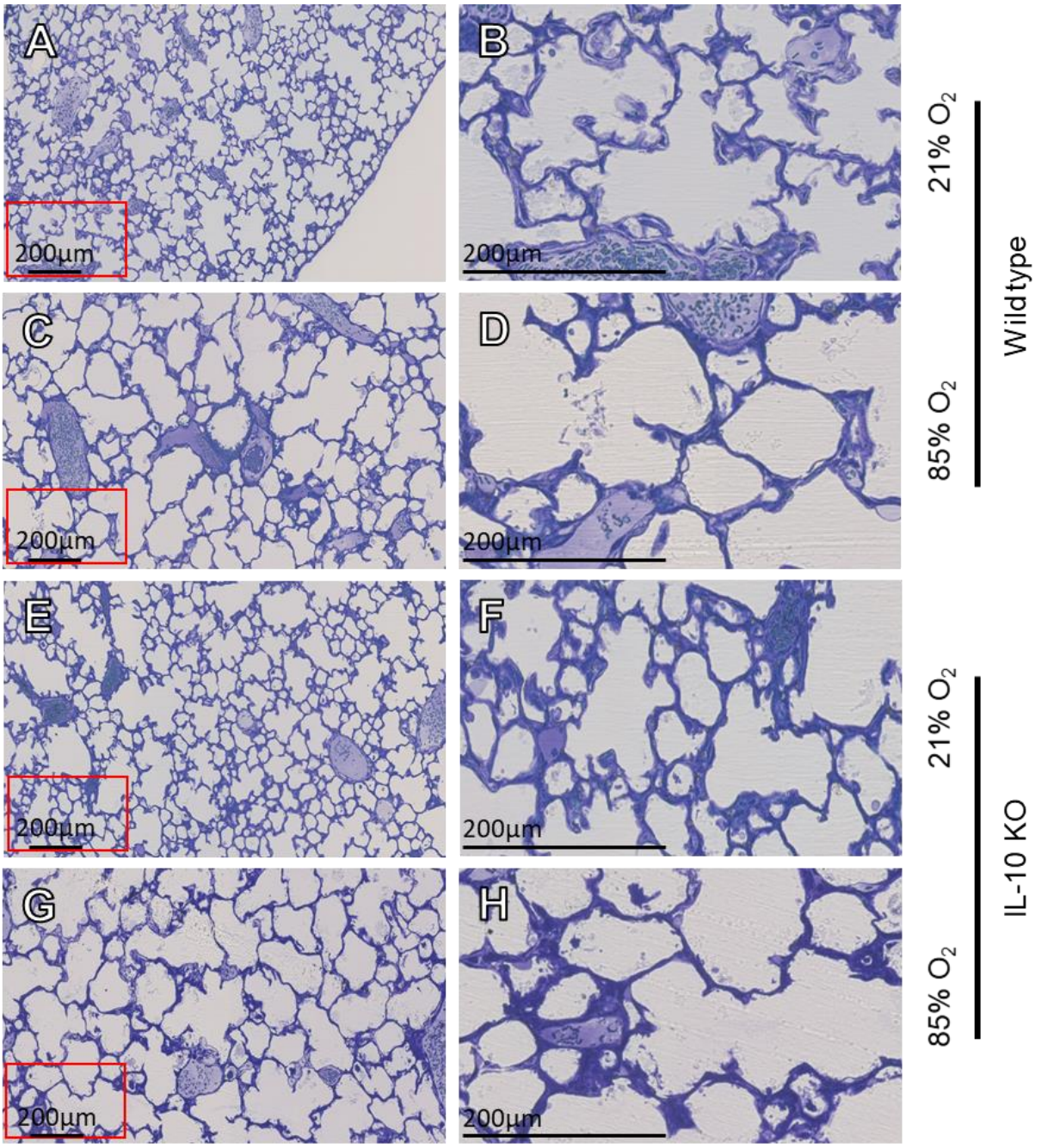

Figure 15. Stereological analysis of lung structure in wild type and IL-10 knockout P14 mice.
C57BL/6J (wild type, WT) mice and C57BL/6J.129P2-Il10^{tm1Cgn} (KO) mice were exposed to normoxia (21% O_2) or hyperoxia (85% O_2) from P1 to P14. Lungs were harvested and processed for analysis of the lung structure by design-based stereology on P14. (A, C, E, G) Lower magnification images from lungs. (B, D, F, H) Higher magnification images derived from the red rectangle on the corresponding image on the bottom left, to highlight changes in septal thickness. Each image is representative of images of lung sections obtained from four other mice within each experimental group. Design-based stereology was employed to assess (I) volume/mass ratios, (J) septal thickness, (K) surface area of gas exchange, (L) mean linear intercept (MLI), (M) alveolar density and (N) number of alveoli. Data represent mean ± S.D. Data comparisons were made by one-way ANOVA with Tukey's *post hoc* test (N=5). Only the statistical comparisons where $P < 0.05$ are presented. Blue square: males; red circles: females.

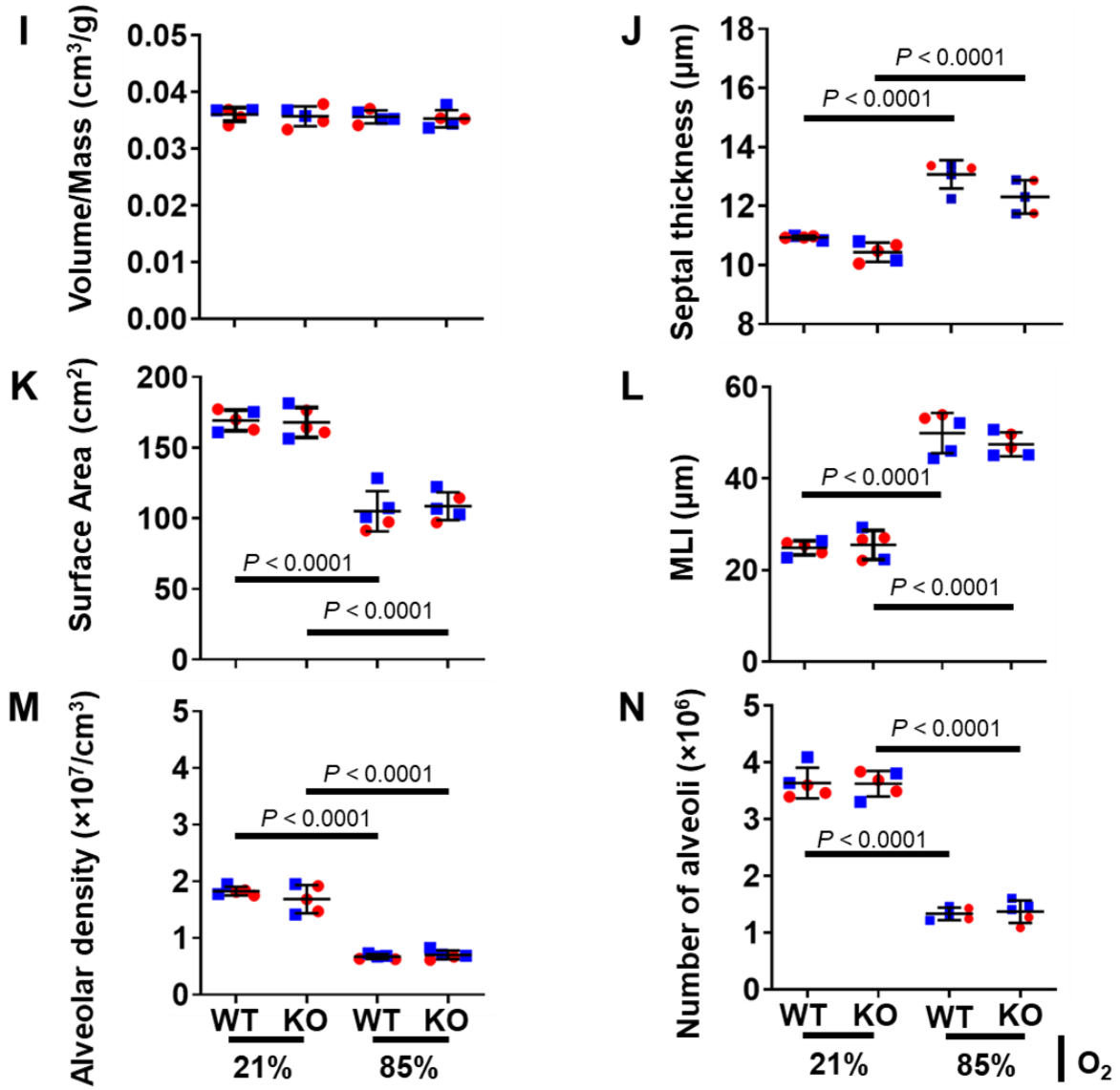

Figure 15, continued.

Table 19. Full stereological analysis of lung structure at P14 in wild type or C57BL/6J.129P2-Il10^{tm1Cgn} mice.

Parameter			21% O_2						85% O_2					
			Wild type			C57BL/6J.129P2-*Il10*^{tm1Cgn}			Wild type			C57BL/6J.129P2-*Il10*^{tm1Cgn}		
			mean ± SD			mean ± SD			mean ± SD		*P* value *vs.* Wild type /21% O_2	mean ± SD		*P* value *vs.* Wild type /85% O_2
V (lung) [cm^3]			0.22 ± 0.03			0.21 ± 0.07			0.23 ± 0.08		0.9923	0.21 ± 0.07		0.9931
CE	*CV*	*CE^2/CV^2*	0.007	0.11	0.25	0.016	0.03	0.25	0.019	0.05	0.25	0.018	0.03	0.25
V_V (par/lung) [%]			91.31 ± 1.99			91.01 ± 2.96			88.74 ± 5.59		0.9730	90.48 ± 7.46		0.6373
N (alv, lung) 10^6			3.68 ± 0.25			3.13 ± 0.50			1.32 ± 0.10		<0.0001	1.57 ± 0.29		0.9922
CE	*CV*	*CE^2/CV^2*	0.019	0.06	0.2	0.079	0.15	0.2	0.027	0.08	0.2	0.038	0.14	0.2
N_V (alv/par) 10^7 [cm^{-3}]			1.82 ± 0.07			1.70 ± 0.28			0.72 ± 0.04		<0.0001	0.78 ± 0.06		0.9825
S_V [cm^{-1}]			774.41 ± 36.16			781.78 ± 37.08			532.52 ± 28.42		<0.0001	490.98 ± 52.26		0.8433
S (alv epi, lung) [cm^2]			170.84 ± 6.34			198.41 ± 7.60			118.01 ± 4.97		<0.0001	96.66 ± 11.64		0.9528
CE	*CV*	*CE^2/CV^2*	0.016	0.03	0.2	0.017	0.03	0.2	0.018	0.04	0.2	0.053	0.12	0.2
τ (sep) [µm]			10.50 ± 0.28			10.14 ± 0.26			12.79 ± 0.41		<0.0001	13.11 ± 0.42		0.0611
CE	*CV*	*CE^2/CV^2*	0.011	0.02	0.2	0.011	0.02	0.2	0.014	0.03	0.2	0.014	0.03	0.2
MLI [µm]			24.59 ± 1.41			25.45 ± 3.35			51.67 ± 1.69		<0.0001	53.62 ± 3.66		0.6032
CE	*CV*	*CE^2/CV^2*	0.025	0.05	0.2	0.058	0.13	0.2	0.014	0.03	0.2	0.030	0.06	0.2

Abbreviations: alv, alveoli; alv epi, alveolar epithelium; *CV*, coefficient of variation; IL-10, interleukin-10; MLI, mean linear intercept; *N*, number; N_V, numerical density; par, parenchyma; *S*, surface area; S_V, surface density; τ (sep), arithmetic mean septal thickness; *V*, volume; V_V, volume density. Values are presented as mean ± SD, $n = 5$ lungs for each group. One-way ANOVA with Tukey's *post hoc* analysis was used to determine *P* values.

10.5 Impact of a single IL-10 injection administered at P1 on normal and aberrant lung development

The lack of significant impact on newborn mouse lungs from either daily IL-10 administration or from complete absence of this cytokine indicated that a more focused approach should be considered (106). A dose of 50 µg/kg recombinant IL-10 was then administered once via IP injection, at P1, to C57BL/6J wild type mouse pups then exposed to normoxia or hyperoxia from P1 to P14. To verify the efficacy of the single dose treatment, steady-state mRNA levels of *Ifng*, (Figure 16A), *Tnf* (Figure 16B) and *Tnfrsf1b* (Figure 16C) mRNA levels were assessed by qPCR, suggesting that a persistent effect of IL-10 administration could still be detected at P14. Administration of a single dose of IL-10 at P1 severely affected lung architecture development in IL-10-injected mouse pups exposed to hyperoxia, but not in IL-10-injected pups exposed to normoxia, compared to vehicle-injected pups exposed to the same oxygen concentrations (FiguG, H *versus* E, F, and *versus* C, D and A, B, complete data set in Table 20). A direct comparison between hyperoxia-exposed IL-10-injected mouse pups and vehicle-injected pups detected that septal thickness was increased from 12.67 µm to 21.88 µm (Figure 17J), surface area of gas exchange was decreased from 77.39 cm^2 to 58.72 cm^2 (Figure 17J), and MLI was decreased from 57.22 µm to 48.64 µm (Figure 17K). Volume/mass ratio (Figure 17I), alveolar density (Figure 17M) and total number of alveoli (Figure 17N) were not affected. These data indicate that a single injection of IL-10 at P1 is sufficient to elicit further, severe remodelling of lung architecture in the aberrant lung development associated to the hyperoxia mouse model of BPD.

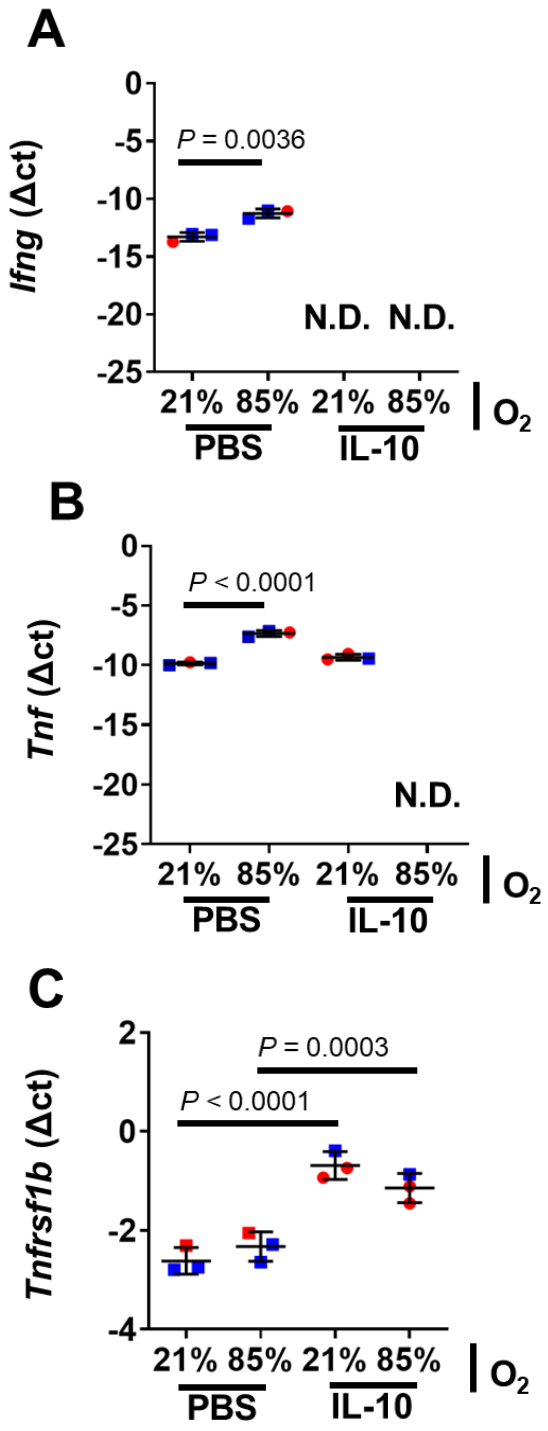

Figure 16. Steady-state mRNA levels of *Ifng*, *Tnf* and *Tnfrsf1b* in the lungs of P14 mice treated at P1 with IL-10.

Steady-state mRNA levels for (A) *Ifng*, (B) *Tnf* and (C) *Tnfrsf1b* were assessed by RT-PCR in total RNA pools isolated from the lungs of mouse pups at P14 that had been exposed to normoxia or hyperoxia since P1. Pups were injected IP at P1 with 50 µg/kg of recombinant IL-10. Data represent mean ± S.D. Data comparisons were made by one-way ANOVA with Tukey's *post hoc* test (N=3). Only the statistical comparisons where $P < 0.05$ are presented. Blue square: males; red circles: females.

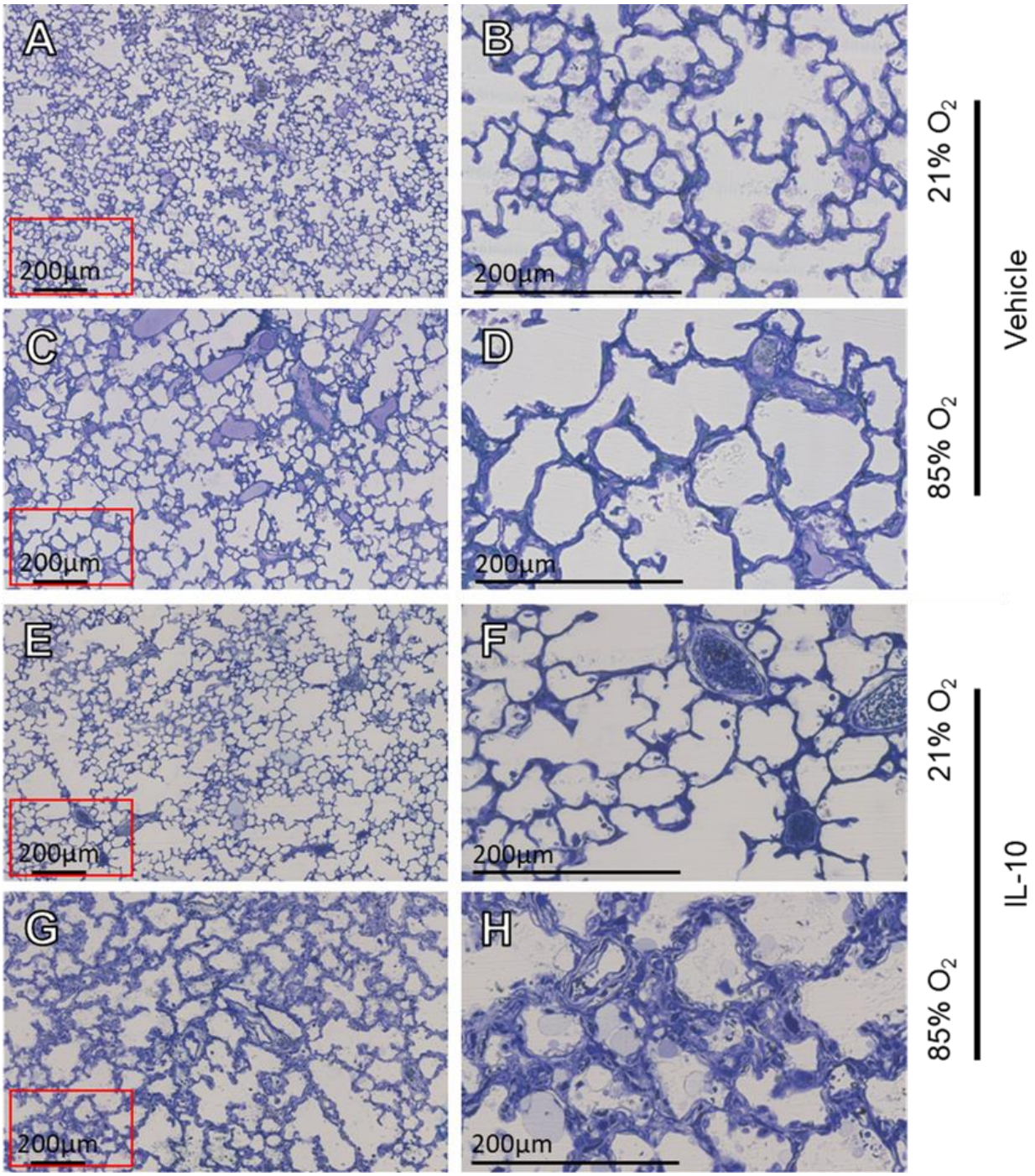

Figure 17. Stereological analysis of lung structure in PBS- and P1 IL-10-single injected P14 mice.
C57BL/6J wild type mice were injected at P1 with PBS or recombinant IL-10 and exposed to normoxia (21% O_2) or hyperoxia (85% O_2) from P1 to P14. Lungs were harvested and processed for analysis of the lung structure by design-based stereology on P14. (A, C, E, G) Lower magnification images from lungs. (B, D, F, H) Higher magnification images derived from the red rectangle on the corresponding image on the bottom left, to highlight changes in septal thickness. Each image is representative of images of lung sections obtained from four other mice within each experimental group. Design-based stereology was employed to assess (I) volume/mass ratios, (J) septal thickness, (K) surface area of gas exchange, (L) mean linear intercept (MLI), (M) alveolar density and (N) number of alveoli. Data represent mean ± S.D. Data comparisons were made by one-way ANOVA with Tukey's *post hoc* test (N=5). Only the statistical comparisons where $P < 0.05$ are presented. Blue square: males; red circles: females.

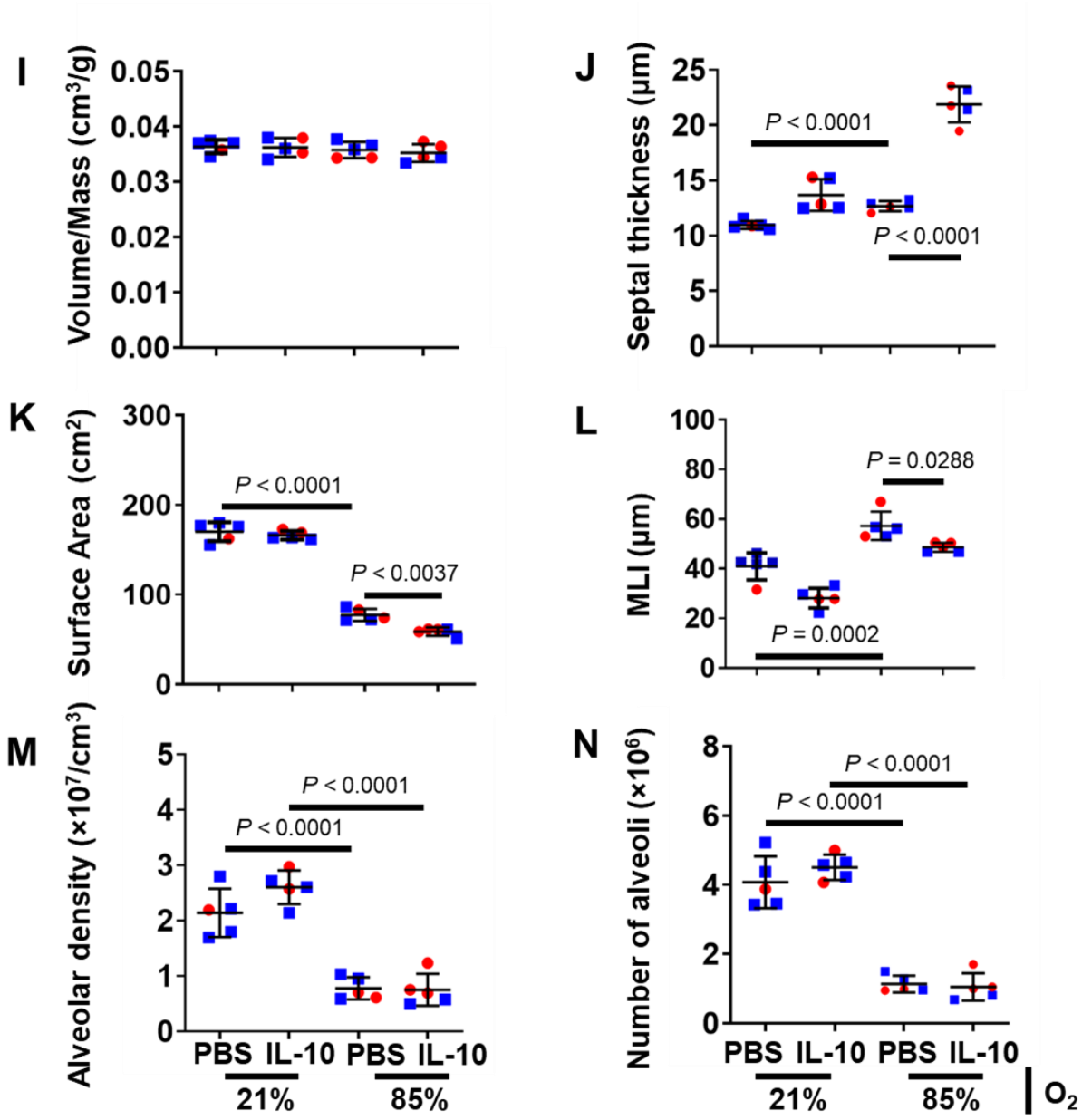

Figure 17, continued.

Table 20. Full stereological analysis of lung structure at P14 in mice injected at P1 with PBS or IL-10.

Parameter			21% O_2						85% O_2					
			PBS			IL-10			PBS			IL-10		
			mean ± SD			mean ± SD			mean ± SD		*P* value *vs.* PBS /21% O_2	mean ± SD		*P* value *vs.* PBS /85% O_2
V (lung) [cm^3]			0.22 ± 0.04			0.22 ± 0.07			0.22 ± 0.07		0.9998	0.21 ± 0.01		0.9993
CE	*CV*	CE^2/CV^2	0.008	0.01	0.2	0.014	0.03	0.2	0.017	0.03	0.2	0.030	0.01	0.2
V_V (par/lung) [%]			0.85 ± 0.05			0.90 ± 0.03			0.86 ± 0.03		0.9342	0.82 ± 0.03		0.4254
N (alv, lung) 10^6			4.07 ± 0.74			4.50 ± 0.36			1.13 ± 0.24		<0.0001	1.04 ± 0.39		0.9915
CE	*CV*	CE^2/CV^2	0.082	0.18	0.2	0.035	0.08	0.2	0.096	0.21	0.2	0.167	0.17	0.2
N_V (alv/par) 10^7 [cm^{-3}]			2.14 ± 0.04			2.60 ± 0.03			0.77 ± 0.02		<0.0001	0.75 ± 0.08		<0.0001
S_V [cm^{-1}]			870.31 ± 31.38			705.28 ± 45.55			496.16 ± 34.56		<0.0001	420.65 ± 34.11		0.3880
S (alv epi, lung) [cm^2]			170.10 ± 5.58			166.10 ± 4.70			77.39 ± 6.78		<0.0001	58.72 ± 4.54		0.0037
CE	*CV*	CE^2/CV^2	0.027	0.06	0.2	0.012	0.02	0.2	0.039	0.08	0.2	0.034	0.07	0.2
τ (sep) [µm]			10.97 ± 0.35			13.67 ± 0.43			12.67 ± 0.45		<0.0001	21.87 ± 0.62		<0.0001
CE	*CV*	CE^2/CV^2	0.014	0.03	0.2	0.046	0.04	0.2	0.016	0.03	0.2	0.033	0.07	0.2
MLI [µm]			40.92 ± 5.48			32.12 ± 3.96			57.22 ± 5.71		0.0002	48.64 ± 1.84		0.0288
CE	*CV*	CE^2/CV^2	0.059	0.13	0.2	0.063	0.14	0.2	0.044	0.09	0.2	0.016	0.03	0.2

Abbreviations: alv, alveoli; alv epi, alveolar epithelium; *CV*, coefficient of variation; IL-10, interleukin-10; MLI, mean linear intercept; *N*, number; N_V, numerical density; par, parenchyma; *S*, surface area; S_V, surface density; τ (sep), arithmetic mean septal thickness; *V*, volume; V_V, volume density. Values are presented as mean ± SD, $n = 5$ lungs for each group. One-way ANOVA with Tukey's *post hoc* analysis was used to determine *P* values.

10.6 Impact of a single IL-10 injection administered at P3 on normal and aberrant lung development

To further delineate the time frame in which the administration of a single IL-10 injection impacts postnatal lung development, a second time point preceding peak bulk secondary septation, P3, was selected. A single administration of recombinant IL-10 at P3 did not impact lung architecture over the period between P1 to P14 in newborn mice pups exposed to normoxia, compared to newborn mouse pups injected at the same time point with PBS (Figure 19E, F *versus* A, B, complete data set in Table 21). No impact was also detected at P14 in newborn mice pups injected with IL-10 at P3 and exposed to hyperoxia compared to newborn mouse pups injected with PBS at P3 and exposed to hyperoxia (Figure 19G, H *versus* C, D). No significant change was observed in the volume/body mass ratio (Figure 19I), septal thickness (Figure 19J), surface area of gas exchange (Figure 19K), MLI (Figure 19L), alveolar density (Figure 19M) or total number of alveoli (Figure 19N). These findings indicate that IL-10 significantly impacts the aberrant lung development associated to the hyperoxia mouse model of BPD when administered on P1, but not at P3.

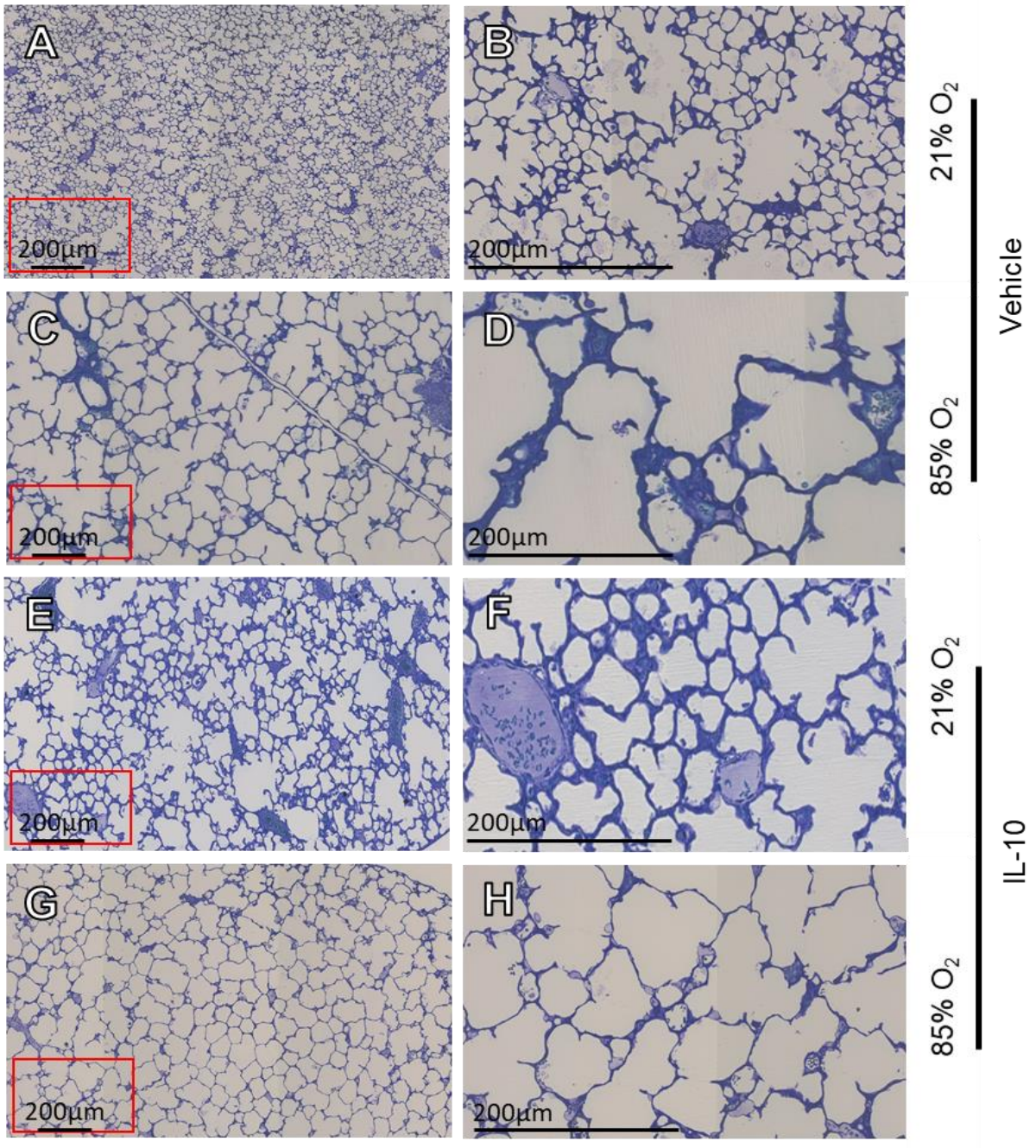

Figure 18. Stereological analysis of lung structure in PBS- and P3 IL-10-single injected P14 mice.
C57BL/6J wild type mice were injected at P3 with PBS or recombinant IL-10 and exposed to normoxia (21% O_2) or hyperoxia (85% O_2) from P1 to P14. Lungs were harvested and processed for analysis of the lung structure by design-based stereology on P14. (A, C, E, G) Lower magnification images from lungs. (B, D, F, H) Higher magnification images derived from the red rectangle on the corresponding image on the bottom left, to highlight changes in septal thickness. Each image is representative of images of lung sections obtained from four other mice within each experimental group. Design-based stereology was employed to assess (I) volume/mass ratios, (J) septal thickness, (K) surface area of gas exchange, (L) mean linear intercept (MLI), (M) alveolar density and (N) number of alveoli. Data represent mean ± S.D. Data comparisons were made by one-way ANOVA with Tukey's *post hoc* test (N=5). Only the statistical comparisons where $P < 0.05$ are presented. Blue square: males; red circles: females.

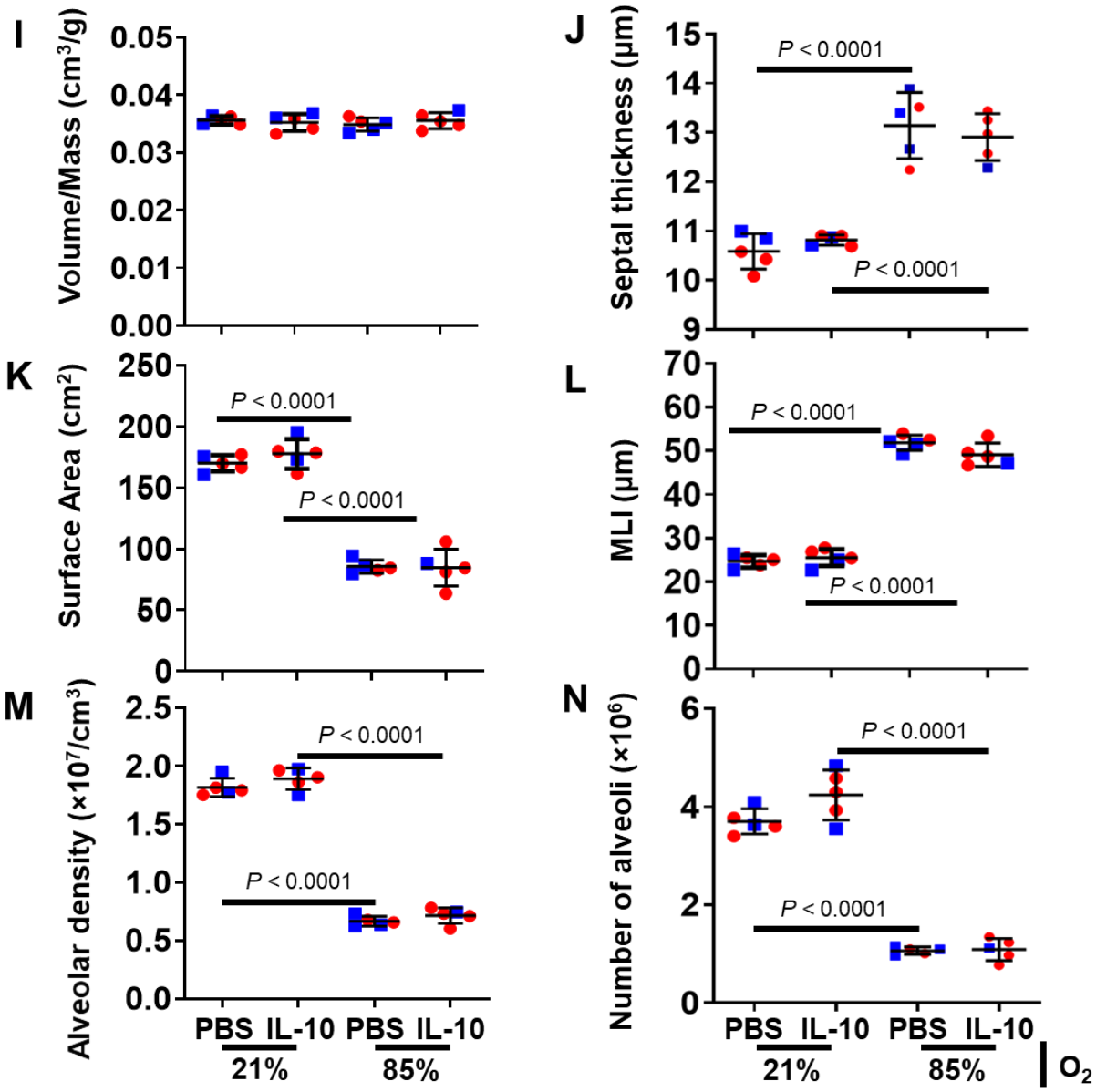

Figure 19, continued.

Table 21. Full stereological analysis of lung structure at P14 in mice injected at P3 with PBS or IL-10.

Parameter			21% O_2						85% O_2					
			PBS			IL-10			PBS			IL-10		
			mean ± SD			mean ± SD			mean ± SD		*P* value *vs.* PBS /21% O_2	mean ± SD		*P* value *vs.* PBS /85% O_2
V (lung) [cm^3]			0.22 ± 0.02			0.24 ± 0.01			0.18 ± 0.01		0.0609	0.19 ± 0.03		0.9603
CE	*CV*	CE^2/CV^2	0.005	0.013	0.2	0.024	0.051	0.2	0.043	0.082	0.2	0.072	0.073	0.2
V_V (par/lung) [%]			0.91 ± 0.01			0.92 ± 0.02			0.89 ± 0.04		0.9855	0.83 ± 0.06		0.3229
N (alv, lung) 10^6			3.70 ± 0.25			4.24 ± 0.51			1.06 ± 0.07		<0.0001	1.09 ± 0.22		0.9993
CE	*CV*	CE^2/CV^2	0.031	0.063	0.2	0.053	0.087	0.2	0.032	0.074	0.2	0.092	0.092	0.2
N_V (alv/par) 10^7 [cm^{-3}]			1.82 ± 0.07			1.89 ± 0.09			0.67 ± 0.04		<0.0001	0.72 ± 0.06		<0.0001
S_V [cm^{-1}]			849.16 ± 48.67			815.02 ± 27.66			532.53 ± 24.61		<0.0001	550.56 ± 35.09		0.9216
S (alv epi, lung) [cm^2]			170.04 ± 6.59			177.72 ± 9.21			85.64 ± 5.49		<0.0001	84.73 ± 5.09		0.9991
CE	*CV*	CE^2/CV^2	0.017	0.034	0.2	0.030	0.063	0.2	0.028	0.066	0.2	0.079	0.072	0.2
τ (sep) [µm]			10.59 ± 0.35			10.82 ± 0.10			13.14 ± 0.67		<0.0001	12.91 ± 0.47		0.8411
CE	*CV*	CE^2/CV^2	0.015	0.032	0.2	0.004	0.095	0.2	0.022	0.053	0.2	0.016	0.036	0.2
MLI [µm]			24.69 ± 1.43			25.52 ± 1.95			51.83 ± 1.73		<0.0001	49.09 ± 1.67		0.1752
CE	*CV*	CE^2/CV^2	0.025	0.053	0.2	0.034	0.075	0.2	0.014	0.036	0.2	0.024	0.056	0.2

Abbreviations: alv, alveoli; alv epi, alveolar epithelium; *CV*, coefficient of variation; IL-10, interleukin-10; MLI, mean linear intercept; *N*, number; N_V, numerical density; par, parenchyma; *S*, surface area; S_V, surface density; τ (sep), arithmetic mean septal thickness; *V*, volume; V_V, volume density. Values are presented as mean ± SD, $n = 5$ lungs for each group. One-way ANOVA with Tukey's post-hoc analysis was used to determine *P* values.

10.7 Impact of a single IL-10 injection at P1 and P3 on the cell composition of the septa

To discern possible changes in the main cellular components of the septa resulting from IL-10 administration and to compare the effects of single injection administration in both P1 and P3 time points, immunohistochemical staining for several different cell markers was carried out. The selected markers, podoplanin, prosurfactant protein C (pro-SPC), vimentin and epithelial cell adhesion molecule (EpCAM), are routinely employed for the staining of AECI, AECII, fibroblasts and endothelial cells, respectively. Additional staining for pan-leukocyte protein CD45, to assess the extent of leukocyte infiltration in the thickened septa, was also performed. Counterstaining with DAPI was carried out in all experiments. Newborn mouse pups were injected with PBS or with IL-10, either on P1 or on P3, and exposed to normoxia and hyperoxia until P14. Isolated lungs were embedded in paraffin, sectioned, and stained with the appropriate antibodies, then mounted and stored at 4 °C. Pictures were taken no later than seven days after staining. In all confocal microscopy pictures taken for this experiment, DAPI counterstaining revealed an abnormal accumulation of cells in the septa of mice injected with IL-10 at P1 and exposed to hyperoxia, while no difference was observed in the normoxia counterparts injected with PBS or IL-10 at P3 (Figure 20, Figure 21, Figure 22, Figure 23 and Figure 24). Staining with anti-EpCAM antibodies highlights no changes in the epithelial cell population in the developing septa of newborn mice injected with PBS or with IL-10 at P3 and exposed to either normoxia or hyperoxia (Figure 20A, B, E, F), and no impact was detected in newborn mice injected with IL-10 at P1 and exposed to normoxia (Figure 20C). No increase in the number of $EpCAM^+$ cells is detectable in the septa of mice exposed to hyperoxia (Figure 20D). These observations suggest that injection of IL-10 at P1 does not impact the abundance of epithelial cells in the septa of newborn mice exposed to hyperoxia.

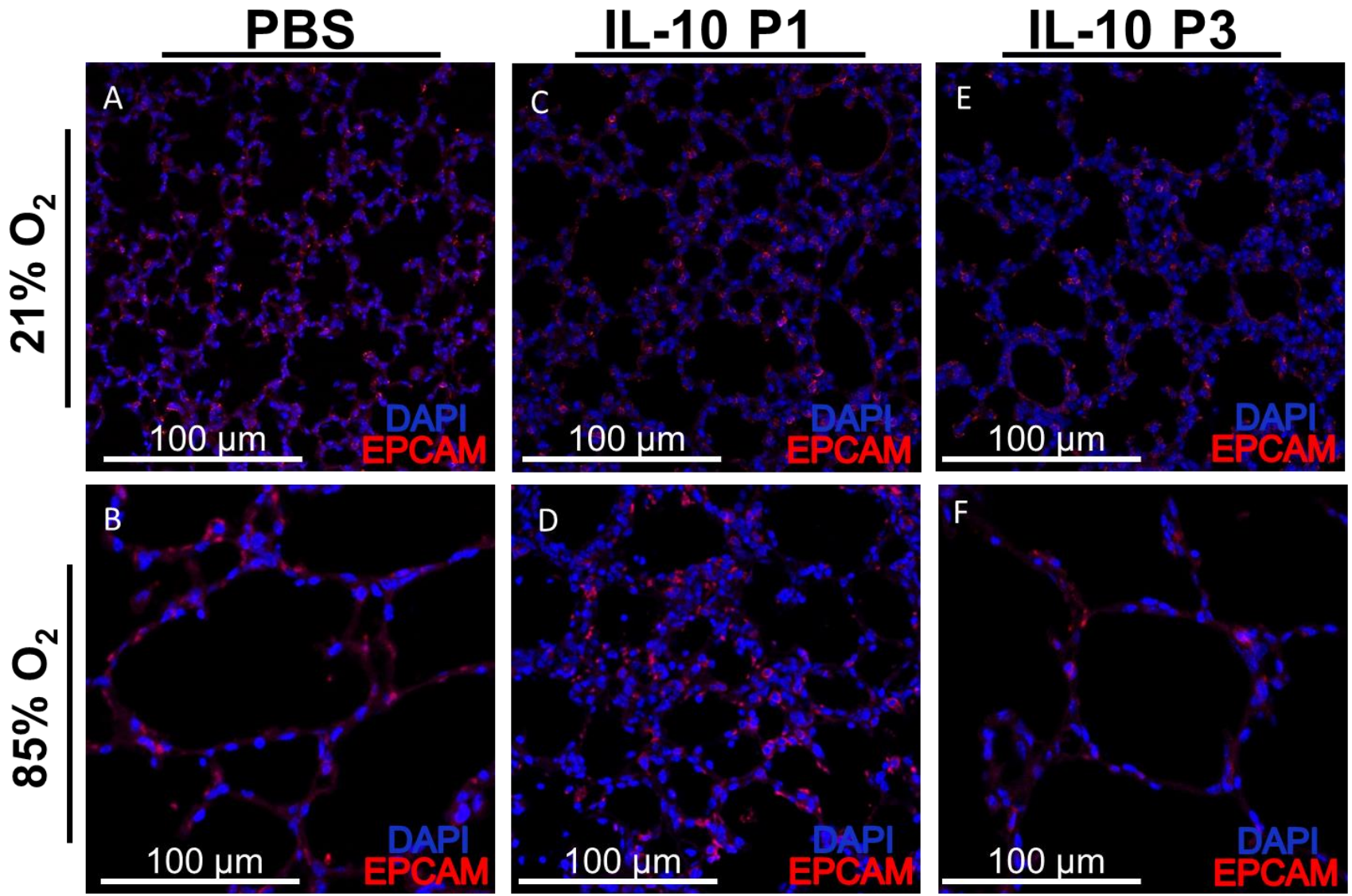

Figure 20. Detection of epithelial cell adhesion molecule in the septa of the normal and aberrant developing lung following treatment with IL-10.
C57BL/6J wild type mice were injected at P1 or at P3 with PBS or recombinant IL-10. Lungs were embedded in paraffin at P14 and stained for epithelia cell adhesion molecule (EPCAM, red) and DAPI (blue), to visualize respectively epithelial cells and the nuclei of all cells present in the section. For clarity, only one PBS control is reported; the trends of all controls are comparable.

Staining with anti-podoplanin antibodies revealed no evident change in the AECI population between mice injected with PBS and mice injected with IL-10 at P3 and exposed to either normoxia or hyperoxia (Figure 21A, B, E, F). No change was observed in podoplanin-positive cells abundance in the thickened septa of mice injected with IL-10 at P1 and exposed to either normoxia or hyperoxia (Figure 21C, D). These data suggest that AECI are not impacted by IL-10 injections. Staining with anti-pro-SPC antibodies revealed no marked change in AECII abundance in the developing septa of newborn mice injected with PBS or with IL-10 at P3 and exposed to either normoxia or hyperoxia (Figure 22A, B, E, F). AECII abundance was also not impacted in newborn mice injected with IL-10 at P1 and exposed to normoxia (Figure 22C), or to hyperoxia (Figure 22D). These observations suggest that injection of IL-10 at P1 does not impact the abundance of pro-SPC cells in the septa of newborn mice exposed to hyperoxia.

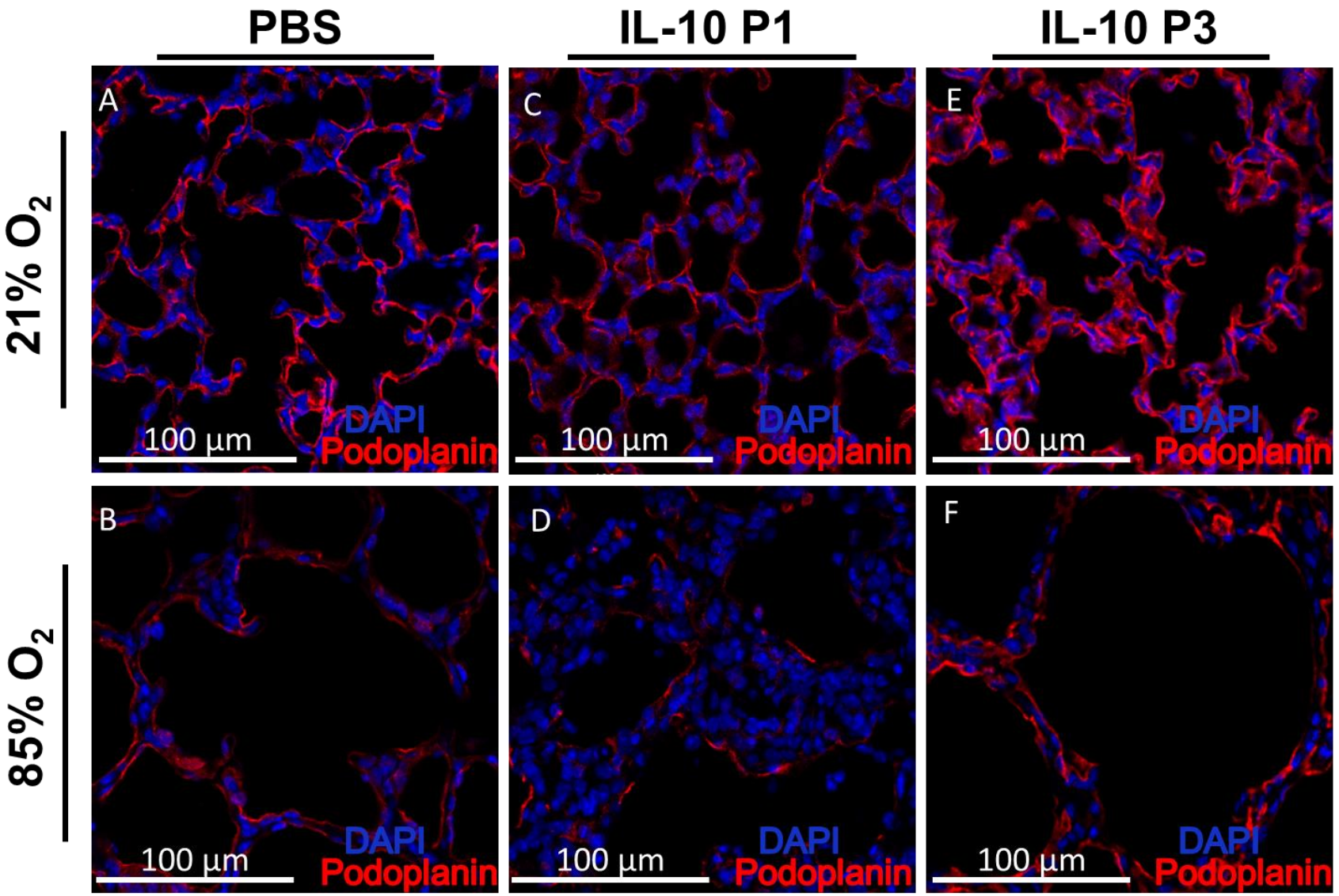

Figure 21. Detection of podoplanin in the septa of the normal and aberrant developing lung following treatment with IL-10.
C57BL/6J wild type mice were injected at P1 or at P3 with PBS or recombinant IL-10. Lungs were embedded in paraffin at P14 and stained for podoplanin (red) and DAPI (blue), to visualize respectively AECI and the nuclei of all cells present in the section. For clarity, only one PBS control is reported; the trends of both controls are comparable.

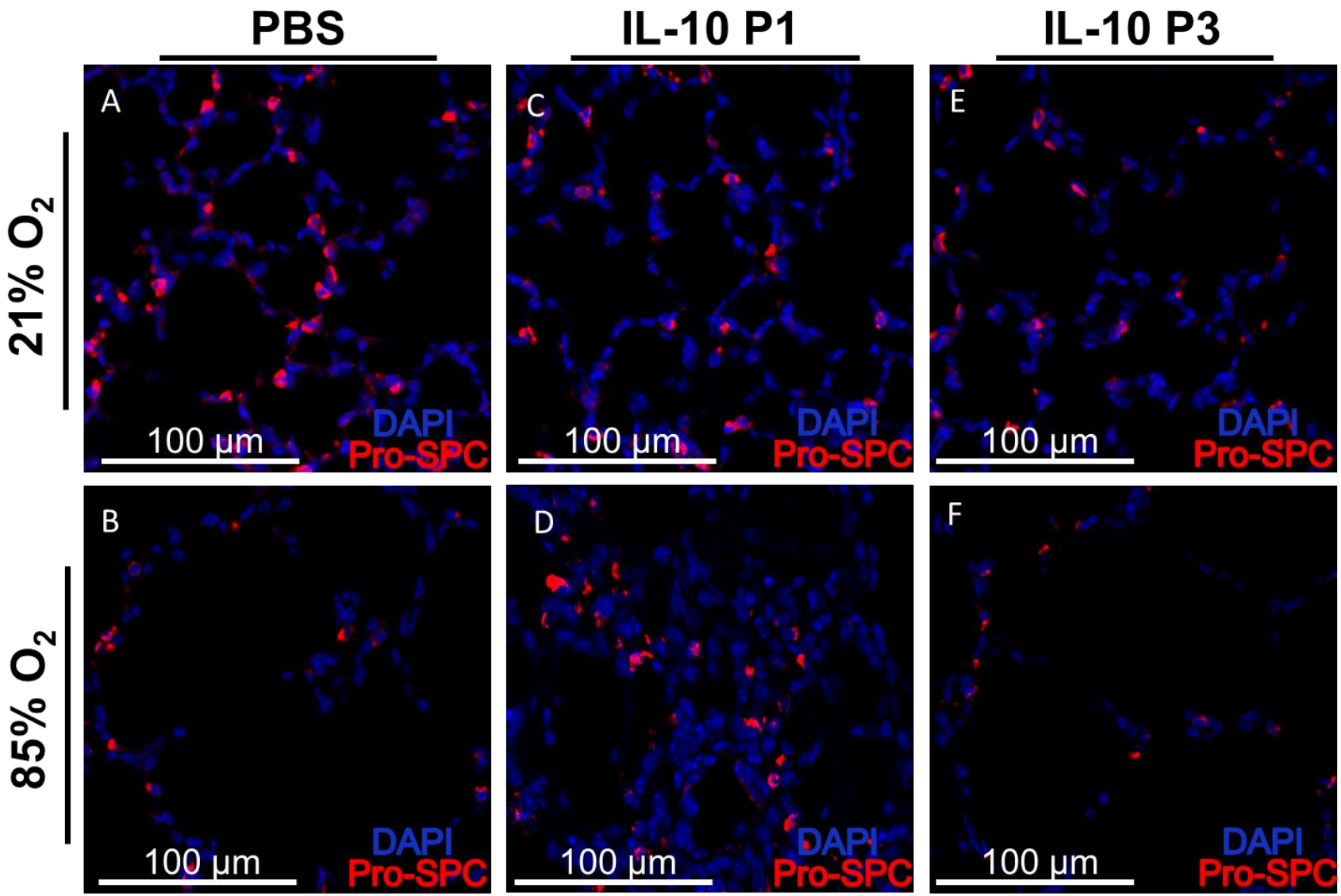

Figure 22. Detection of prosurfactant protein C in the septa of the normal and aberrant developing lung following treatment with IL-10.
C57BL/6J wild type mice were injected at P1 or at P3 with PBS or recombinant IL-10. Lungs were embedded in paraffin at P14 and stained for prosurfactant protein C (pro-SPC, red) and DAPI (blue), to visualize respectively AECII and the nuclei of all cells present in the section. For clarity, only one PBS control is reported; the trends of both controls are comparable.

A staining assay with anti-vimentin antibodies was performed to visualize fibroblasts in the developing septum. No change was observed in fibroblast abundance in the developing septa of newborn mice injected with PBS or with IL-10 at P3 and exposed to either normoxia or hyperoxia (Figure 23A, B, E, F). No impact was also observed in fibroblasts abundance in newborn mice injected with IL-10 at P1 and exposed to normoxia (Figure 23C), while a higher number of vimentin-positive cells was observed in the thickened septa of mice exposed to hyperoxia (Figure 23D). These data indicate that injection of IL-10 at P1 impacts the abundance of vimentin-positive cells in the septa of newborn mice exposed to hyperoxia. To elucidate wherever high levels of leukocyte infiltration could significantly contribute to the thickening of the septa, staining with anti-CD45 antibodies was carried out, revealing no evident change in the abundance of leukocytes in the septa of mice injected with PBS and in the septa of mice injected with IL-10 at P3 and exposed to either normoxia or hyperoxia (Figure 24A, B, E, F). No change was also observed in CD45-positive cell abundance in the thickened septa of mice injected with IL-10 at P1 and exposed to either normoxia or hyperoxia (Figure 24C, 24D). These data suggest that the localization of leukocytes in the septa is not impacted by IL-10 injections. All negative controls for the stainings are reported in Figure 33, Figure 34, Figure 35, Figure 36 and Figure 37. Steady-state levels of *Vim* and *Col1a1* mRNAs, genes coding respectively for fibroblast markers vimentin and collagen type I, are reported in Figure 25. Taken together, these data suggest that a single injection of IL-10 at P1 impacts the abundance of fibroblasts, but not of AECI, AECII or leukocytes in the septa of newborn mice exposed to hyperoxia.

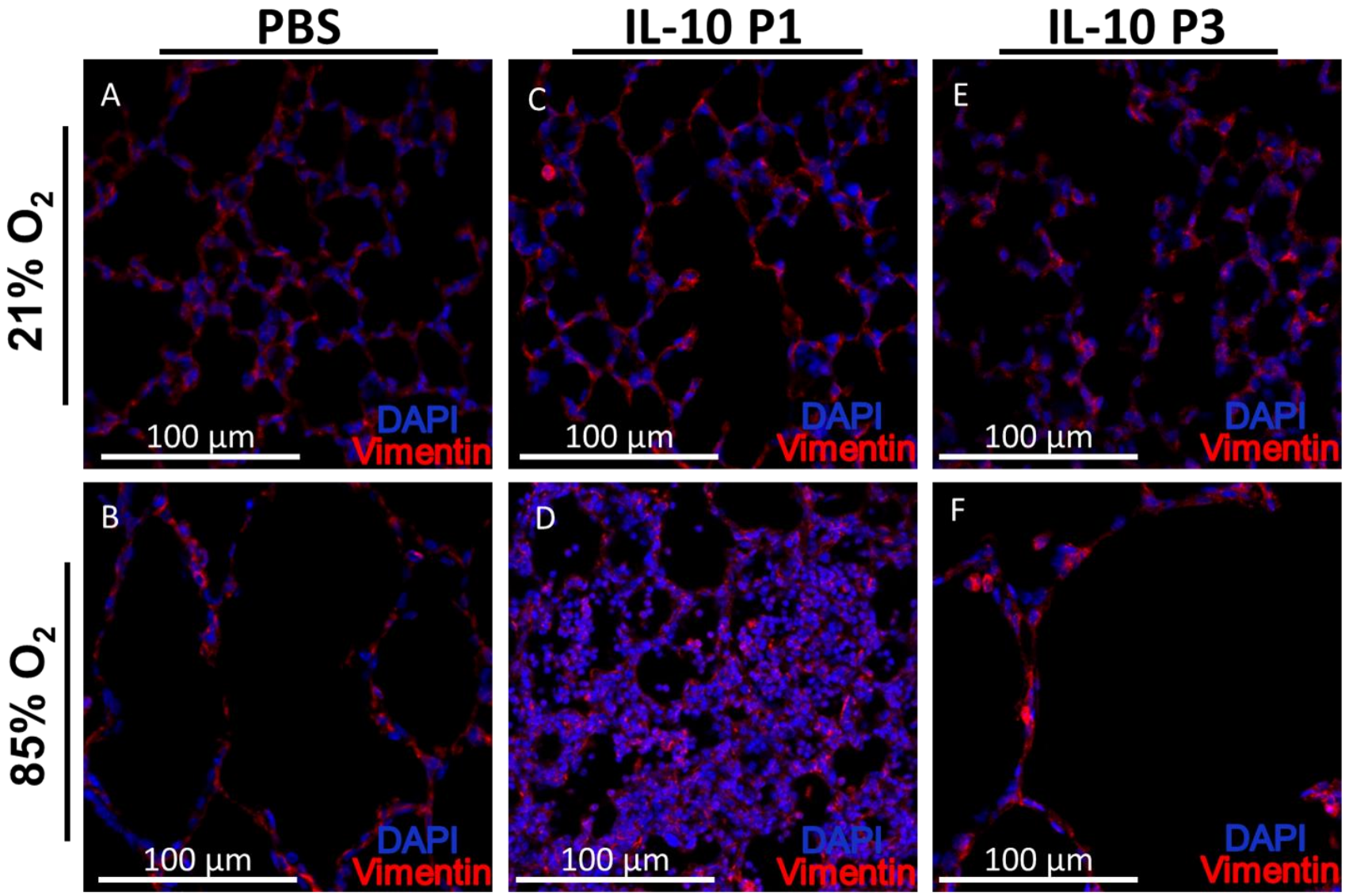

Figure 23. Detection of vimentin in the septa of the normal and aberrant developing lung following treatment with IL-10.
C57BL/6J wild type mice were injected at P1 or at P3 with PBS or recombinant IL-10. Lungs were embedded in paraffin at P14 and stained for vimentin (red) and DAPI (blue), to visualize respectively mesenchymal cells and the nuclei of all cells present in the section. For clarity, only one PBS control is reported; the trends of both controls are comparable.

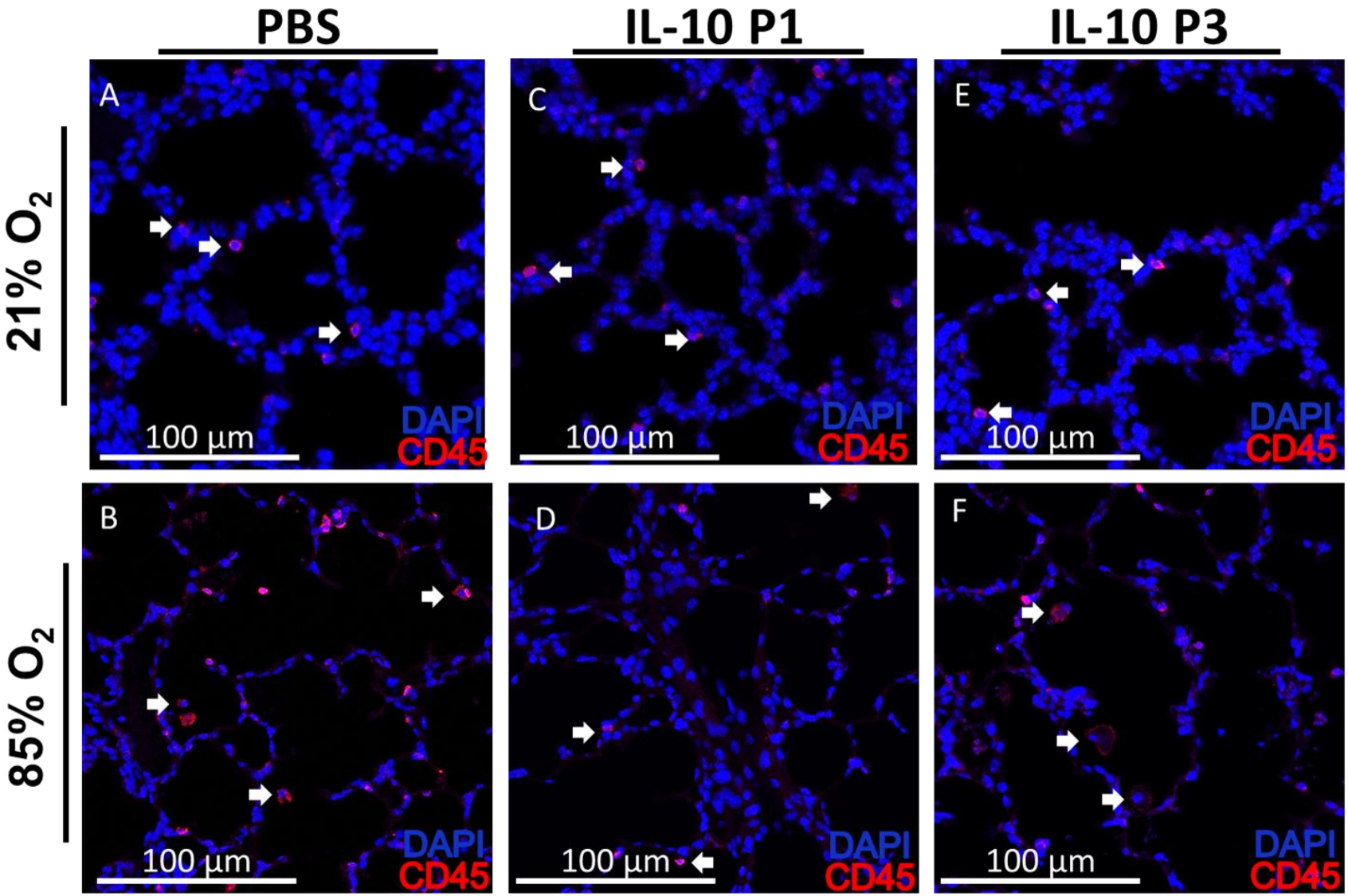

Figure 24. Detection of CD45 in the septa of the normal and aberrant developing lung following treatment with IL-10.
C57BL/6J wild type mice were injected at P1 or at P3 with PBS or recombinant IL-10. Lungs were embedded in paraffin at P14 and stained for CD45 (red) and DAPI (blue), to visualize respectively mesenchymal cells and the nuclei of all cells present in the section. For clarity, only one PBS control is reported; the trends of both controls are comparable.

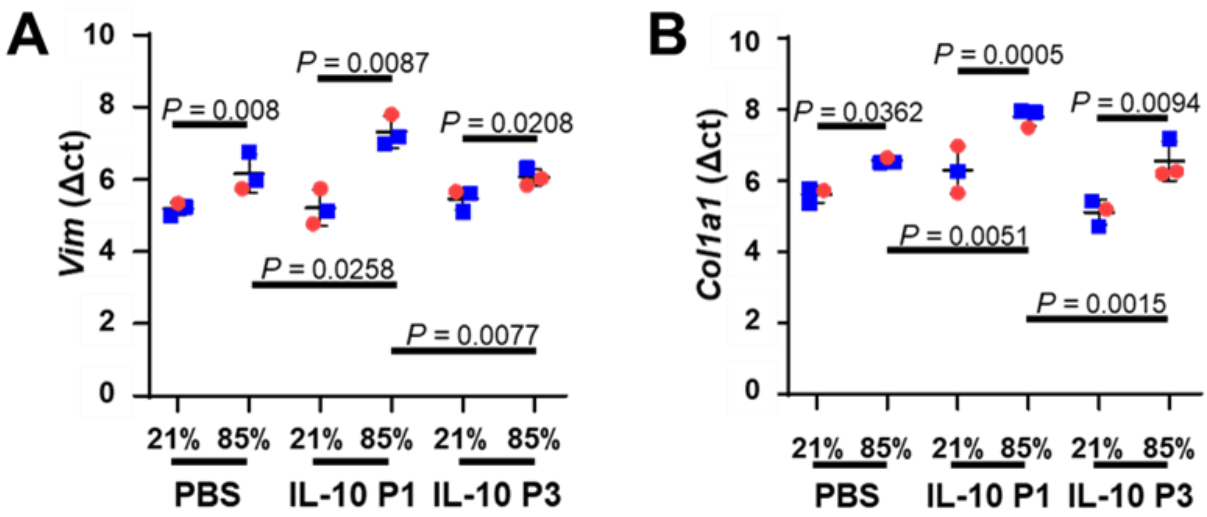

Figure 25. Steady-state mRNA levels of *Vim* and *Col1a1* in the lungs of P14 mice treated at P1 or P3 with IL-10.
Steady-state mRNA levels for (A) *Vim* and (B) *Col1a1* were assessed by RT-PCR in total RNA pools isolated from the lungs of mouse pups at P14 that had been exposed to normoxia or hyperoxia since P1. Pups were injected IP at P1 or at P3 with 50 µg/kg of recombinant IL-10 or PBS. Data represent mean ± S.D. Data comparisons were made by one-way ANOVA with Tukey's *post hoc* test (N=3). Only the statistical comparisons where $P < 0.05$ are presented. Blue square: males; red circles: females. For clarity, only one PBS control is reported; the trends of all controls are comparable.

10.8 Impact of a single IL-10 injection administered at P1 or P3 on innate and adaptive cellular immune response

To assess the impact of IL-10 administration on the cellular immune response in the chronic inflammation milieu associated to BPD, whole lungs isolated from P14 mice injected with PBS or IL-10 at P1 or P3 were isolated and digested via mechanical and enzymatic processing. Resulting cell suspensions were stained with the appropriate cell marker antibodies for select innate and adaptive immune cells and analysed via flow cytometry. The leukocyte subsets selected for analysis in the innate immunity compartment were tissue resident alveolar macrophages (TR-AM) and eosinophils (Figure 26), while in the adaptive immunity compartment total T cells and the $CD4^+$ T helper cells, $CD8^+$ T cytotoxic cells and $CD4^+$ $CD25^+$ T regulatory cells subsets were analysed (Figure 26, Figure 27). Exposure to hyperoxia induced severe loss of TR-AM, and as expected treatment with IL-10 does not rescue the number of resident macrophages in the lungs, neither at P1 nor at P3. TR-AMs detected in lungs of mice exposed to normoxia populate, regardless of treatment, a range between averages of 16,600 and 22,100 units, which drops to a range between averages of 1,500 and 3,300 units in the lungs of mice exposed to hyperoxia (Figure 26A). Conversely, eosinophils levels, which significantly rise in mice exposed to hyperoxia from an average of 6,100 to an average of 14,100 units, are restored, in mice injected with IL-10 at P1 and P3, to levels that closely

resemble those observed in mice exposed to normoxia. The eosinophil count for mice injected at P1 and exposed to normoxia is an average of 8,900 units, which drops to an average of 6,800 units in those exposed to hyperoxia; the eosinophil count for mice injected at P3 and exposed to normoxia is an average of 7,400 units, which drops to an average of 5,700 units (Figure 26B). Total T cells count significantly decreases in mice injected with PBS and exposed to hyperoxia, compared to mice exposed to normoxia; the T cell count drops from an average of 10,500 units to an average of 5,700 units. Treatment with IL-10 at P1 all but restores levels of T cells to those of the normoxia counterparts, rising to an average of 9,500 units *versus* a normoxia cell count of an average of 10,400 units. Treatment with IL-10 at P3 does not significantly impact T cells abundance in mice exposed to either normoxia or hyperoxia; cell count in normoxia achieves an average of 8,900 units *versus* an average of 4,600 units in hyperoxia (Figure 26C). Treatment with IL-10 significantly impacted T cells subsets. Cell counts for $CD4^+$ cells decrease sharply in mice injected with PBS and exposed to hyperoxia compared to mice exposed to normoxia, from an average of 7,000 units to an average of 3,600 units. These levels are restored to an average of 6,500 units in hyperoxia by IL-10 treatment at P1. No significant changes were observed between $CD4^+$ cell counts in mice exposed to normoxia and injected with PBS *versus* mice injected with IL-10, or between mice injected with PBS and mice injected with IL-10 at P3, regardless of the exposure to normoxia or hyperoxia (Figure 27A). Conversely, no significant changes were observed among cell counts of $CD8^+$ T cytotoxic cells in all groups of mice exposed to hyperoxia, with the average cell counts populating a range between 244 and 306 units. However, treatment with IL-10 at P1 and P3 markedly reduces $CD8^+$ cell counts in mice exposed to normoxia compared to the cell counts of mice injected with PBS. The average cell count for mice injected with PBS achieves an average of 339 units, while mice injected at P1 achieve an average of 150 units and mice injected at P3 an average of 199 units (Figure 27B). Treatment with IL-10, regardless of the day in which it was administered, significantly impacts T regulatory cell numbers, which drop, in mice exposed to normoxia, from an average of 600 units in mice injected with PBS to an average of 390 units in mice injected with IL-10 at P1 and to an average of 300 units to mice treated with IL-10 at P3. In mice exposed to hyperoxia, these numbers drop from an average of 550 units in mice injected with PBS to an average of 350 units in mice injected with IL-10 at P1 and 290 units in mice injected with IL-10 at P3 (Figure 27C). Taken together, these data outline a significant impact of IL-10 treatment on the innate and immune cell compartments. Administered at P1, IL-10 does not influence total macrophages cell count in either normoxia or hyperoxia, but it does induce a sharp decrease in the total cell count of eosinophils and an

equally sharp increase in total T cells count at 85% O_2, which can in turn be partly attributed to the significant increase in abundance of the $CD4^+$ T cell subset.

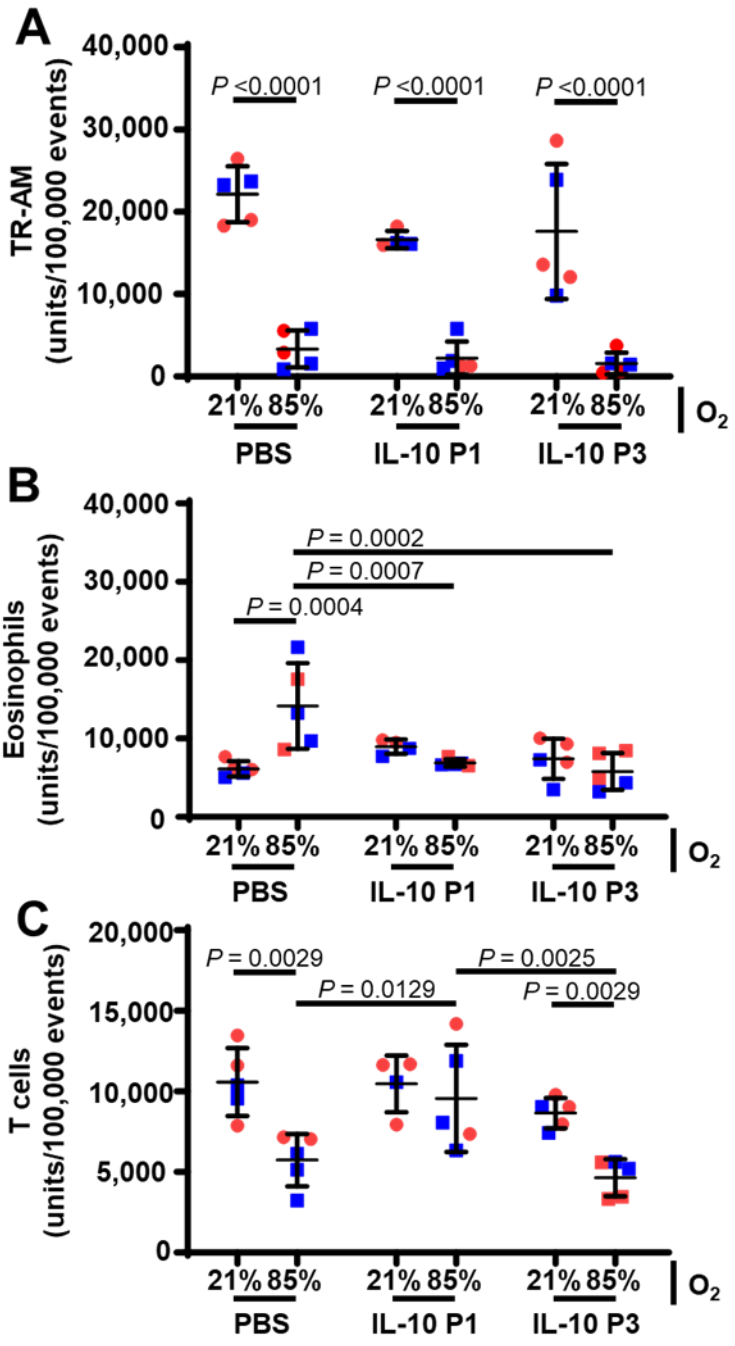

Figure 26. Impact of IL-10 treatment on lung tissue resident macrophages, eosinophils, and T cells.
IL-10 administration on P1 or P3 impacts eosinophils and T cells, but not macrophages, total cell numbers. Tissue resident alveolar macrophages (TR-AM), A), eosinophils (B), and T cells (C) total numbers were assessed at P14 at a counting-stop setting of 100,000 events per lung. Data represent mean ± S.D. Data comparisons were made by two-way ANOVA with Bonferroni's multiple comparisons test (N=5). Only the statistical comparisons where $P < 0.05$ are presented. Blue square: males; red circles: females. For clarity, only one PBS control is reported; the trends of all controls are comparable.

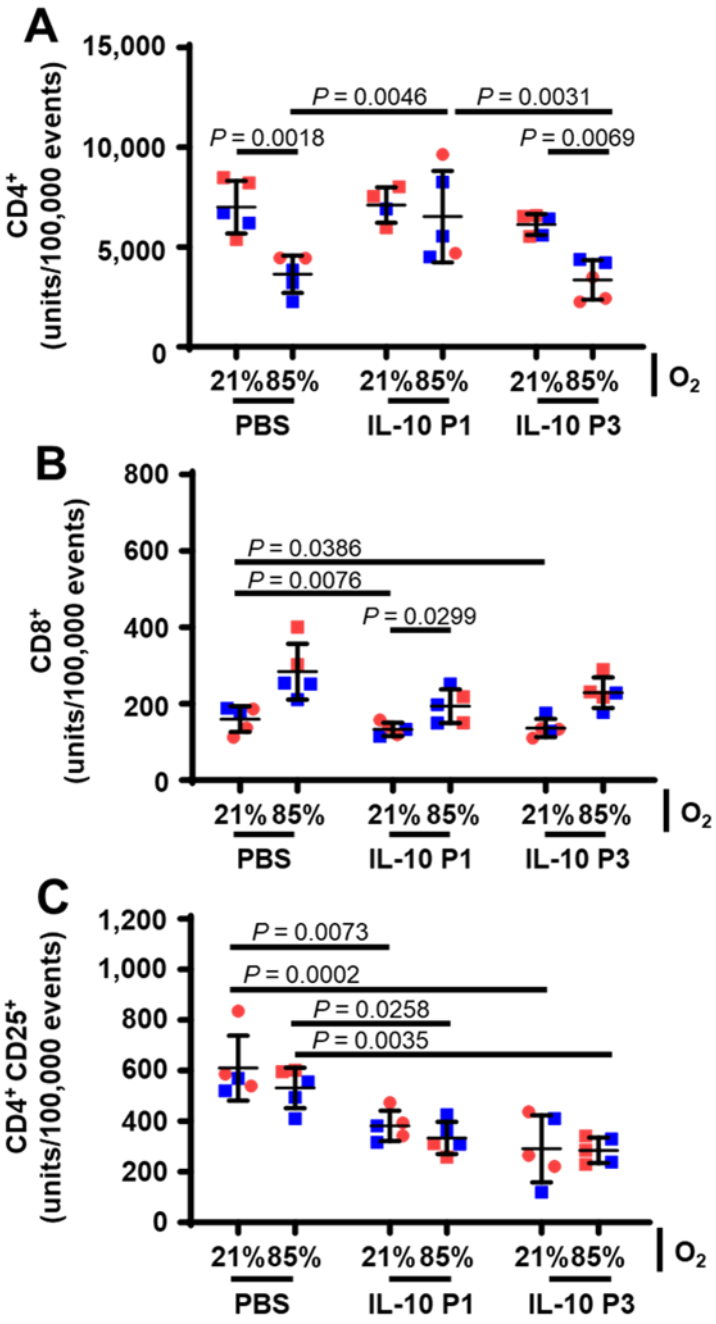

Figure 27. Impact of interleukin-10 treatment on T cell subsets.
Interleukin-10 administration on P1 or P3 significantly impacts total cell numbers of various T cells subsets. $CD4^+$ T helper cells (A), $CD8^+$ T cytotoxic cells (B), and $CD4^+$ $CD25^+$ T regulatory cells (C) total numbers were assessed at P14 at a counting-stop setting of 100,000 events per lung. Data represent mean ± S.D. Data comparisons were made by two-way ANOVA with Holm-Sidak's multiple comparisons test (N=5). Only the statistical comparisons where $P < 0.05$ are presented. Blue square: males; red circles: females. For clarity, only one PBS control is reported; the trends of all controls are comparable.

Cell counts for $CD8^+$ T cells are not majorly impacted by IL-10 treatment in mice exposed to hyperoxia but are significantly reduced in normoxia. While the stark reduction in T regulatory cell numbers after IL-10 treatment suggests lack of tight regulation as a potential explanation

for the increase in $CD4^+$ cell numbers in mice treated at P1 (an effect not seen in mice treated at P3), this reduction in suppressive capabilities is not evident in the altered $CD8^+$ cell numbers of mice treated with IL-10 regardless of the day of administration. These observations indicate that, in addition to subverting the canonical proliferative role played by IL-10 on $CD8^+$ cells, administration of this cytokine induces an alteration of the total cell count of $CD4^+$ $CD25^+$ T regulatory cells, and, potentially synergizing with the P1 administration, increases the count of $CD4^+$ T cells in hyperoxia.

10.9 Impact on the lung transcriptome at P2 and P3 of a single IL-10 injection administered at P1

To investigate the impact of IL-10 administration on a transcriptomic level, RNA sequence analysis on mRNA libraries isolated from whole lung homogenates of newborn mouse lungs was undertaken. The lungs of mouse pups treated with IL-10 or injected with PBS at P1 and exposed to hyperoxia were isolated at P2 and P3 and the transcriptome was sequenced and analysed on a NextSeq500 Illumina sequencing system. The most upregulated and downregulated transcripts are reported in Table 22 and Table 23 for lungs isolated at P2 from mice exposed to hyperoxia, and Table 24 and Table 25 for lungs isolated at P3 from mice exposed to hyperoxia. Volcano plot representations of upregulated (log_2 fold change ≥ 1 in treated mice versus untreated mice) and downregulated (log_2 fold change ≤ -1 in treated mice versus untreated mice) gene transcripts are reported in Figure 30A for libraries isolated at P2 and in Figure 30B for libraries isolated at P3, while RT-PCR validation of the most deregulated transcripts is reported in Figure 31 and Figure 32. Extensive alterations of the transcriptome were identified; 674 transcripts were found to be upregulated and 133 downregulated at P2, while 761 transcripts were found to be upregulated and 493 downregulated at P3. Treatment with IL-10 induces downregulation of crucial, immune-related genes at P2. The expression of *Rag1*, coding for the recombination-activating protein 1, necessary for immunoglobulin class switching, as well as of *Cd8a* and *Cd8b1*, coding surface glycoproteins regulating $CD8^+$ T cell maturation, is strongly downregulated. Conversely, treatment with IL-10 induces, in mice exposed to hyperoxia, upregulation of a subset of genes linked to the epithelial-mesenchymal transition (EMT), at both P2 and P3. The expression of *Lama5*, coding for laminin-5, a mediator of cell migration in EMT, was upregulated at P2, as well as the expression of *Twist1* and *Foxc2*, coding for indirect E-cadherin repressors Twist-1 and FOXC2. These findings outline an early, canonical anti-inflammatory profile of the transcriptome, achieved by IL-10

treatment, which is suggested to switch to a more EMT-oriented profile at P3 in mice exposed to hyperoxia, thus providing a framework through which to interpret the increase in the abundance of fibroblasts in the septa observed at P14.

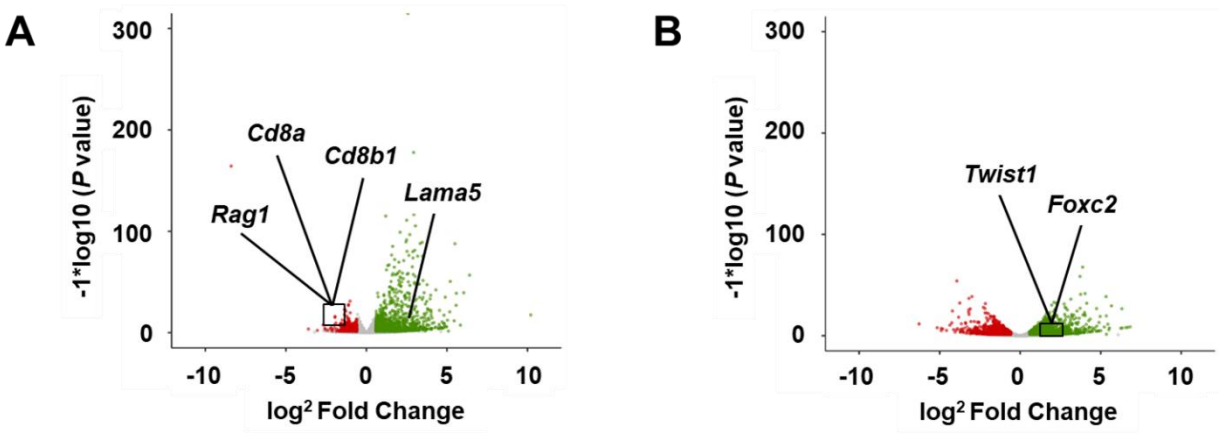

Figure 28.Volcano plots representing relative gene expression in the lungs at P2 and P3 in IL-10-treated and untreated mouse pups exposed to hyperoxia.
Plots represent deregulated genes detected at P2 (A) and at P3 (B) in mouse pups exposed to hyperoxia. Plotted values are colour-coded, representing upregulated genes in green and downregulated genes in red, in treated mice, after comparison to untreated mice.

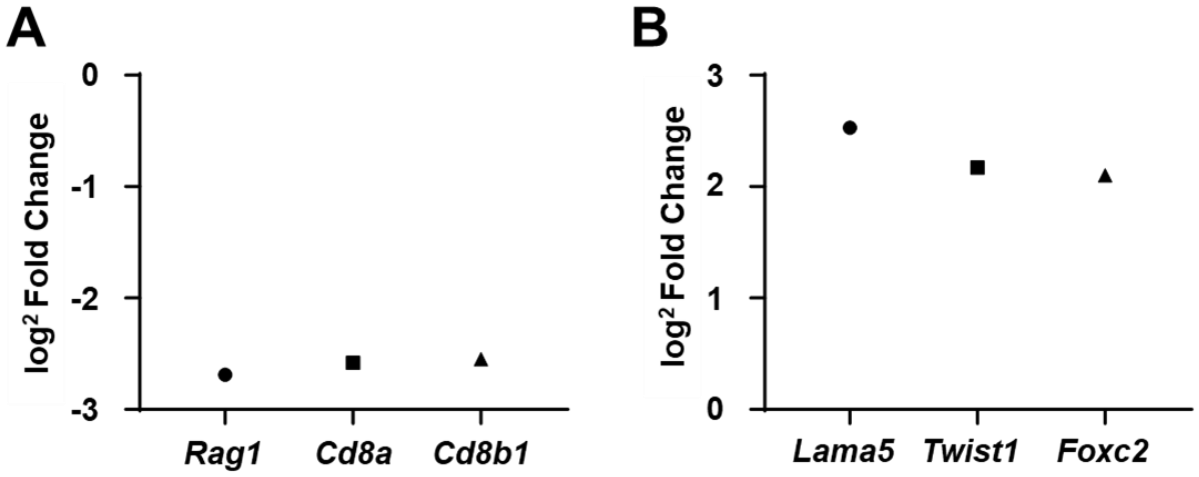

Figure 29. Expression of deregulated genes at P2 and P3 in mice treated with IL-10 at P1 and exposed to hyperoxia.
Data represent the change in the expression of mRNAs of the plotted genes in mice treated with IL-10, as compared to the expression of mRNAs of these genes in mice injected with PBS at P1.

Table 22. Top upregulated genes in whole lung extracts isolated at P2 from mice treated with recombinant IL-10 at P1 and exposed to 85% O_2 *versus* extracts from untreated mice exposed to 85% O_2.

Rank	P (corr)	FC	Gene symbol	Full name
1	0.00	10.20	*Bmp10*	Bone morphogenetic protein 10
2	0.00	6.40	*Nppa*	Natriuretic peptide A
3	0.00	6.04	*Alpk2*	Alpha-protein kinase 2
4	0.00	5.83	*Adipoq*	Adiponectin
5	0.00	5.58	*Ca3*	Carbonic anhydrase 3
6	0.00	5.57	*Ahsg*	Alpha-2-HS-glycoprotein
7	0.00	5.50	*Cacna2d2*	Voltage-dependent calcium channel subunit alpha2/delta2
8	0.00	5.45	*Nppb*	Natriuretic peptide B
9	0.00	5.21	*Sbk2*	Serine/threonine-protein kinase SBK2
10	0.00	5.17	*Xirp2*	Xin actin-binding repeat-containing protein 2
11	0.17	5.09	*Uty*	Histone demethylase UTY
12	0.00	5.03	*Capn11*	Calpain-11
13	0.00	4.98	*Cd207*	C-type lectin domain family 4 member K
14	0.00	4.94	*Tyrp1*	Tyrosinase-related protein 1
15	0.00	4.89	*Alox8*	Arachidonate 8S-lipoxygenase

Abbreviations: FC, fold change; *P* (corr), corrected *P*-value.

Table 23. Top downregulated genes in whole lung extracts isolated at P2 from mice treated with recombinant IL-10 at P1 and exposed to 85% O_2 *versus* extracts from untreated mice exposed to 85% O_2.

Rank	P (corr)	FC	Gene symbol	Full name
1	0.00	-2.69	*Rag1*	V(D)J recombination-activating protein 1
2	0.00	-2.58	*Cd8a*	T-cell surface glycoprotein CD8 alpha chain
3	0.01	-2.55	*Cd8b1*	T-cell surface glycoprotein CD8 beta chain
4	0.03	-2.41	*Crh*	Corticoliberin
5	0.00	-2.25	*Cxcl5*	C-X-C motif chemokine 5
6	0.00	-2.17	*Ibsp*	Bone sialoprotein 2
7	0.02	-2.13	*Bdnf*	Brain-derived neurotrophic factor
8	0.00	-1.99	*Mxd3*	MAX dimerization protein 3
9	0.00	-1.98	*B3galt5*	Beta-1.3-galactosyltransferase 5
10	0.00	-1.95	*Ptpn5*	Tyrosine-protein phosphatase non-receptor type 5
11	0.00	-1.95	*Hoxa7*	Homeobox protein Hox-A7
12	0.00	-1.90	*Pimreg*	Protein FAM64A
13	0.06	-1.78	*H2-Q7*	H-2 class I histocompatibility antigen. Q7 alpha chain
14	0.04	-1.65	*Lrr1*	Leucine-rich repeat protein 1
15	0.00	-1.64	*Pnoc*	Prepronociceptin

Abbreviations: FC, fold change; *P* (corr), corrected *P*-value.

Table 24. Top upregulated genes in whole lung extracts isolated at P3 from mice treated with recombinant IL-10 at P1 and exposed to 85% O_2 *versus* extracts from untreated mice exposed to 85% O_2.

Rank	P (corr)	FC	Gene symbol	Full name
1	0.00	6.83	*Mmp10*	Stromelysin-2
2	0.00	6.68	*Serpina3m*	Serine protease inhibitor A3M
3	0.00	6.34	*Kcng1*	Potassium voltage-gated channel subfamily G member 1
4	0.00	6.32	*Mmp3*	Matrix metallopeptidase 3
5	0.00	6.25	*Tnfsf18*	Tumor necrosis factor ligand superfamily member 18
6	0.00	5.66	*Pla1a*	Phospholipase A1 member A
7	0.00	5.54	*Clec2e*	C-type lectin domain family 2 member E
8	0.00	5.51	*Calcr*	Calcitonin receptor
9	0.00	5.44	*Prmt8*	Protein arginine N-methyltransferase 8
10	0.00	5.35	*Lrtm2*	Leucine-rich repeat and transmembrane domain-containing protein 2
11	0.00	5.33	*Ereg*	Proepiregulin
12	0.00	5.22	*Dclk3*	Serine/threonine-protein kinase DCLK3
13	0.00	5.01	*Oas1e*	2-5 oligoadenylate synthetase 1E
14	0.00	4.96	*Fosl1*	Fos-related antigen 1
15	0.00	4.89	*Sall1*	Sal-like 1 (Drosophila),Sal-like protein 1

Abbreviations: FC, fold change; *P* (corr), corrected *P*-value.

Table 25. Top downregulated genes in whole lung isolated at P3 from mice treated with recombinant IL-10 at P1 and exposed to 85% O_2 *versus* extracts from untreated mice exposed to 85% O_2.

Rank	P (corr)	FC	Gene symbol	Full name
1	0.00	-6.28	*Cyp1a1*	Cytochrome P450 1A1
2	0.00	-5.16	*Slc22a19*	Solute carrier family 22 member 19
3	0.00	-4.90	*Tmem233*	Transmembrane protein 233
4	0.00	-4.90	*4833423E24Rik*	Fatty acid desaturase 2-like protein FADS2P1
5	0.00	-4.82	*Pnoc*	Prepronociceptin
6	0.00	-4.37	*Colec10*	Collectin-10
7	0.00	-4.25	*Zfp663*	Zinc finger protein 663
8	0.00	-4.21	*Cpa1*	Carboxypeptidase A1
9	0.00	-4.13	*Clca3a2*	Chloride channel accessory 3A2
10	0.00	-4.04	*Magel2*	MAGE-like protein 2
11	0.00	-3.97	*Cst8*	Cystatin-8
12	0.00	-3.93	*Dlk1*	Protein delta homolog 1
13	0.00	-3.89	*Dcx*	Neuronal migration protein doublecortin
14	0.00	-3.83	*Treml4*	Trem-like transcript 4 protein
15	0.00	-3.75	*Slc7a10*	Asc-type amino acid transporter 1

Abbreviations: FC, fold change; *P* (corr), corrected *P*-value.

11 Discussion

Bronchopulmonary dysplasia develops from a multitude of factors, from prematurity to barotrauma, volutrauma and high oxygen toxicity resulting from ventilation. Although lifesaving, the outcome of the combination of these factors is invariably, among other complications, chronic inflammation, which leads to aberrant lung development and stunted alveolarization through repeated cycles of lung damage and impaired repair (54). Interleukin-10, a cytokine considered the main mediator of the anti-inflammatory response, has long been regarded as one of the most promising molecules to be harnessed for countering the immune imbalance underpinning the structural changes in lung architecture in BPD. However, IL-10 administration elicits pleiotropic, often contrasting effects, cascading through a dense network of interactions (81, 147). To date, this is the first study to investigate the impact of IL-10 administration in normal and aberrant lung development, employing a severe hyperoxia mouse model to recapitulate the main hallmarks of BPD. After establishing an effective IL-10 administration protocol, lung morphology, septal cell composition, leukocyte populations and gene expression regulation have been investigated as the main areas of inquiry for this study.

11.1 Assessment of IL-10 expression levels in mouse late lung development

Due to the prominent anti-inflammatory role IL-10 plays in the immune response, this cytokine has been extensively studied, both in humans and in mouse models of disease, with the ultimate objective of manipulating it as a therapeutic modality. This has been especially true in relation to BPD, where the prominence of chronic inflammation among the root causes of the disease has prompted wide-ranging efforts with the aim to modulate inflammation. Adding a layer of complexity to IL-10 studies is the lack of consensus on the link between expression of this cytokine and severity of BPD in preterm infants. While some studies promote high levels of IL-10 as a risk factor (5, 27), others describe a link between reduced expression of IL-10 and worse outcomes (42, 96). In our lab, a study by Madurga and coworkers (94) confirmed a significant reduction in IL-10 levels in our mouse model of BPD. Additionally, to date there is no available data on IL-10 modulation over the course of mouse late lung development. Therefore, steady-state levels of mRNA for the genes coding for IL-10 and both subunits of the IL-10 receptor (respectively *Il10*, *Ilra* and *Ilrb*) and the relative abundance of mature IL-10 protein have been assessed throughout late lung development, normal and aberrant, in our mouse model of BPD. To gather a comprehensive overview of IL-10 expression throughout

the postnatal lung development process, three time points have been chosen, P3, P5 and P14, corresponding respectively to the pre-, peak, and post-alveolarization phase of postnatal mouse lung development. Although steady-state mRNA levels of *Il10* do not seem to differ between mice subjected to normoxia and hyperoxia at P3, a reduced abundance of the protein has been detected; nevertheless, at P5 and P14, in both mRNA steady-state levels and protein abundance in mice exposed to hyperoxia a significant drop compared to normoxia was detected, thus aligning these findings with those previously reported by our lab and other groups and adding important information on the regulation of IL-10 during lung development. Of note, steady-state mRNA levels of *Ilra* and *Ilrb* appear to follow an opposite trend, being significantly higher towards the end phase of the alveolarization process in mice exposed to hyperoxia compared to levels in mice exposed to normoxia. This suggests that the IL-10 signalling machinery is ready and primed in the context of BPD, with the relative scarcity of IL-10 as the limiting factor of the activation of the signalling cascade.

11.2 Establishment of an effective experimental IL-10 dosage

The complex network of factors involving IL-10 activity has proven to be a severe hurdle in the standardization of the dosage of exogenous administration of IL-10, both in adult and newborn mice. To date, the approaches employed have varied wildly, and a general consensus has not been firmly established (36, 77, 83, 85, 100). In this study, to ensure constant availability of IL-10 to the lungs, a daily IP injection regime was initially undertaken, and to better identify the dose of recombinant protein most likely to induce a robust anti-inflammatory response, a trio of doses, 50, 100 and 150 μg/kg, were tested on different mouse cohorts exposed to normoxia or hyperoxia. Directly detecting changes in IL-10 levels following the treatment has proved technically unreliable; changes in the gene expression of three key factors of the inflammation process, two cytokines, IFNγ and TNF-α, and the soluble form of the receptor for TNF-α, TNFR1B, have been assessed instead, functioning as indirect reporters of the modulation of the inflammatory milieu. IFNγ and TNF-α have been selected due to the well-documented pro-inflammatory activity these molecules exhibit (69, 75), while TNFR1B has been reported to stimulate T regulatory cells and is often indicated as a marker of anti-inflammatory immune activity (23, 151). Steady-state levels for all three genes were found to be elevated in mice exposed to hyperoxia, compared to normoxia, as expected in a chronic inflammation environment, where a balance of pro- and anti-inflammatory factors effectively impedes a successful resolution of the inflammation (149). In mice treated daily with IL-10 at

a dose of 50 μg/kg, diametrically opposed effects have been achieved in the cohorts of mice exposed to normoxia compared to those exposed to hyperoxia. In mice exposed to 21% O_2, IL-10 treatment elicits a pattern of expression of *Ifng, Tnf* and *Tnfrsf1b* with strong links to inflammation; while in the case of *Tnf* the levels of expression achieved are lower compared to those detected in mice injected with PBS and exposed to hyperoxia, in both other genes an increase in the expression level, which is fully comparable to the levels detected in mice injected with PBS and exposed to hyperoxia, was detected. Conversely, the treated cohorts exposed to hyperoxia were found to express undetectable levels of mRNA for *Ifng* and *Tnf* and an even more marked increase in the mRNA levels of *Tnfrsf1b*. These results clearly indicate both sides of IL-10 action. A potent pro-inflammatory activity is detected in mice with no ongoing inflammation, while an incisive anti-inflammatory milieu is suggested to be achieved in mice exposed to hyperoxia and suffering from chronic inflammation. Of note, previous studies have also reported that relatively higher doses of IL-10 induces either no effect or a trend towards the switch to a pro-inflammatory immune response (97, 167). Taken together, these data indicate that, among those tested, treatment with 50 μg/kg is best suited to elicit an anti-inflammatory response in the lungs of mice exposed to hyperoxia and was therefore selected and employed in all subsequent experiments.

11.3 Daily IL-10 administration treatment and global IL-10 deletion do not impact normal or aberrant lung development

To date, no study has addressed the impact of constant, elevated IL-10 systemic availability on mouse lung development. Hence, C57BL/6J wild type mice received daily IP IL-10 injections and were exposed to either normoxia or hyperoxia from the day of birth to P14. Stereological analysis of the lungs isolated from these mice indicates that IL-10 daily administration had no impact on lung architecture, normal or aberrant. While the cytokine response to IL-10 administration in mice exposed to 21% O_2 suggests a switch of the immune activity towards a pro-inflammatory environment, this response is potentially not intense or pervasive enough to induce any structural alteration in the lung morphology. The lack of any detectable effect in mice exposed to hyperoxic conditions indicates, on the other hand, that although constant availability of IL-10 does constitute a factor capable of tilting the balance towards an effective anti-inflammatory response, a simple abatement of this inflammatory milieu is not sufficient to improve aberrant lung development. As BPD is a complex, multifactorial disease, mechanisms of pathogenesis other than inflammation are considered equally responsible for

stunted lung alveolarization. As an example, the oxidative stress resulting from hyperoxia leads to disruption of growth factor signalling, cell proliferation, apoptosis and vasculogenesis (93), thus significantly contributing to aberrant lung development. To assess the impact of *Il10* deletion in postnatal mouse lung development, a global IL-10 knockout mouse model was employed. This model, first reported by Kühn and coworkers in 1993, is widely used in studies on autoimmunity and is especially useful to model enterocolitis, which these mice develop spontaneously when not housed in specific pathogen-free facilities (79). Due to the lack of inflammation, a reduced role (and, consequently, no impact) of IL-10 deletion in the lung of mice exposed to normoxia conforms to expectations; however, in this model, global deletion of IL-10 also does not impact aberrant lung development. In this instance, the balancing act of competing factors during chronic inflammation could explain the lack of impact of IL-10 scarcity on aberrant lung architecture. Interleukin-4, for example, has been proven to exhibit strong compensatory effects in IL-10 deficient mice (6), while low-dose oestrogen has been reported to be able to orchestrate an anti-inflammatory immune response in the nervous system in the absence of IL-10 (153).

11.4 Single IL-10 injection treatment at P1, but not at P3, significantly impacts hyperoxia-induced aberrant lung development

The wide range of IL-10 administration modalities employed in literature is a clear indication that adjustments in IL-10 dosage could introduce new perspectives and have a different impact on the normal and aberrant lung development. It has been demonstrated, in a plurality of experiments by different research groups, that a single injection of recombinant IL-10 can be successfully employed, at a variety of concentrations and at a variety of time points, to achieve experimental goals (36, 85, 100, 106). To assess whether this approach could be feasible for the present study, a single IP injection of 50 μg/kg was administered at P1 to newborn mouse pups subsequently exposed to normoxia and hyperoxia until P14. Strikingly, profound effects on the inflammatory response were detected even at such a late time point from the date of injection, indicating that a marked anti-inflammatory response was still active in mice exposed to hyperoxia. Additionally, mice exposed to normoxia also exhibit abatement of *Ifng* and raised levels of *Tnf* and *Tnfrsf1b*, which could be linked to the TNFR1B-mediated immunosuppressive activity of TNF-α (151), thus pointing towards an anti-inflammatory environment stimulated by the single IL-10 injection. Strikingly, lung architecture in mice exposed to hyperoxia was severely affected compared to mice exposed to normoxia. Septa are

markedly thickened and exhibit an altered morphology, compared to the septa of mice exposed to hyperoxia which did not receive IL-10, resulting in a marked reduction in the surface area of gas exchange. No changes were observed in the lungs of mice injected with IL-10 and exposed to normoxia. The role of IL-10 as an indirect actor in cell proliferation or as a growth factor has been already established by various groups in the last decade (29, 30, 134), including the implication of direct IL-10 trophic activity in cancer progression (41, 126). However, to date, available information on the activity of IL-10 as a growth factor in the lung is scarce, although previous studies have reported that IL-10 administration is indeed capable of countering the inhibitory effect of IFNγ on lung fibroblast proliferation during inflammation (53). To further elucidate the impact of single-injection IL-10 administration in the developing lung, a second time point, P3, was selected, as a later time point meant to coincide with the beginning of peak secondary septation. Strikingly, no impact was detected in the lung architecture of mice injected with IL-10 and exposed to normoxia or hyperoxia, compared to that of mice injected with PBS. These data suggest that exogenous IL-10 severely impacts lung architecture in the hyperoxia model of BPD when administered in a time frame restricted to the first 24 hours of postnatal lung development.

11.5 Single IL-10 injection treatment at P1, but not at P3, impacts the abundance of fibroblasts in the developing mouse lung exposed to hyperoxia

The observed further thickening of the septa in the lungs of mice exposed to hyperoxia following IL-10 injection could be attributable to a change in the quantity of cells composing the septum itself. To elucidate the impact of IL-10 administration on the cell abundance in the septa of the developing mouse lung, a series of immunohistochemistry stainings were carried out. Paraffin sections from the lungs of P14 newborn mice treated at P1 or P3 with IL-10 or with PBS were stained with different cell markers to visualize the main structural components of the lung septum, epithelial cells (AECI and AECII) and fibroblasts. Additionally, to investigate whether leukocyte infiltration could contribute to the thickening of the septa, a staining against CD45 was performed. Counterstaining with DAPI detected a marked increase in the number of cells in the thickened septa of mice exposed to hyperoxia after IL-10 injection at P1, while no change was observed in mice injected with PBS or with IL-10 at P3. When compared with the other experimental cohorts, an increase in the abundance of fibroblasts was detected in mice injected at P1 and exposed to hyperoxia. An indirect role played by IL-10 in the proliferation of fibroblasts through the activation of macrophages has been reported (162);

furthermore, in studies on the impact of IL-10 administration in wound healing, this cytokine has been also reported to induce de-differentiation of myofibroblasts into non-fibrotic fibroblasts (70). It is possible therefore to speculate on a potential proliferative activity of exogenous IL-10, which, through the activation of the epithelial-mesenchymal transition machinery, results in the formation of thickened septa. In this regard and considering the observed impact of IL-10 administration on the architecture of the lung exposed to hyperoxia, the application of this cytokine as a therapeutic modality for improving the fate of lung epithelium requires a careful approach and further investigation.

11.6 Single IL-10 injection treatment rescues eosinophilia and alters T cell count in the developing lung

The activity exerted by IL-10 is primarily indirect, acting on a deep and complex network of interactions to inhibit most pro-inflammatory cytokines and to induce production of anti-inflammatory factors, thus blocking the activation of inflammatory pathways (106). In the context of chronic lung inflammation, this activity impacts primarily macrophages, eosinophils, and T cells. The key role played by resident macrophages in inflammation and defence from pathogen is to the forefront of BPD research, due to the complications that arise from macrophage abatement, immaturity, and polarization towards a pro-inflammatory response, which are hallmarks of the disease (141, 156). The recent identification of a possible causal link between resident macrophages activated by hyperoxia and aberrant lung development casts a light on a new, trophic potential of the monocyte/macrophage lineage (72). Additionally, the impact of eosinophilia in chronic diseases like asthma and BPD has been widely reported; activation and infiltration of eosinophils has indeed been reported to positively correlate with the severity of BPD, although the underlying pathological mechanisms have not been completely elucidated (180, 182). Lastly, a dysregulation of T cells activation and proliferation has been suggested to play a major role in the chronic inflammatory milieu of BPD; the most reported lymphocyte profile consists of a reduction in the total count of T cells, paired with a higher fraction of activated cells and a further reduction in T regulatory cells, indicating the presence of an unchecked inflammatory response, which leads to tissue damage and remodelling (104, 159, 171). In the present study, IL-10 administration to mice exposed to normoxia or hyperoxia is reported to impact quite dramatically the cellular immune response compartment. Total eosinophil cell counts, raised by hyperoxia exposure, are rescued by IL-10 treatment at P1 and at P3, in accordance with the classical role of IL-10 as an inducer of

eosinophil apoptosis (1). However, tissue resident macrophages cell counts, already dramatically abated in mice exposed to hyperoxia, are not significantly impacted by IL-10 treatment, most likely due to the potent antiproliferative activity of this cytokine (119). Although not introducing any significant variation in macrophage abundance, a trend can nonetheless be observed where the cell counts of tissue-resident macrophages appear to decline in hyperoxia-exposed mice, following IL-10 treatment at P1 or P3, compared to PBS-injected mice, suggesting a moderate inhibition of macrophage proliferation. Strikingly, the impact of IL-10 treatment at P1 on T cells appears to deviate from the established canonical roles of this molecule. An almost doubling of the cell count for lymphocytes in mice exposed to hyperoxia was observed, mostly due to a $CD4^+$ cell count increase of about 50%, while no significant impact was observed in mice treated at P3. Conversely, no significant change was detected in $CD8^+$ cell count in mice treated at P1 and P3 and exposed to hyperoxia, while a stark drop in cell count was detected in treated mice exposed to normoxia, resulting in another deviation from the established $CD8^+$ stimulatory role played by IL-10. The generalized reduction in $CD4^+$ $CD25^+$ T regulatory cell numbers following IL-10 treatment at both P1 and P3 in mice exposed to either normoxia or hyperoxia offers a partial explanation for the changes observed in $CD4^+$ cell numbers; exogenous IL-10 very possibly adds to the levels of endogenous IL-10 secreted by T regulatory cells, thus deactivating lymphocytes through a feedback loop. The count of $CD8^+$ cells exhibits no significant variation in mice exposed to hyperoxia, regardless of the treatment administered; due to the mainly cytotoxic role exhibited by these cells, it is plausible to speculate that a sterile inflammation milieu like the one induced by hyperoxia does not result in significant activation of this subset, and consequently no impact from IL-10 could be detected. Interestingly, in a study by Sawant and co-workers (146) IL-10 has indeed been reported to promote $CD8^+$ depletion in chronic inflammation, an impact observed in a non-inflammatory environment in the present study. These data depict novel, potentially non-canonical avenues of activity of IL-10 on the immune cell response mobilized by hyperoxia and add to the rich tapestry of interaction of this molecule, at the same time introducing additional caveats to the administration of IL-10 as a therapeutic modality.

11.7 IL-10 treatment induces a late switch to an epithelial-mesenchymal transition transcriptomic profile in mouse pups exposed to hyperoxia

To further elucidate the mechanisms leading to the observed impact of IL-10 on the morphology of the developing neonatal lung, an RNA sequencing analysis was undertaken on

lungs isolated from P2 and P3 mouse pups treated at P1 and exposed to hyperoxia from birth *versus* lungs of newborn mice exposed to hyperoxia but injected with PBS. This specific methodology and its application to the whole lung were selected to gain an overview of the complex, pleiotropic effects of IL-10 and the impact of the administration of this cytokine on multiple compartments of the organ at once. As expected, a rather strong early anti-inflammatory effect was detectable 24 h after administration, as indicated by the upregulation of genes coding for anti-inflammatory molecules like natriuretic peptides A and B (101), and, more extensively, by the downregulation of key mediators of the immune response like, among others, *Rag1*, responsible for coding V(D)J recombination-activating protein 1, involved in the antibody and T cell receptor V(D)J recombination, as well as *Cd8a* and *Cd8b1*, coding for the alpha and beta chains of the T cell coreceptor for the MHC class I of peptide receptors. What could be defined as a late switch towards an EMT profile of expression was detectable at P3 in mice exposed to hyperoxia; genes found to be upregulated at such time point include genes coding for factors involved in the promotion of EMT, like laminin 5, Twist-1 and FOXC2. Aside from the widely reported and firmly proven trophic role for IL-10 in $CD8^+$ T cells, observations involving a positive correlation of IL-10 with the proliferation of non-immune cells have been sparsely documented, and never in the lungs (3, 189). These observations hint to potential mechanisms through which IL-10 administration could induce the development of the severely affected septa observed in the lungs of mice exposed to hyperoxia. Taken together, the data reported by this study offer the first report of a potential synergy between chronic lung injury and IL-10 towards the further aggravation of the aberrant lung development phenotype induced by hyperoxia. This suggests once more that a cautious approach towards IL-10 as a clinical modality is to be preferred.

12 Outlook and limitations of the study

Interleukin-10 is a powerful, pleiotropic cytokine described as the key regulator of the anti-inflammatory component of the immune response. As a chronic respiratory disease with a crucial inflammatory component, bronchopulmonary dysplasia was considered the ideal background for an investigation of the potential of the administration of IL-10 as a therapeutic modality. An analysis of the impact of IL-10 in the normal and aberrant lung development has been provided, utilizing a murine model of BPD based on hyperoxia for all animal studies. After the identification of a dosage more likely to exert an anti-inflammatory effect, an analysis

of how the constant availability or the complete lack of IL-10 impacted newborn lung development followed, reporting a remarkable dearth of changes. An adjustment to a single injection on the day of birth, as opposed to a daily administration regime, induced a significant aggravation of the septal structure in the lungs of mice exposed to hyperoxia, a result that a later injection at postnatal day 3 failed to replicate. A more in-depth analysis of the affected septal structures revealed an increase in the abundance of fibroblasts; this deregulation of the processes leading to the formation of the septa is mirrored by the switch from an anti-inflammatory transcriptomic profile, observed 24 h after IL-10 injection in mice exposed to hyperoxia, to a later one more committed to epithelial-mesenchymal transition. To date, this study is the first to report on a relevant impact of interleukin-10 on the architecture of the developing lung afflicted by chronic inflammation. Thus, to elucidate the impact of IL-10 administration in the immune compartment of the developing lung, an analysis of the relative abundance of selected immune cell types was undertaken, indicating that IL-10 treatment rescues the eosinophilic milieu associated to BPD, while at the same time greatly increasing the absolute numbers of T cells when administered at P1, but not at P3. A deeper observation of the main T cell subsets, $CD4^+$, $CD8^+$, and $CD4^+$ $CD25^+$, reveals that the main increase in T cell number at P1 can be ascribed to an almost doubling of $CD4^+$ cell numbers, while $CD4^+$ $CD25^+$ cells undergo a significant reduction. No changes were detected in the abundance of $CD8^+$ cells in hyperoxia, regardless of the day in which the treatment was administered. While exogenous IL-10 could enter a feedback loop with the endogenous counterpart secreted by T regulatory cells, thus inhibiting proliferation, a lack of regulation could also be a factor in the rise in $CD4^+$ cell numbers, although this increase is visible only in mice injected at P1. This reveals a deeper, more complex layer of interactions between interleukin-10 and the immune system, that calls for further exploration, especially in consideration of the fact that more specialized subsets of T cells, especially $CD4^+$ subsets like Th1, pro-inflammatory, and the anti-inflammatory Th17, Th2 and Th3 (44), which could play a more nuanced role in the observed impact of IL-10 administration, were out of the scope of this study.

13 Appendix

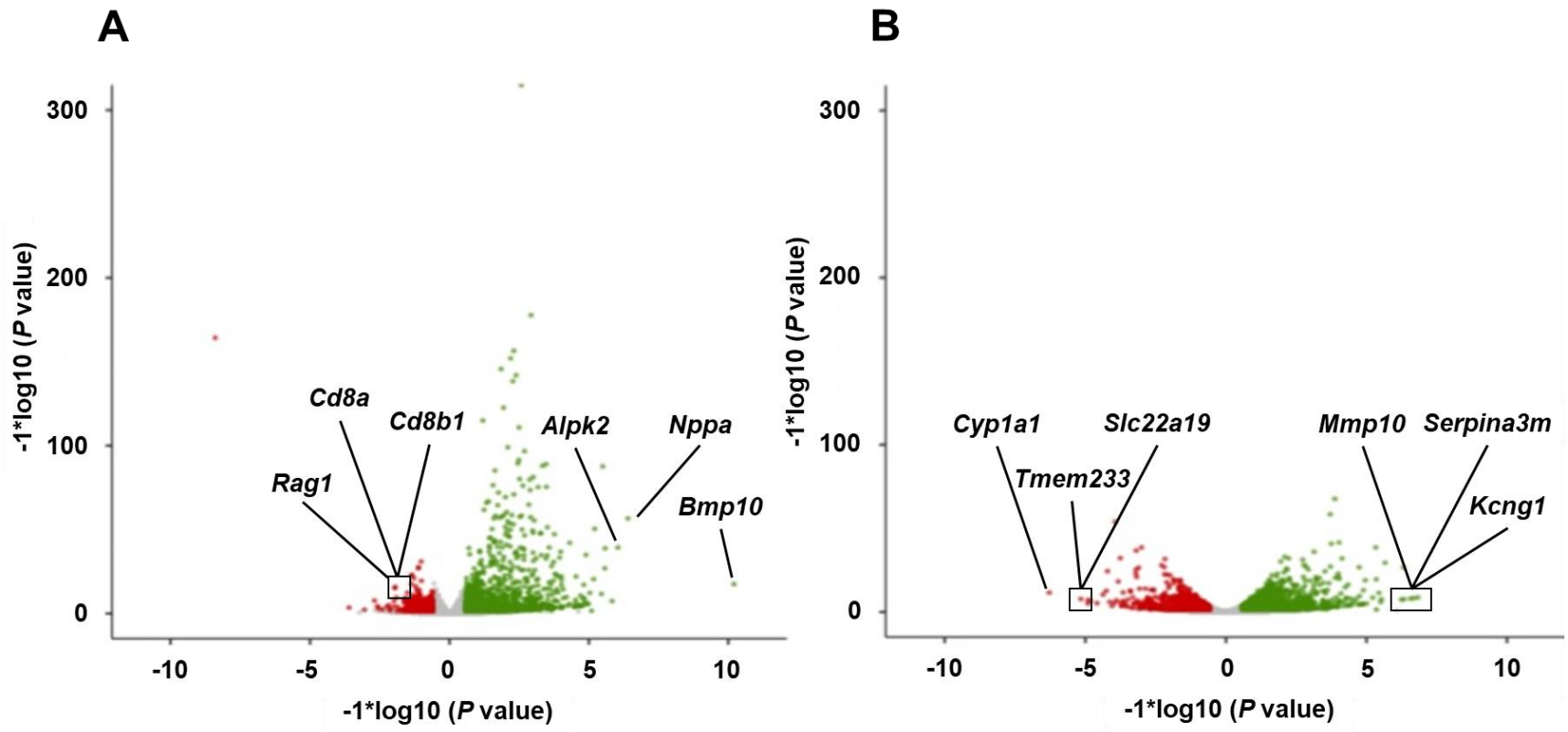

Figure 30. Volcano plots representing relative gene expression in the lungs at P2 and P3 in treated and untreated mouse pups exposed to hyperoxia.
Plots represents deregulated genes detected at P2 (A) and P3 (B). Genes are colour-coded as upregulated, green, or downregulated, red, in treated mice after comparison to untreated mice. Genes whose steady-state levels were assessed for the validation of the sequencing analysis (Figure 31) are reported on the plots.

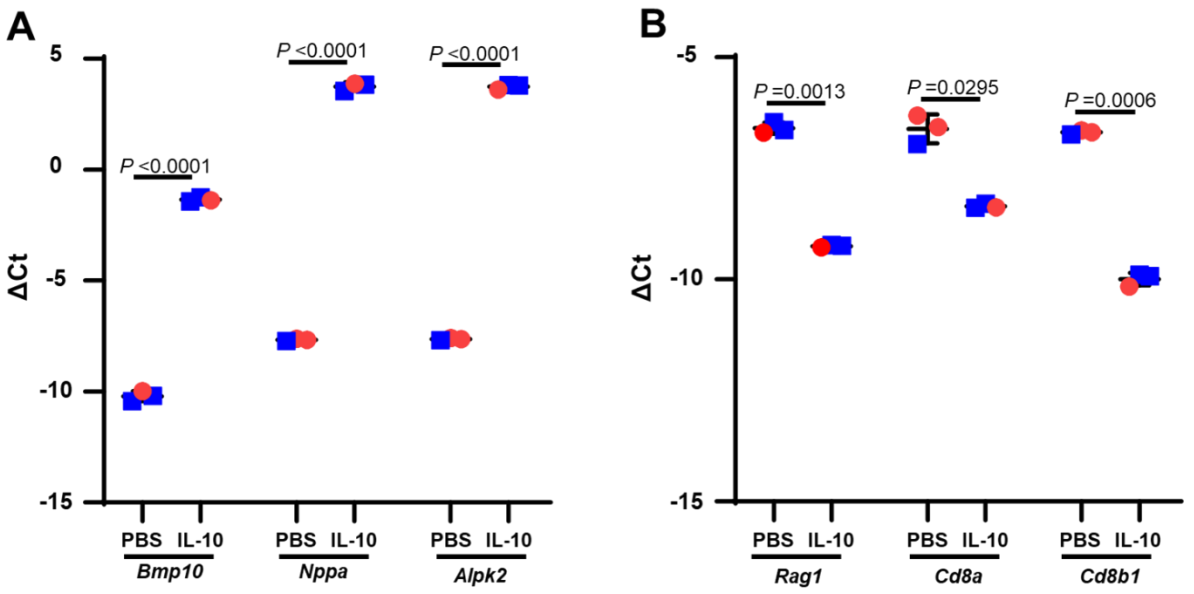

Figure 31. Steady-state mRNA levels of the most deregulated genes at P2 in the treated and untreated neonatal mouse lung exposed to hyperoxia.
Steady-state mRNA levels for (A) the 3 most upregulated and (B) the 3 most downregulated genes identified in the lung transcriptome at P2 were assessed by RT-PCR in total RNA pools isolated from the lungs of mouse pups that had been exposed to hyperoxia since P1. Pups were injected at P1 with 50 µg/kg recombinant IL-10 or PBS. Data represent mean ± SD. *P* values were determined by one-way ANOVA with Tukey's *post hoc* test (N=3). Only the statistical comparisons where $P < 0.05$ are presented. Blue square: males; red circles: females.

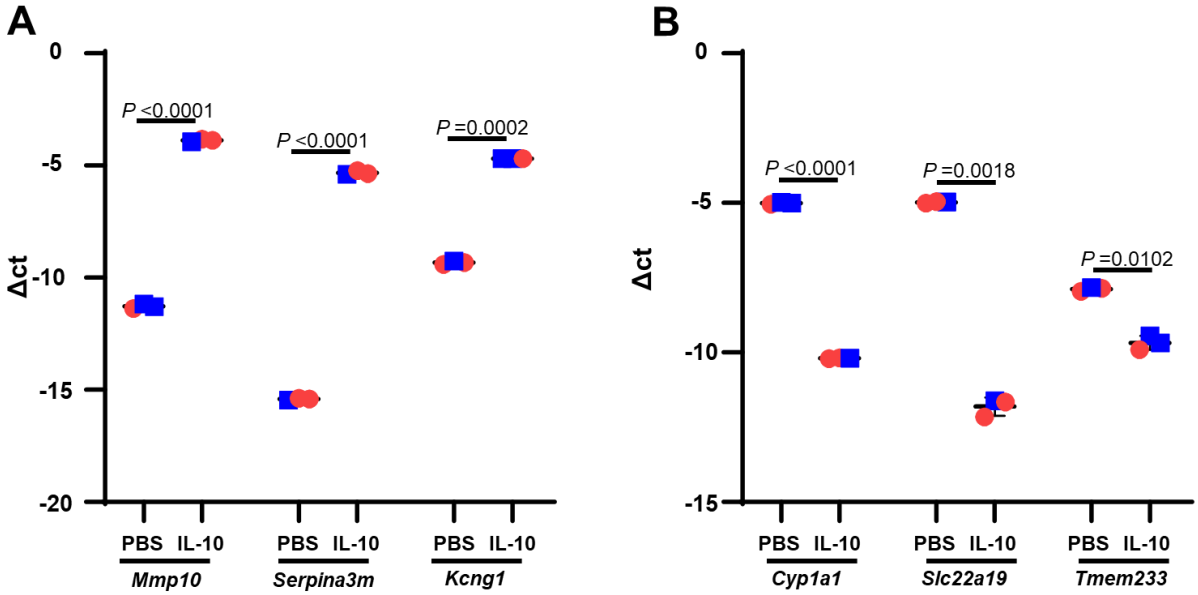

Figure 32.Steady-state mRNA levels of the most deregulated genes at P3 in the treated and untreated neonatal mouse lung exposed to hyperoxia.
Steady-state mRNA levels for (A) the 3 most upregulated and (B) the 3 most downregulated genes identified in the lung transcriptome at P3 were assessed by RT-PCR in total RNA pools isolated from the lungs of mouse pups that had been exposed to hyperoxia since P1. Pups were injected at P1 with 50 µg/kg recombinant IL-10 or PBS. Data represent mean ± SD. *P* values were determined by one-way ANOVA with Tukey's post hoc test (n=3). Only the statistical comparisons where $P < 0.05$ are presented. Blue square: males; red circles: females.

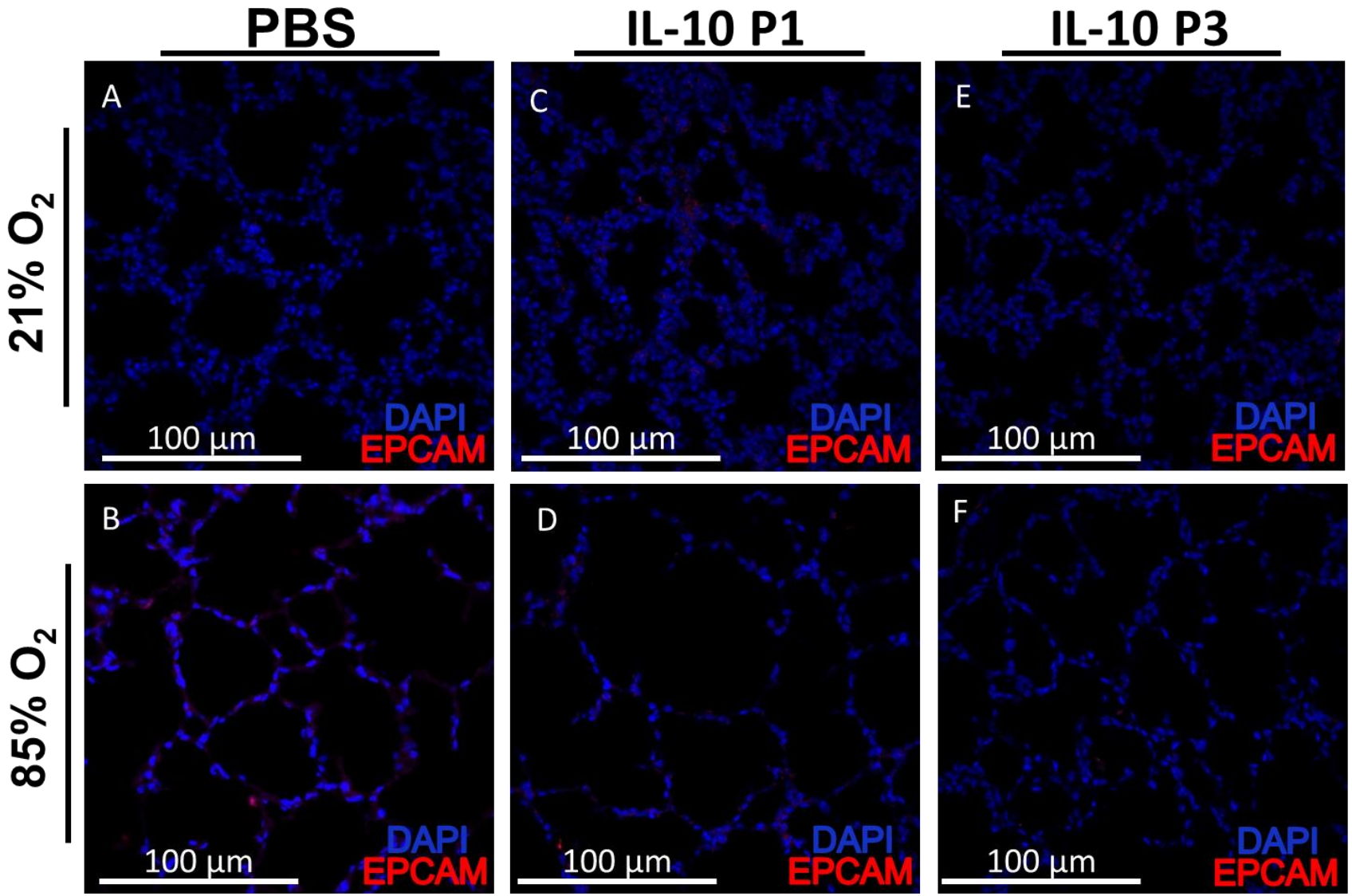

Figure 33. Control stainings for the epithelial cell adhesion molecule stainings in Figure 20.
Control staining images were taken at the same time as those in Figure 20, from samples incubated with isotype control antibodies as a replacement for primary anti-epithelia cell adhesion molecule (EPCAM) antibody (red). DAPI (blue) staining was employed to visualize the nuclei of all cells present in the section. For clarity, only one PBS control is reported; the trends of all controls are comparable.

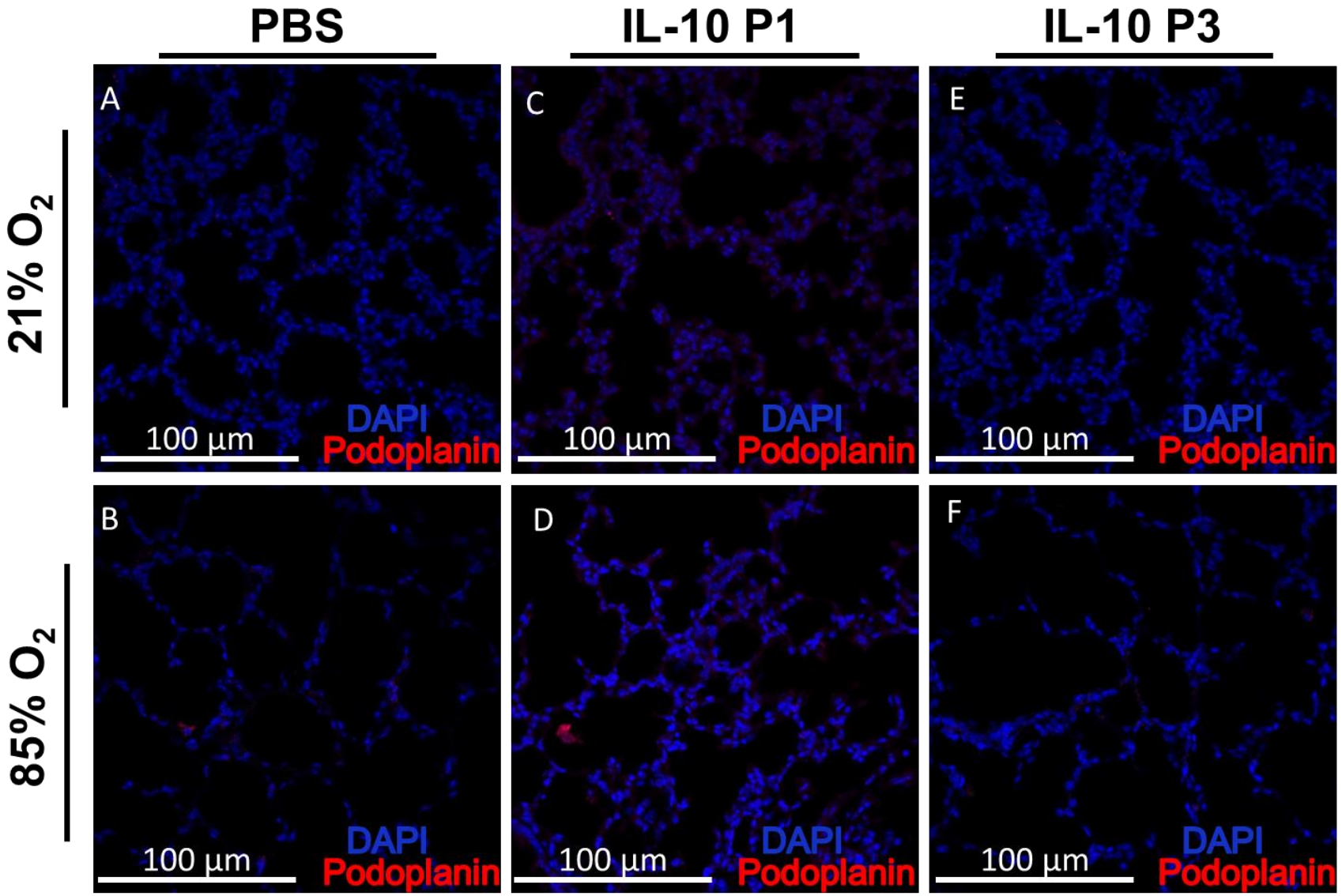

Figure 34. Control stainings for the podoplanin stainings in Figure 21.
Control staining images were taken at the same time as those in Figure 21, from samples incubated with isotype control antibodies as a replacement for primary anti-podoplanin antibody (red). DAPI (blue) staining was employed to visualize the nuclei of all cells present in the section. For clarity, only one PBS control is reported; the trends of all controls are comparable.

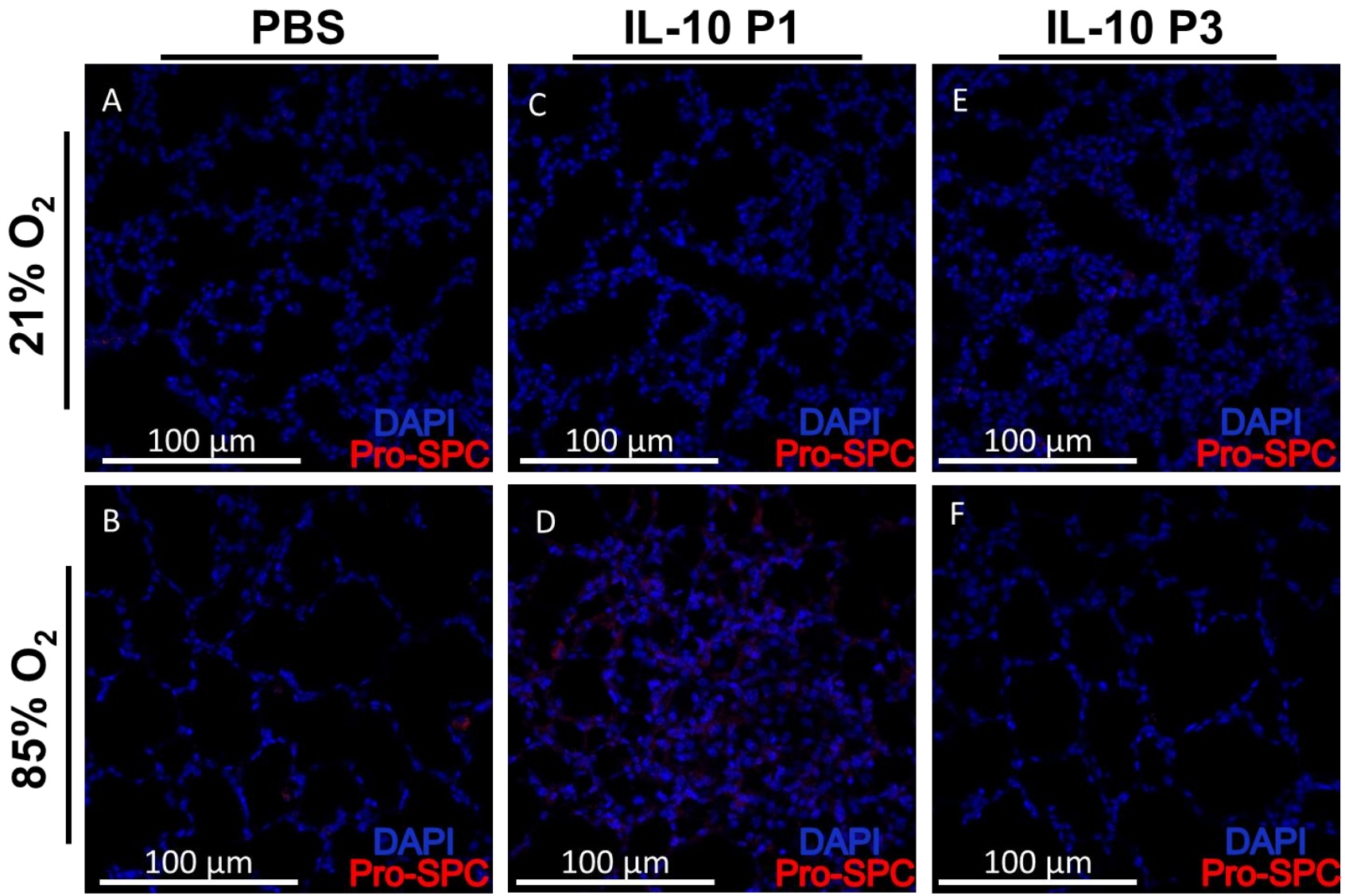

Figure 35. Control stainings for the prosurfactant protein C stainings in Figure 22.
Control staining images were taken at the same time as those in Figure 22, from samples incubated with isotype control antibodies as a replacement for primary anti-prosurfactant protein C (pro-SPC) antibody (red). DAPI (blue) staining was employed to visualize the nuclei of all cells present in the section. For clarity, only one PBS control is reported; the trends of all controls are comparable.

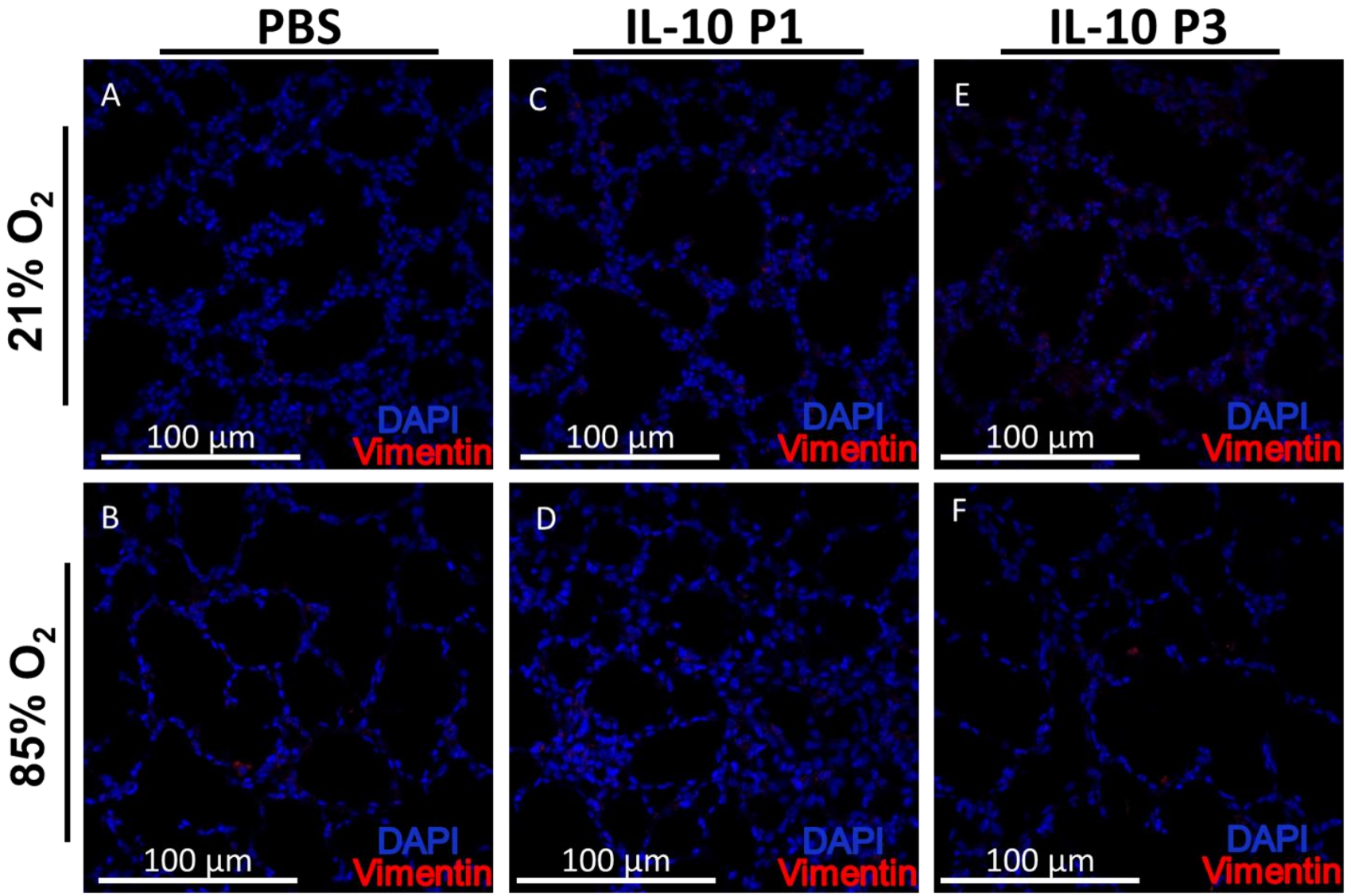

Figure 36. Control stainings for the vimentin stainings in Figure 23.
Control staining images were taken at the same time as those in Figure 23 from samples incubated with isotype control antibodies as a replacement for primary anti-vimentin antibody (red). DAPI (blue) staining was employed to visualize the nuclei of all cells present in the section. For clarity, only one PBS control is reported; the trends of all controls are comparable.

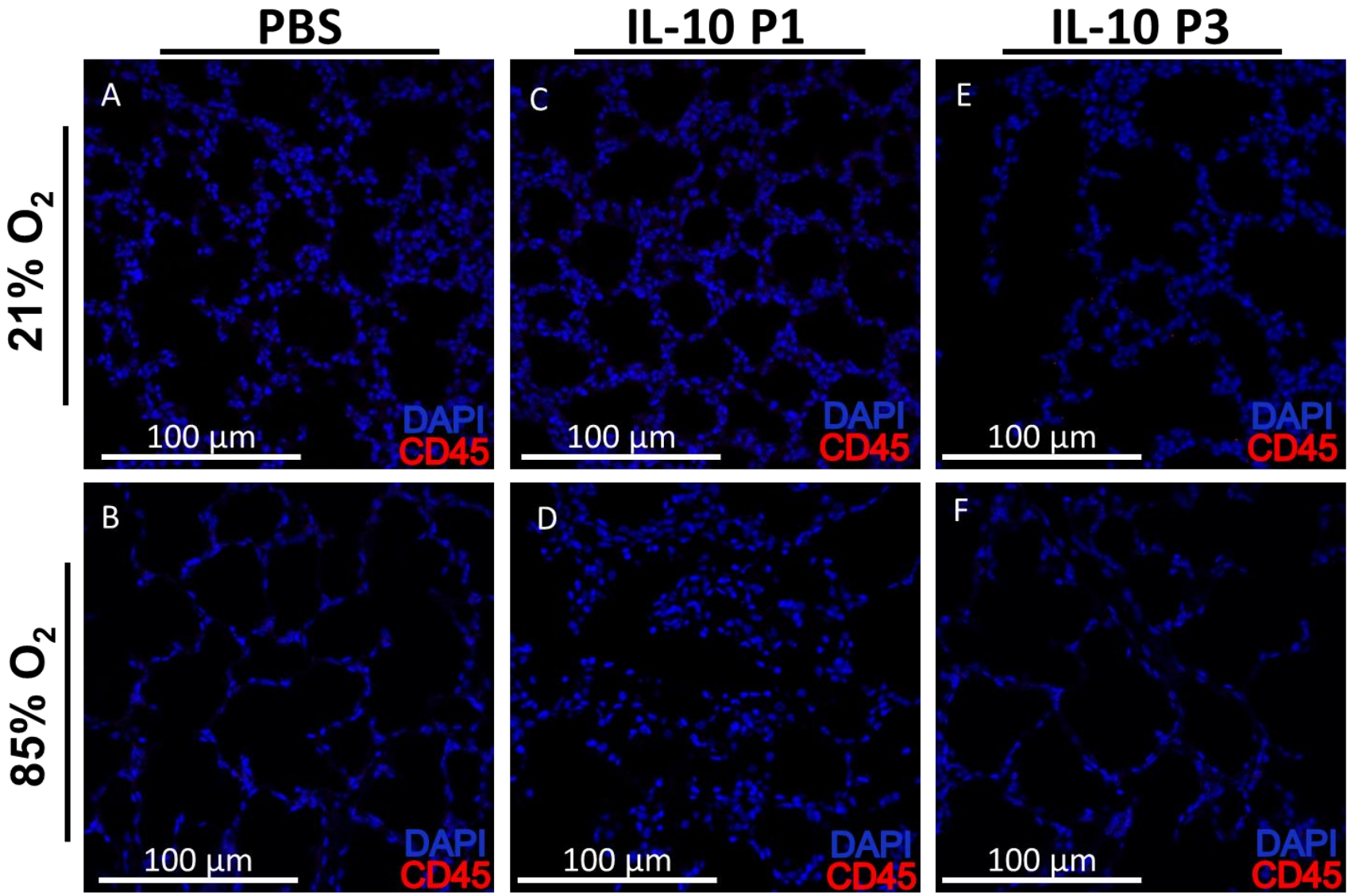

Figure 37. Control stainings for the CD45 stainings in Figure 24.
Control staining images were taken at the same time as those in Figure 24 from samples incubated with isotype control antibodies as a replacement for primary anti-CD45 antibody (red). DAPI (blue) staining was employed to visualize the nuclei of all cells present in the section. For clarity, only one PBS control is reported; the trends of all controls are comparable.

14 Bibliography

1. Akdis CA, Blaser K. IL-10-induced anergy in peripheral T cell and reactivation by microenvironmental cytokines: two key steps in specific immunotherapy. FASEB J. 1999;13(6):603-9.
2. Alejandre-Alcázar MA, Kwapiszewska G, Reiss I, Amarie OV, Marsh LM, Sevilla-Pérez J, et al. Hyperoxia modulates TGF-beta/BMP signaling in a mouse model of bronchopulmonary dysplasia. Am J Physiol Lung Cell Mol Physiol. 2007;292(2):L537-49.
3. Alexandrakis MG, Goulidaki N, Pappa CA, Boula A, Psarakis F, Neonakis I, et al. Interleukin-10 Induces Both Plasma Cell Proliferation and Angiogenesis in Multiple Myeloma. Pathol Oncol Res. 2015;21(4):929-34.
4. Ali Z, Schmidt P, Dodd J, Jeppesen DL. Bronchopulmonary dysplasia: a review. Arch Gynecol Obstet. 2013;288(2):325-33.
5. Ambalavanan N, Carlo WA, D'Angio CT, McDonald SA, Das A, Schendel D, et al. Cytokines associated with bronchopulmonary dysplasia or death in extremely low birth weight infants. Pediatrics. 2009;123(4):1132-41.
6. Ameredes BT, Zamora R, Sethi JM, Liu HL, Kohut LK, Gligonic AL, et al. Alterations in nitric oxide and cytokine production with airway inflammation in the absence of IL-10. J Immunol. 2005;175(2):1206-13.
7. Andrews S, Stephens LR, Hawkins PT. PI3K class IB pathway. Sci STKE. 2007;2007(407):cm2.
8. Awasthi A, Carrier Y, Peron JP, Bettelli E, Kamanaka M, Flavell RA, et al. A dominant function for interleukin 27 in generating interleukin 10-producing anti-inflammatory T cells. Nat Immunol. 2007;8(12):1380-9.
9. Baier RJ, Majid A, Parupia H, Loggins J, Kruger TE. CC chemokine concentrations increase in respiratory distress syndrome and correlate with development of bronchopulmonary dysplasia. Pediatr Pulmonol. 2004;37(2):137-48.
10. Balaji S, Wang X, King A, Le LD, Bhattacharya SS, Moles CM, et al. Interleukin-10-mediated regenerative postnatal tissue repair is dependent on regulation of hyaluronan metabolism via fibroblast-specific STAT3 signaling. FASEB J. 2017;31(3):868-81.
11. Balany J, Bhandari V. Understanding the impact of infection, inflammation, and their persistence in the pathogenesis of bronchopulmonary dysplasia. Front Med (Lausanne). 2015;2:90.
12. Ballabh P, Simm M, Kumari J, Krauss AN, Jain A, Auld PA, et al. Lymphocyte subpopulations in bronchopulmonary dysplasia. Am J Perinatol. 2003;20(8):465-75.
13. Barry BE, Crapo JD. Patterns of accumulation of platelets and neutrophils in rat lungs during exposure to 100% and 85% oxygen. Am Rev Respir Dis. 1985;132(3):548-55.
14. Bolger AM, Lohse M, Usadel B. Trimmomatic: a flexible trimmer for Illumina sequence data. Bioinformatics. 2014;30(15):2114-20.
15. Bose CL, Dammann CE, Laughon MM. Bronchopulmonary dysplasia and inflammatory biomarkers in the premature neonate. Arch Dis Child Fetal Neonatal Ed. 2008;93(6):F455-61.
16. Breedveld A, Groot Kormelink T, van Egmond M, de Jong EC. Granulocytes as modulators of dendritic cell function. J Leukoc Biol. 2017;102(4):1003-16.
17. Broekelmann TJ, Limper AH, Colby TV, McDonald JA. Transforming growth factor beta 1 is present at sites of extracellular matrix gene expression in human pulmonary fibrosis. Proc Natl Acad Sci U S A. 1991;88(15):6642-6.

18. Brostrom EB, Katz-Salamon M, Lundahl J, Hallden G, Winbladh B. Eosinophil activation in preterm infants with lung disease. Acta Paediatr. 2007;96(1):23-8.
19. Bruder D, Westendorf AM, Geffers R, Gruber AD, Gereke M, Enelow RI, et al. CD4 T Lymphocyte-mediated lung disease: steady state between pathological and tolerogenic immune reactions. Am J Respir Crit Care Med. 2004;170(11):1145-52.
20. Burri PH. Postnatal growth and maturation of the lung. Chest. 1975;67(2 Suppl):2S-3S.
21. Burri PH. Structural aspects of postnatal lung development - alveolar formation and growth. Biol Neonate. 2006;89(4):313-22.
22. Cardoso WV, Lu J. Regulation of early lung morphogenesis: questions, facts and controversies. Development (Cambridge, England). 2006;133(9):1611-24.
23. Chopra M, Biehl M, Steinfatt T, Brandl A, Kums J, Amich J, et al. Exogenous TNFR2 activation protects from acute GvHD via host T reg cell expansion. J Exp Med. 2016;213(9):1881-900.
24. Colombel JF, Rutgeerts P, Malchow H, Jacyna M, Nielsen OH, Rask-Madsen J, et al. Interleukin 10 (Tenovil) in the prevention of postoperative recurrence of Crohn's disease. Gut. 2001;49(1):42-6.
25. Crapo JD, Barry BE, Foscue HA, Shelburne J. Structural and biochemical changes in rat lungs occurring during exposures to lethal and adaptive doses of oxygen. Am Rev Respir Dis. 1980;122(1):123-43.
26. Cunha FQ, Moncada S, Liew FY. Interleukin-10 (IL-10) inhibits the induction of nitric oxide synthase by interferon-gamma in murine macrophages. Biochem Biophys Res Commun. 1992;182(3):1155-9.
27. D'Angio CT, Ambalavanan N, Carlo WA, McDonald SA, Skogstrand K, Hougaard DM, et al. Blood Cytokine Profiles Associated with Distinct Patterns of Bronchopulmonary Dysplasia among Extremely Low Birth Weight Infants. J Pediatr. 2016;174:45-51.e5.
28. de Waal Malefyt R, Abrams J, Bennett B, Figdor CG, de Vries JE. Interleukin 10(IL-10) inhibits cytokine synthesis by human monocytes: an autoregulatory role of IL-10 produced by monocytes. J Exp Med. 1991;174(5):1209-20.
29. Deng G, Li K, Chen S, Chen P, Zheng H, Yu B, et al. Interleukin-10 promotes proliferation and migration, and inhibits tendon differentiation via the JAK/Stat3 pathway in tendon-derived stem cells in vitro. Mol Med Rep. 2018;18(6):5044-52.
30. Dinant S, Veteläinen RL, Florquin S, van Vliet AK, van Gulik TM. IL-10 attenuates hepatic I/R injury and promotes hepatocyte proliferation. J Surg Res. 2007;141(2):176-82.
31. Ding L, Shevach EM. IL-10 inhibits mitogen-induced T cell proliferation by selectively inhibiting macrophage costimulatory function. J Immunol. 1992;148(10):3133-9.
32. Dobin A, Davis CA, Schlesinger F, Drenkow J, Zaleski C, Jha S, et al. STAR: ultrafast universal RNA-seq aligner. Bioinformatics. 2013;29(1):15-21.
33. Dordelmann M, Kerk J, Dressler F, Brinkhaus MJ, Bartels DB, Dammann CE, et al. Interleukin-10 high producer allele and ultrasound-defined periventricular white matter abnormalities in preterm infants: a preliminary study. Neuropediatrics. 2006;37(3):130-6.
34. El Kasmi KC, Smith AM, Williams L, Neale G, Panopoulos AD, Watowich SS, et al. Cutting edge: A transcriptional repressor and corepressor induced by the STAT3-regulated anti-inflammatory signaling pathway. J Immunol. 2007;179(11):7215-9.
35. Eldredge LC, Treuting PM, Manicone AM, Ziegler SF, Parks WC, McGuire JK. CD11b(+) Mononuclear Cells Mitigate Hyperoxia-Induced Lung Injury in Neonatal Mice. Am J Respir Cell Mol Biol. 2016;54(2):273-83.

36. Emami CN, Chokshi N, Wang J, Hunter C, Guner Y, Goth K, et al. Role of interleukin-10 in the pathogenesis of necrotizing enterocolitis. Am J Surg. 2012;203(4):428-35.
37. Fiorentino DF, Bond MW, Mosmann TR. Two types of mouse T helper cell. IV. Th2 clones secrete a factor that inhibits cytokine production by Th1 clones. J Exp Med. 1989;170(6):2081-95.
38. Fox RB, Hoidal JR, Brown DM, Repine JE. Pulmonary inflammation due to oxygen toxicity: involvement of chemotactic factors and polymorphonuclear leukocytes. Am Rev Respir Dis. 1981;123(5):521-3.
39. Frank L, Bucher JR, Roberts RJ. Oxygen toxicity in neonatal and adult animals of various species. J Appl Physiol Respir Environ Exerc Physiol. 1978;45(5):699-704.
40. Gabryšová L, Howes A, Saraiva M, O'Garra A. The regulation of IL-10 expression. Curr Top Microbiol Immunol. 2014;380:157-90.
41. Gao Y, Lu J, Zeng C, Yang J, Huang B, Zhang N, et al. IL-10 suppresses IFN-γ-mediated signaling in lung adenocarcinoma. Clin Exp Med. 2020;20(3):449-59.
42. Garingo A, Tesoriero L, Cayabyab R, Durand M, Blahnik M, Sardesai S, et al. Constitutive IL-10 expression by lung inflammatory cells and risk for bronchopulmonary dysplasia. Pediatr Res. 2007;61(2):197-202.
43. Glehen O, Mithieux F, Traverse-Glehen A, Isaac S, Bienvenu J, François Y, et al. Enteral immunotherapy in the treatment of chronic enterocolitis in interleukin-10-deficient mice. Hepatogastroenterology. 2003;50(51):670-5.
44. Golubovskaya V, Wu L. Different Subsets of T Cells, Memory, Effector Functions, and CAR-T Immunotherapy. Cancers (Basel). 2016;8(3).
45. González-Aragoneses F, Moreno-Mata N, Cebollero-Presmanes M, García-Yuste M, Cañizares-Carretero MA, Molins-López-Rodó L, et al. Prognostic significance of synaptophysin in stage I of squamous carcinoma and adenocarcinoma of the lung. Cancer. 2007;110(8):1776-81.
46. Greenough A, Premkumar M, Patel D. Ventilatory strategies for the extremely premature infant. Paediatr Anaesth. 2008;18(5):371-7.
47. Groneck P, Götze-Speer B, Oppermann M, Eiffert H, Speer CP. Association of pulmonary inflammation and increased microvascular permeability during the development of bronchopulmonary dysplasia: a sequential analysis of inflammatory mediators in respiratory fluids of high-risk preterm neonates. Pediatrics. 1994;93(5):712-8.
48. Groneck P, Speer CP. Inflammatory mediators and bronchopulmonary dysplasia. Arch Dis Child Fetal Neonatal Ed. 1995;73(1):F1-3.
49. Groux H, Bigler M, de Vries JE, Roncarolo MG. Interleukin-10 induces a long-term antigen-specific anergic state in human CD4+ T cells. J Exp Med. 1996;184(1):19-29.
50. Grünig G, Corry DB, Leach MW, Seymour BW, Kurup VP, Rennick DM. Interleukin-10 is a natural suppressor of cytokine production and inflammation in a murine model of allergic bronchopulmonary aspergillosis. J Exp Med. 1997;185(6):1089-99.
51. Guilliams M, De Kleer I, Henri S, Post S, Vanhoutte L, De Prijck S, et al. Alveolar macrophages develop from fetal monocytes that differentiate into long-lived cells in the first week of life via GM-CSF. J Exp Med. 2013;210(10):1977-92.
52. Hagenbaugh A, Sharma S, Dubinett SM, Wei SH, Aranda R, Cheroutre H, et al. Altered immune responses in interleukin 10 transgenic mice. J Exp Med. 1997;185(12):2101-10.
53. Hashimoto T, Nakamura M, Oshika Y, Tsuchida T, Yamazaki H, Kijima H, et al. Interleukin-10 relieves the inhibitory effects of interferon-gamma on normal human lung fibroblasts. Int J Mol Med. 2001;7(2):149-54.

54. Hayes D, Meadows JT, Murphy BS, Feola DJ, Shook LA, Ballard HO. Pulmonary function outcomes in bronchopulmonary dysplasia through childhood and into adulthood: implications for primary care. Prim Care Respir J. 2011;20(2):128-33.
55. Haynes BF, Markert ML, Sempowski GD, Patel DD, Hale LP. The role of the thymus in immune reconstitution in aging, bone marrow transplantation, and HIV-1 infection. Annu Rev Immunol. 2000;18:529-60.
56. Herriges M, Morrisey EE. Lung development: orchestrating the generation and regeneration of a complex organ. Development (Cambridge, England). 2014;141(3):502-13.
57. Higgins RD, Jobe AH, Koso-Thomas M, Bancalari E, Viscardi RM, Hartert TV, et al. Bronchopulmonary Dysplasia: Executive Summary of a Workshop. J Pediatr. 2018;197:300-8.
58. Hikino S, Ohga S, Kinjo T, Kusuda T, Ochiai M, Inoue H, et al. Tracheal aspirate gene expression in preterm newborns and development of bronchopulmonary dysplasia. Pediatr Int. 2012;54(2):208-14.
59. Hirahara K, Nakayama T. CD4+ T-cell subsets in inflammatory diseases: beyond the Th1/Th2 paradigm. Int Immunol. 2016;28(4):163-71.
60. Hislop AA. Airway and blood vessel interaction during lung development. J Anat. 2002;201(4):325-34.
61. Holgersen K, Kvist PH, Markholst H, Hansen AK, Holm TL. Characterisation of enterocolitis in the piroxicam-accelerated interleukin-10 knock out mouse--a model mimicking inflammatory bowel disease. J Crohns Colitis. 2014;8(2):147-60.
62. Hsia CC, Hyde DM, Ochs M, Weibel ER, Structure AEJTFoQAoL. An official research policy statement of the American Thoracic Society/European Respiratory Society: standards for quantitative assessment of lung structure. Am J Respir Crit Care Med. 2010;181(4):394-418.
63. Hutchins AP, Takahashi Y, Miranda-Saavedra D. Genomic analysis of LPS-stimulated myeloid cells identifies a common pro-inflammatory response but divergent IL-10 anti-inflammatory responses. Sci Rep. 2015;5:9100.
64. Hyde DM, Tyler NK, Putney LF, Singh P, Gundersen HJ. Total number and mean size of alveoli in mammalian lung estimated using fractionator sampling and unbiased estimates of the Euler characteristic of alveolar openings. Anat Rec A Discov Mol Cell Evol Biol. 2004;277(1):216-26.
65. Itakura E, Huang RR, Wen DR, Paul E, Wünsch PH, Cochran AJ. IL-10 expression by primary tumor cells correlates with melanoma progression from radial to vertical growth phase and development of metastatic competence. Mod Pathol. 2011;24(6):801-9.
66. Jarry A, Bossard C, Bou-Hanna C, Masson D, Espaze E, Denis MG, et al. Mucosal IL-10 and TGF-beta play crucial roles in preventing LPS-driven, IFN-gamma-mediated epithelial damage in human colon explants. J Clin Invest. 2008;118(3):1132-42.
67. Jobe AH, Bancalari E. Bronchopulmonary dysplasia. Am J Respir Crit Care Med. 2001;163(7):1723-9.
68. Jones CA, Cayabyab RG, Kwong KY, Stotts C, Wong B, Hamdan H, et al. Undetectable interleukin (IL)-10 and persistent IL-8 expression early in hyaline membrane disease: a possible developmental basis for the predisposition to chronic lung inflammation in preterm newborns. Pediatr Res. 1996;39(6):966-75.
69. Jónsson B, Tullus K, Brauner A, Lu Y, Noack G. Early increase of TNF alpha and IL-6 in tracheobronchial aspirate fluid indicator of subsequent chronic lung disease in preterm infants. Arch Dis Child Fetal Neonatal Ed. 1997;77(3):F198-201.

70. Jung M, Ma Y, Iyer RP, DeLeon-Pennell KY, Yabluchanskiy A, Garrett MR, et al. IL-10 improves cardiac remodeling after myocardial infarction by stimulating M2 macrophage polarization and fibroblast activation. Basic Res Cardiol. 2017;112(3):33.
71. Kajekar R. Environmental factors and developmental outcomes in the lung. Pharmacol Ther. 2007;114(2):129-45.
72. Kalymbetova TV, Selvakumar B, Rodríguez-Castillo JA, Gunjak M, Malainou C, Heindl MR, et al. Resident alveolar macrophages are master regulators of arrested alveolarization in experimental bronchopulmonary dysplasia. J Pathol. 2018;245(2):153-9.
73. Kim BI, Lee HE, Choi CW, Jo HS, Choi EH, Koh YY, et al. Increase in cord blood soluble E-selectin and tracheal aspirate neutrophils at birth and the development of new bronchopulmonary dysplasia. J Perinat Med. 2004;32(3):282-7.
74. Kim EY, Priatel JJ, Teh SJ, Teh HS. TNF receptor type 2 (p75) functions as a costimulator for antigen-driven T cell responses in vivo. J Immunol. 2006;176(2):1026-35.
75. Kim KB, Choi YH, Kim IK, Chung CW, Kim BJ, Park YM, et al. Potentiation of Fas- and TRAIL-mediated apoptosis by IFN-gamma in A549 lung epithelial cells: enhancement of caspase-8 expression through IFN-response element. Cytokine. 2002;20(6):283-8.
76. Kinnula VL, Crapo JD. Superoxide dismutases in the lung and human lung diseases. Am J Respir Crit Care Med. 2003;167(12):1600-19.
77. Kondo H, Abe I, Gotoh K, Fukui A, Takanari H, Ishii Y, et al. Interleukin 10 Treatment Ameliorates High-Fat Diet-Induced Inflammatory Atrial Remodeling and Fibrillation. Circ Arrhythm Electrophysiol. 2018;11(5):e006040.
78. Kotecha S, Wilson L, Wangoo A, Silverman M, Shaw RJ. Increase in interleukin (IL)-1 beta and IL-6 in bronchoalveolar lavage fluid obtained from infants with chronic lung disease of prematurity. Pediatr Res. 1996;40(2):250-6.
79. Kühn R, Löhler J, Rennick D, Rajewsky K, Müller W. Interleukin-10-deficient mice develop chronic enterocolitis. Cell. 1993;75(2):263-74.
80. Kumar H, Kawai T, Akira S. Pathogen recognition by the innate immune system. Int Rev Immunol. 2011;30(1):16-34.
81. Kwilasz AJ, Grace PM, Serbedzija P, Maier SF, Watkins LR. The therapeutic potential of interleukin-10 in neuroimmune diseases. Neuropharmacology. 2015;96(Pt A):55-69.
82. Lang R, Patel D, Morris JJ, Rutschman RL, Murray PJ. Shaping gene expression in activated and resting primary macrophages by IL-10. J Immunol. 2002;169(5):2253-63.
83. Laumet G, Edralin JD, Chiang AC, Dantzer R, Heijnen CJ, Kavelaars A. Resolution of inflammation-induced depression requires T lymphocytes and endogenous brain interleukin-10 signaling. Neuropsychopharmacology. 2018;43(13):2597-605.
84. Lauw FN, Pajkrt D, Hack CE, Kurimoto M, van Deventer SJ, van der Poll T. Proinflammatory effects of IL-10 during human endotoxemia. J Immunol. 2000;165(5):2783-9.
85. Li HD, Zhang QX, Mao Z, Xu XJ, Li NY, Zhang H. Exogenous interleukin-10 attenuates hyperoxia-induced acute lung injury in mice. Exp Physiol. 2015;100(3):331-40.
86. Liao Y, Smyth GK, Shi W. featureCounts: an efficient general purpose program for assigning sequence reads to genomic features. Bioinformatics. 2014;30(7):923-30.
87. Lira FS, Rosa JC, Pimentel GD, Seelaender M, Damaso AR, Oyama LM, et al. Both adiponectin and interleukin-10 inhibit LPS-induced activation of the NF-κB pathway in 3T3-L1 adipocytes. Cytokine. 2012;57(1):98-106.

88. Llorente L, Richaud-Patin Y, Garcia-Padilla C, Claret E, Jakez-Ocampo J, Cardiel MH, et al. Clinical and biologic effects of anti-interleukin-10 monoclonal antibody administration in systemic lupus erythematosus. Arthritis Rheum. 2000;43(8):1790-800.
89. Loser K, Apelt J, Voskort M, Mohaupt M, Balkow S, Schwarz T, et al. IL-10 controls ultraviolet-induced carcinogenesis in mice. J Immunol. 2007;179(1):365-71.
90. Love MI, Huber W, Anders S. Moderated estimation of fold change and dispersion for RNA-seq data with DESeq2. Genome Biol. 2014;15(12):550.
91. Macatonia SE, Doherty TM, Knight SC, O'Garra A. Differential effect of IL-10 on dendritic cell-induced T cell proliferation and IFN-gamma production. J Immunol. 1993;150(9):3755-65.
92. Madurga A, Golec A, Pozarska A, Ishii I, Mižíková I, Nardiello C, et al. The H2S-generating enzymes cystathionine β-synthase and cystathionine γ-lyase play a role in vascular development during normal lung alveolarization. Am J Physiol Lung Cell Mol Physiol. 2015;309(7):L710-24.
93. Madurga A, Mizikova I, Ruiz-Camp J, Morty RE. Recent advances in late lung development and the pathogenesis of bronchopulmonary dysplasia. Am J Physiol Lung Cell Mol Physiol. 2013;305(12):L893-905.
94. Madurga A, Mizikova I, Ruiz-Camp J, Vadasz I, Herold S, Mayer K, et al. Systemic hydrogen sulfide administration partially restores normal alveolarization in an experimental animal model of bronchopulmonary dysplasia. Am J Physiol Lung Cell Mol Physiol. 2014;306(7):L684-97.
95. McCoy CE, Sheedy FJ, Qualls JE, Doyle SL, Quinn SR, Murray PJ, et al. IL-10 inhibits miR-155 induction by toll-like receptors. J Biol Chem. 2010;285(27):20492-8.
96. McGowan EC, Kostadinov S, McLean K, Gotsch F, Venturini D, Romero R, et al. Placental IL-10 dysregulation and association with bronchopulmonary dysplasia risk. Pediatr Res. 2009;66(4):455-60.
97. McInnes IB, Illei GG, Danning CL, Yarboro CH, Crane M, Kuroiwa T, et al. IL-10 improves skin disease and modulates endothelial activation and leukocyte effector function in patients with psoriatic arthritis. J Immunol. 2001;167(7):4075-82.
98. Meiron M, Zohar Y, Anunu R, Wildbaum G, Karin N. CXCL12 (SDF-1alpha) suppresses ongoing experimental autoimmune encephalomyelitis by selecting antigen-specific regulatory T cells. J Exp Med. 2008;205(11):2643-55.
99. Merritt TA, Stuard ID, Puccia J, Wood B, Edwards DK, Finkelstein J, et al. Newborn tracheal aspirate cytology: classification during respiratory distress syndrome and bronchopulmonary dysplasia. J Pediatr. 1981;98(6):949-56.
100. Mesples B, Plaisant F, Gressens P. Effects of interleukin-10 on neonatal excitotoxic brain lesions in mice. Brain Res Dev Brain Res. 2003;141(1-2):25-32.
101. Mezzasoma L, Peirce MJ, Minelli A, Bellezza I. Natriuretic peptides: the case of prostate cancer. Molecules. 2017;22(10).
102. Michel RP, Cruz-Orive LM. Application of the Cavalieri principle and vertical sections method to lung: estimation of volume and pleural surface area. J Microsc. 1988;150(Pt 2):117-36.
103. Miller MD, Marty MA. Impact of environmental chemicals on lung development. Environ Health Perspect. 2010;118(8):1155-64.
104. Misra R, Shah S, Fowell D, Wang H, Scheible K, Misra S, et al. Preterm cord blood $CD4^+$ T cells exhibit increased IL-6 production in chorioamnionitis and decreased $CD4^+$ T cells in bronchopulmonary dysplasia. Hum Immunol. 2015;76(5):329-38.

105. Mizikova I, Ruiz-Camp J, Steenbock H, Madurga A, Vadasz I, Herold S, et al. Collagen and elastin cross-linking is altered during aberrant late lung development associated with hyperoxia. Am J Physiol Lung Cell Mol Physiol. 2015;308(11):L1145-58.
106. Moore KW, de Waal Malefyt R, Coffman RL, O'Garra A. Interleukin-10 and the interleukin-10 receptor. Annu Rev Immunol. 2001;19:683-765.
107. Morty RE. Recent advances in the pathogenesis of BPD. Semin Perinatol. 2018;42(7):404-12.
108. Mühlfeld C, Hegermann J, Wrede C, Ochs M. A review of recent developments and applications of morphometry/stereology in lung research. Am J Physiol Lung Cell Mol Physiol. 2015;309(6):L526-36.
109. Mühlfeld C, Knudsen L, Ochs M. Stereology and morphometry of lung tissue. Methods Mol Biol. 2013;931:367-90.
110. Mühlfeld C, Ochs M. Measuring structure - What's the point in counting? Ann Anat. 2014;196(1):1-2.
111. Mumm JB, Emmerich J, Zhang X, Chan I, Wu L, Mauze S, et al. IL-10 elicits IFNγ-dependent tumor immune surveillance. Cancer Cell. 2011;20(6):781-96.
112. Naing A, Infante JR, Papadopoulos KP, Chan IH, Shen C, Ratti NP, et al. PEGylated IL-10 (Pegilodecakin) induces systemic immune activation, CD8. Cancer Cell. 2018;34(5):775-91.e3.
113. Nakanishi H, Sugiura T, Streisand JB, Lonning SM, Roberts JD, Jr. TGF-beta-neutralizing antibodies improve pulmonary alveologenesis and vasculogenesis in the injured newborn lung. Am J Physiol Lung Cell Mol Physiol. 2007;293(1):L151-61.
114. Nardiello C, Mizikova I, Morty RE. Looking ahead: where to next for animal models of bronchopulmonary dysplasia? Cell Tissue Res. 2017;367(3):457-68.
115. Nardiello C, Mizikova I, Silva DM, Ruiz-Camp J, Mayer K, Vadasz I, et al. Standardisation of oxygen exposure in the development of mouse models for bronchopulmonary dysplasia. Dis Model Mech. 2017;10(2):185-96.
116. Nardiello C, Morty RE. MicroRNA in late lung development and bronchopulmonary dysplasia: the need to demonstrate causality. Mol Cell Pediatr. 2016;3(1):19.
117. Nemunaitis J, Fong T, Shabe P, Martineau D, Ando D. Comparison of serum interleukin-10 (IL-10) levels between normal volunteers and patients with advanced melanoma. Cancer Invest. 2001;19(3):239-47.
118. Northway WH, Jr., Rosan RC, Porter DY. Pulmonary disease following respirator therapy of hyaline-membrane disease. Bronchopulmonary dysplasia. N Engl J Med. 1967;276(7):357-68.
119. O'Farrell AM, Liu Y, Moore KW, Mui AL. IL-10 inhibits macrophage activation and proliferation by distinct signaling mechanisms: evidence for Stat3-dependent and -independent pathways. EMBO J. 1998;17(4):1006-18.
120. Ochs M, Mühlfeld C. Quantitative microscopy of the lung: a problem-based approach. Part 1: basic principles of lung stereology. Am J Physiol Lung Cell Mol Physiol. 2013;305(1):L15-22.
121. Ogden BE, Murphy SA, Saunders GC, Pathak D, Johnson JD. Neonatal lung neutrophils and elastase/proteinase inhibitor imbalance. Am Rev Respir Dis. 1984;130(5):817-21.
122. Orkin SH, Zon LI. SnapShot: hematopoiesis. Cell. 2008;132(4):712.
123. Ouyang W, O'Garra A. IL-10 Family Cytokines IL-10 and IL-22: from Basic Science to Clinical Translation. Immunity. 2019;50(4):871-91.
124. Ovchinnikov DA. Macrophages in the embryo and beyond: much more than just giant phagocytes. Genesis. 2008;46(9):447-62.

125. Parimi PS, Birnkrant DJ, Rao LV, Diaz G, Moore JJ. Effect of dexamethasone on lymphocyte subpopulations in premature infants with bronchopulmonary dysplasia. J Perinatol. 1999;19(5):347-51.
126. Patel S, Vetale S, Teli P, Mistry R, Chiplunkar S. IL-10 production in non-small cell lung carcinoma patients is regulated by ERK, P38 and COX-2. J Cell Mol Med. 2012;16(3):531-44.
127. Pestka S, Krause CD, Sarkar D, Walter MR, Shi Y, Fisher PB. Interleukin-10 and related cytokines and receptors. Annu Rev Immunol. 2004;22:929-79.
128. Pollard JW. Trophic macrophages in development and disease. Nat Rev Immunol. 2009;9(4):259-70.
129. Pozarska A, Rodríguez-Castillo JA, Surate Solaligue DE, Ntokou A, Rath P, Mižíková I, et al. Stereological monitoring of mouse lung alveolarization from the early postnatal period to adulthood. Am J Physiol Lung Cell Mol Physiol. 2017;312(6):L882-L95.
130. Pryhuber GS. Postnatal Infections and Immunology Affecting Chronic Lung Disease of Prematurity. Clin Perinatol. 2015;42(4):697-718.
131. Quiros M, Nishio H, Neumann PA, Siuda D, Brazil JC, Azcutia V, et al. Macrophage-derived IL-10 mediates mucosal repair by epithelial WISP-1 signaling. J Clin Invest. 2017;127(9):3510-20.
132. RICHARDSON KC, JARETT L, FINKE EH. Embedding in epoxy resins for ultrathin sectioning in electron microscopy. Stain Technol. 1960;35:313-23.
133. Riese DJ, Cullum RL. Epiregulin: roles in normal physiology and cancer. Semin Cell Dev Biol. 2014;28:49-56.
134. Robertson TE, Nikolic-Paterson DJ, Hurst LA, Atkins RC, Chadban SJ. IL-10 induces mesangial cell proliferation via a PDGF-dependent mechanism. Clin Exp Immunol. 2002;130(2):241-4.
135. Rocha G, Proença E, Guedes A, Carvalho C, Areias A, Ramos JP, et al. Cord blood levels of IL-6, IL-8 and IL-10 may be early predictors of bronchopulmonary dysplasia in preterm newborns small for gestational age. Dis Markers. 2012;33(1):51-60.
136. Rosen D, Lee JH, Cuttitta F, Rafiqi F, Degan S, Sunday ME. Accelerated thymic maturation and autoreactive T cells in bronchopulmonary dysplasia. Am J Respir Crit Care Med. 2006;174(1):75-83.
137. Roth-Kleiner M, Post M. Similarities and dissimilarities of branching and septation during lung development. Pediatr Pulmonol. 2005;40(2):113-34.
138. Rubtsov YP, Rasmussen JP, Chi EY, Fontenot J, Castelli L, Ye X, et al. Regulatory T cell-derived interleukin-10 limits inflammation at environmental interfaces. Immunity. 2008;28(4):546-58.
139. Ryan RM, Ahmed Q, Lakshminrusimha S. Inflammatory mediators in the immunobiology of bronchopulmonary dysplasia. Clin Rev Allergy Immunol. 2008;34(2):174-90.
140. Sahni M, Mowes AK. Bronchopulmonary Dysplasia. StatPearls. Treasure Island (FL)2020.
141. Sahoo D, Zaramela LS, Hernandez GE, Mai U, Taheri S, Dang D, et al. Transcriptional profiling of lung macrophages identifies a predictive signature for inflammatory lung disease in preterm infants. Commun Biol. 2020;3(1):259.
142. Sakaguchi S. Naturally arising Foxp3-expressing CD25+CD4+ regulatory T cells in immunological tolerance to self and non-self. Nat Immunol. 2005;6(4):345-52.
143. Saraiva M, Christensen JR, Veldhoen M, Murphy TL, Murphy KM, O'Garra A. Interleukin-10 production by Th1 cells requires interleukin-12-induced STAT4 transcription factor and ERK MAP kinase activation by high antigen dose. Immunity. 2009;31(2):209-19.

144. Saraiva M, O'Garra A. The regulation of IL-10 production by immune cells. Nat Rev Immunol. 2010;10(3):170-81.
145. Saraiva M, Vieira P, O'Garra A. Biology and therapeutic potential of interleukin-10. J Exp Med. 2020;217(1).
146. Sawant DV, Yano H, Chikina M, Zhang Q, Liao M, Liu C, et al. Adaptive plasticity of IL-10. Nat Immunol. 2019;20(6):724-35.
147. Saxena A, Khosraviani S, Noel S, Mohan D, Donner T, Hamad AR. Interleukin-10 paradox: A potent immunoregulatory cytokine that has been difficult to harness for immunotherapy. Cytokine. 2015;74(1):27-34.
148. Schaljo B, Kratochvill F, Gratz N, Sadzak I, Sauer I, Hammer M, et al. Tristetraprolin is required for full anti-inflammatory response of murine macrophages to IL-10. J Immunol. 2009;183(2):1197-206.
149. Schett G, Neurath MF. Resolution of chronic inflammatory disease: universal and tissue-specific concepts. Nat Commun. 2018;9(1):3261.
150. Schittny JC. Development of the lung. Cell Tissue Res. 2017;367(3):427-44.
151. Schmid T, Falter L, Weber S, Muller N, Molitor K, Zeller D, et al. Chronic inflammation increases the sensitivity of mouse Treg for TNFR2 costimulation. Front Immunol. 2017;8:1471.
152. Schneider JP, Ochs M. Alterations of mouse lung tissue dimensions during processing for morphometry: a comparison of methods. Am J Physiol Lung Cell Mol Physiol. 2014;306(4):L341-50.
153. Seifert HA, Gerstner G, Kent G, Vandenbark AA, Offner H. Estrogen-induced compensatory mechanisms protect IL-10-deficient mice from developing EAE. J Neuroinflammation. 2019;16(1):195.
154. Series IM, Pichette J, Carrier C, Masson M, Bedard PM, Beaudoin J, et al. Quantitative analysis of T and B cell subsets in healthy and sick premature infants. Early Hum Dev. 1991;26(2):143-54.
155. Shachar I, Karin N. The dual roles of inflammatory cytokines and chemokines in the regulation of autoimmune diseases and their clinical implications. J Leukoc Biol. 2013;93(1):51-61.
156. Shahzad T, Radajewski S, Chao CM, Bellusci S, Ehrhardt H. Pathogenesis of bronchopulmonary dysplasia: when inflammation meets organ development. Mol Cell Pediatr. 2016;3(1):23.
157. Shennan AT, Dunn MS, Ohlsson A, Lennox K, Hoskins EM. Abnormal pulmonary outcomes in premature infants: prediction from oxygen requirement in the neonatal period. Pediatrics. 1988;82(4):527-32.
158. Shimotake TK, Izhar FM, Rumilla K, Li J, Tan A, Page K, et al. Interleukin (IL)-1 beta in tracheal aspirates from premature infants induces airway epithelial cell IL-8 expression via an NF-kappa B dependent pathway. Pediatr Res. 2004;56(6):907-13.
159. Shrestha AK, Bettini ML, Menon RT, Gopal VYN, Huang S, Edwards DP, et al. Consequences of early postnatal lipopolysaccharide exposure on developing lungs in mice. Am J Physiol Lung Cell Mol Physiol. 2019;316(1):L229-L44.
160. Silva DM, Nardiello C, Pozarska A, Morty RE. Recent advances in the mechanisms of lung alveolarization and the pathogenesis of bronchopulmonary dysplasia. Am J Physiol Lung Cell Mol Physiol. 2015;309(11):L1239-72.
161. Singh SP, Chand HS, Langley RJ, Mishra N, Barrett T, Rudolph K, et al. Gestational Exposure to Sidestream (Secondhand) Cigarette Smoke Promotes Transgenerational Epigenetic Transmission of Exacerbated Allergic Asthma and Bronchopulmonary Dysplasia. J Immunol. 2017;198(10):3815-22.

162. Steen EH, Wang X, Balaji S, Butte MJ, Bollyky PL, Keswani SG. The Role of the Anti-Inflammatory Cytokine Interleukin-10 in Tissue Fibrosis. Adv Wound Care (New Rochelle). 2020;9(4):184-98.
163. Steidler L, Hans W, Schotte L, Neirynck S, Obermeier F, Falk W, et al. Treatment of murine colitis by Lactococcus lactis secreting interleukin-10. Science. 2000;289(5483):1352-5.
164. Sterio DC. The unbiased estimation of number and sizes of arbitrary particles using the disector. J Microsc. 1984;134(Pt 2):127-36.
165. Sun J, Madan R, Karp CL, Braciale TJ. Effector T cells control lung inflammation during acute influenza virus infection by producing IL-10. Nat Med. 2009;15(3):277-84.
166. Takeda K, Clausen BE, Kaisho T, Tsujimura T, Terada N, Förster I, et al. Enhanced Th1 activity and development of chronic enterocolitis in mice devoid of Stat3 in macrophages and neutrophils. Immunity. 1999;10(1):39-49.
167. Tilg H, van Montfrans C, van den Ende A, Kaser A, van Deventer SJ, Schreiber S, et al. Treatment of Crohn's disease with recombinant human interleukin 10 induces the proinflammatory cytokine interferon gamma. Gut. 2002;50(2):191-5.
168. Trachsel E, Bootz F, Silacci M, Kaspar M, Kosmehl H, Neri D. Antibody-mediated delivery of IL-10 inhibits the progression of established collagen-induced arthritis. Arthritis Res Ther. 2007;9(1):R9.
169. Tripp RA, Oshansky C, Alvarez R. Cytokines and respiratory syncytial virus infection. Proc Am Thorac Soc. 2005;2(2):147-9.
170. Tschanz SA, Salm LA, Roth-Kleiner M, Barre SF, Burri PH, Schittny JC. Rat lungs show a biphasic formation of new alveoli during postnatal development. J Appl Physiol (1985). 2014;117(1):89-95.
171. Turunen R, Vaarala O, Nupponen I, Kajantie E, Siitonen S, Lano A, et al. Activation of T cells in preterm infants with respiratory distress syndrome. Neonatology. 2009;96(4):248-58.
172. Wagenaar GT, ter Horst SA, van Gastelen MA, Leijser LM, Mauad T, van der Velden PA, et al. Gene expression profile and histopathology of experimental bronchopulmonary dysplasia induced by prolonged oxidative stress. Free Radic Biol Med. 2004;36(6):782-801.
173. Wang SH, Tsao PN. Phenotypes of Bronchopulmonary Dysplasia. Int J Mol Sci. 2020;21(17).
174. Warburton D, Bellusci S, De Langhe S, Del Moral PM, Fleury V, Mailleux A, et al. Molecular mechanisms of early lung specification and branching morphogenesis. Pediatr Res. 2005;57(5 Pt 2):26R-37R.
175. Warburton D, Olver BE. Coordination of genetic, epigenetic, and environmental factors in lung development, injury, and repair. Chest. 1997;111(6 Suppl):119S-22S.
176. Ward HE, Nicholas TE. Alveolar type I and type II cells. Aust N Z J Med. 1984;14(5 Suppl 3):731-4.
177. Warner BB, Stuart LA, Papes RA, Wispe JR. Functional and pathological effects of prolonged hyperoxia in neonatal mice. Am J Physiol. 1998;275(1):L110-7.
178. Weber-Nordt RM, Riley JK, Greenlund AC, Moore KW, Darnell JE, Schreiber RD. Stat3 recruitment by two distinct ligand-induced, tyrosine-phosphorylated docking sites in the interleukin-10 receptor intracellular domain. J Biol Chem. 1996;271(44):27954-61.
179. Williams L, Bradley L, Smith A, Foxwell B. Signal transducer and activator of transcription 3 is the dominant mediator of the anti-inflammatory effects of IL-10 in human macrophages. J Immunol. 2004;172(1):567-76.

180. Yamamoto C, Kojima T, Hattori K, Nogi S, Imamura H, Tsubura A, et al. Eosinophilia in premature infants: correlation with chronic lung disease. Acta Paediatr. 1996;85(10):1232-5.
181. Yanamandra K, Boggs P, Loggins J, Baier RJ. Interleukin-10 -1082 G/A polymorphism and risk of death or bronchopulmonary dysplasia in ventilated very low birth weight infants. Pediatr Pulmonol. 2005;39(5):426-32.
182. Yang JY, Cha J, Shim SY, Cho SJ, Park EA. The relationship between eosinophilia and bronchopulmonary dysplasia in premature infants at less than 34 weeks' gestation. Korean J Pediatr. 2014;57(4):171-7.
183. Yoon BH, Romero R, Kim KS, Park JS, Ki SH, Kim BI, et al. A systemic fetal inflammatory response and the development of bronchopulmonary dysplasia. Am J Obstet Gynecol. 1999;181(4):773-9.
184. Zanardo V, Savio V, Giacomin C, Rinaldi A, Marzari F, Chiarelli S. Relationship between neonatal leukemoid reaction and bronchopulmonary dysplasia in low-birth-weight infants: a cross-sectional study. Am J Perinatol. 2002;19(7):379-86.
185. Zdanov A. Structural analysis of cytokines comprising the IL-10 family. Cytokine Growth Factor Rev. 2010;21(5):325-30.
186. Zhang JM, An J. Cytokines, inflammation, and pain. Int Anesthesiol Clin. 2007;45(2):27-37.
187. Zhang Z, Wu W, Hou L, Jiang J, Wan W, Li Z. Cytokines and Exhaled Nitric Oxide Are Risk Factors in Preterm Infants for Bronchopulmonary Dysplasia. Biomed Res Int. 2021;2021:6648208.
188. Zhou Z, Peng X, Insolera R, Fink DJ, Mata M. IL-10 promotes neuronal survival following spinal cord injury. Exp Neurol. 2009;220(1):183-90.
189. Zhou Z, Peng X, Insolera R, Fink DJ, Mata M. Interleukin-10 provides direct trophic support to neurons. J Neurochem. 2009;110(5):1617-27.
190. Zigmond E, Bernshtein B, Friedlander G, Walker CR, Yona S, Kim KW, et al. Macrophage-restricted interleukin-10 receptor deficiency, but not IL-10 deficiency, causes severe spontaneous colitis. Immunity. 2014;40(5):720-33.

15 List of publications

Lignelli, E., Palumbo, F., Myti, D. and Morty, R.E. (2019). **Recent advances in our understanding of the mechanisms of lung alveolarization and bronchopulmonary dysplasia.** American Journal of Physiology-Lung Cellular and Molecular Physi-ology, 317(6), pp.L832-L887.

Lignelli, E., Palumbo, F., Bayindir, S.G., Nagahara, N., Vadász, I., Herold, S., Seeger, W. and Morty, R.E. (2021). **The H2S-generating enzyme 3-mercaptopyruvate sulfurtransferase regulates pulmonary vascular smooth muscle cell migration and proliferation but does not impact normal or aberrant lung development.** Nitric Oxide, 107, pp.31-45.

Looso, M., Preussner, J., Sousounis, K., Bruckskotten, M., Michel, C.S., Lignelli, E., Reinhardt, R., Höffner, S., Krüger, M., Tsonis, P.A. and Borchardt, T. (2013). **A de novo assembly of the newt transcriptome combined with proteomic valida-tion identifies new protein families expressed during tissue regeneration.** Genome biology, 14(2), pp.1-16.

Pfeffer, T., Lignelli, E., Inoue, H., Mižíková, I., Solaligue, D.E.S., Steenbock, H., Myti, D., Vadász, I., Herold, S., Seeger, W. and Brinckmann, J. (2020). **Minoxidil cannot be used to target lysyl hydroxylases during postnatal mouse lung development: a cautionary note**. Journal of Pharmacology and Experimental Therapeutics, 375(3), pp.478-487.

Ruiz-Camp, J., Quantius, J., Lignelli, E., Arndt, P.F., Palumbo, F., Nardiello, C., Surate Solaligue, D.E., Sakkas, E., Mižíková, I., Rodríguez-Castillo, J.A. and Vadász, I. (2019). **Targeting miR-34a/Pdgfra interactions partially corrects alveologenesis in experimental bronchopulmonary dysplasia.** EMBO molecular medicine, 11(3), p.e9448.

16 Curriculum vitae

17 Acknowledgements

My first words of gratitude are for my supervisor, Dr. Rory Morty, for giving me the opportunity to develop my skills in his lab and, eventually, reach my PhD. A heartfelt thank you also goes to Prof. Dr. Werner Seeger, for his unwavering support and critical pointers.

Thanks to all my lab members, because without them, I would not have been able to reach this goal. A deeply felt thank you goes to Claudio and Alberto, my seniors and friends, who taught me so much, in and outside of the lab. An especially warm thank you goes to Jordi, who became family ("famiglia!") to me and who gave me the strength and the knowledge to keep going when all else seemed to fail. And thank you, especially, Francesco, who joined me from the start and was always by my side, with his incomparable artisanship and the bursts of silliness who made the hard times tolerable. Thank you, Francisco, for never doubting me and always having my back – even in online environments, in our shared fandoms and movie tastes! And thank you, Daniel, for the incredibly insightful conversations and the amazing job you have done helping me getting through the finish line. Thank you, Solmaz, because having to be the "mother" of a lab full of loud, funny people did not stop you from showing us how big your heart is, day after day. Thank you, Despina, because impromptu dance parties and convoluted stories are nothing, compared to how much your friendship and warmth helped me. Thank you, Miša, my battle partner, for keeping all my notes and little post-its and cherishing them. Thank you, Reshma, for the hugs and the chats and all the scientific little moments we shared.

Thanks, my special one, David, hermano. I was lucky to have you there, back-to-back, always.

A profound, unpayable debt of gratitude I owe to Christina. I would literally not be writing these words without your support, help, friendship, hard, hard work and limitless chats about superhero fandom. You earned a special place in Heaven amongst saints and martyrs.

Sabrina, my love and wife... my gratitude cannot be described in words. You were there to pick me up for every hard moment, to shield me in the harshest of times, and to help me seeing the joy in the little victories. You are my Light.

Grazie, bro, perché un fratello non si trova mica per strada, eh.

E grazie, all'ultimo posto, il posto speciale, riservato a chi c'è sempre stato; grazie, mammì. Per una vita di supporto e sacrifici. Ti voglio tanto, tanto, tanto bene.

18 Declaration

Hiermit erkläre ich, dass ich die vorliegende Arbeit selbständig und ohne unzulässige Hilfeoder Benutzung anderer als der angegebenen Hilfsmittel angefertigt habe. Alle Textstellen, diewörtlich oder sinngemäß aus veröffentlichten oder nichtveröffentlichten Schriften entnommen sind, und alle Angaben, die auf mündlichen Auskünften beruhen, sind als solche kenntlich gemacht. Bei den von mir durchgeführten und in der Dissertation erwähnten Untersuchungen habe ich die Grundsätze guter wissenschaftlicher Praxis, wie sie in der „Satzung der JustusLiebig-Universität Gießen zur Sicherung guter wissenschaftlicher Praxis“ niedergelegt sind, eingehalten sowie ethische, datenschutzrechtliche und tierschutzrechtliche Grundsätze befolgt. Ich versichere, dass Dritte von mir weder unmittelbar noch mittelbar geldwerte Leistungen für Arbeiten erhalten haben, die im Zusammenhang mit dem Inhalt der vorgelegten Dissertation stehen, oder habe diese nachstehend spezifiziert. Die vorgelegte Arbeit wurde weder im Inland noch im Ausland in gleicher oder ähnlicher Form einer anderen Prüfungsbehörde zum Zweck einer Promotion oder eines anderen Prüfungsverfahrens vorgelegt. Alles aus anderen Quellen und von anderen Personen übernommene Material, das in der Arbeit verwendet wurde oder auf das direkt Bezug genommen wird, wurde als solches kenntlich gemacht. Insbesondere wurden alle Personen genannt, die direkt und indirekt an der Entstehung der vorliegenden Arbeit beteiligt waren. Mit der Überprüfung meiner Arbeit durch eine Plagiatserkennungssoftware bzw. ein internetbasiertes Softwareprogramm erkläre ich mich einverstanden.

Ort, Datum Unterschrift